



UNIVERSITEIT VAN PRETORIA
UNIVERSITY OF PRETORIA
YUNIBESITHI YA PRETORIA



UNIVERSITEIT VAN PRETORIA
UNIVERSITY OF PRETORIA
YUNIBESITHI YA PRETORIA

Denkleiers • Leading Minds • Dikgopolo tša Dihlalefi

INTEGRATED BRAKE BASED TORQUE VECTORING CONTROL OF VEHICLE YAW RATE AND SIDE-SLIP ANGLE

Submitted in partial fulfilment of the requirements for the degree

Master of Engineering

(Mechanical Engineering)

By

Karthik Poovendran

In the Faculty of

Engineering, Built Environment and Information Technology (EBIT)

JUNE 4, 2018

UNIVERSITY OF PRETORIA

Pretoria

Summary

Title: Integrated Brake Based Torque Vectoring Control of Yaw Rate and Side-Slip Angle

Author: Karthik Poovendran

Study Leader: Dr. T.R. Botha

Department: Mechanical and Aeronautical Engineering, University of Pretoria

Degree: Masters in Engineering (Mechanical Engineering)

Sport Utility Vehicle (SUV) sales are increasing globally, even surpassing sedan vehicle sales worldwide. Their increasing popularity is termed a continuous trend that is expected to last. SUVs are known to offer a higher ground clearance which makes them more susceptible to rollover and directional instability during emergency manoeuvres. This dissertation proposes an integrated controller which controls two vehicle states, namely yaw-rate and side-slip angle to improve handling while reducing rollover propensity and improving rollover stability. The control system employs brake based torque vectoring to control the vehicle states, torque vectoring control improves lateral stability by maintaining consistent handling characteristics over all driving conditions and the lateral stability is maintained whilst adhering to a rollover index. The desired vehicle states are obtained from a reference linear two degree of freedom model with tyre characteristics obtained from the linear region of the tyre. A coordinated control strategy is investigated with respect to Direct Yaw Moment Control (DYC) acting on a vehicle through individual brake torques. Two types of controllers are investigated, namely a Linear Quadratic Regulator (LQR) and a Linear Model Predictive Controller (LMPC). It is shown that yaw rate control together with side-slip angle control and the inclusion of a roll index limit allows for better vehicle handling. Simulation tests are done using Simulink/ADAMS and verified experimentally with a SUV undergoing evasive manoeuvres where the vehicle is near its performance limit. The vehicle managed to be successfully navigated through manoeuvres not possible prior to yaw rate and side-slip angle control, with a notable decrease in the vehicle roll.

Acknowledgements

A special word of thanks to the following people who contributed in various ways to this study:

- Dr. T.R Botha for his positive outlook, ability to guide my endeavours, mentorship and overall support.
- My Parents Puvi and Siri Rangini Poovendran, for their motivation and continuous support.
- Prof. P.S Els for allowing me the opportunity and sharing his wise words of encouragement during my postgraduate studies.
- Herman Hamersma, Carl Becker and Wietsche Penny for agreeing to be test drivers on different occasions.
- Matti Noack for sharing his knowledge on Optimal Control and helping me adapt to the state space form.
- My Brother and Sister for their words of encouragement and motivation.
- The Vehicle Dynamics Group for the guidance, positive criticism and support during testing as well as the constructive outings.

Table of Contents

| | |
|---|-----|
| Summary | i |
| Acknowledgements | ii |
| List of Figures..... | v |
| List of Tables | vi |
| List of Symbols and Abbreviations | vii |
| Chapter 1 Literature Study..... | 1 |
| 1.1 Introduction | 1 |
| 1.2 Vehicle Dynamics..... | 6 |
| 1.2.1 Vehicle Navigating a Corner at low speed | 6 |
| 1.2.2 Vehicle Navigating a Corner at high speed..... | 6 |
| 1.3 Control Focus..... | 13 |
| 1.3.1 Yaw Rate and Side Slip Angle | 13 |
| 1.3.2 Types of Roll Prediction | 15 |
| Conclusion from Literature Study | 18 |
| Chapter 2 Experimental Setup and Validation of Vehicle Simulation Model | 19 |
| 2.1 Vehicle..... | 19 |
| 2.1.1 Simulation Model | 19 |
| 2.1.2 Vehicle Tyre | 20 |
| 2.1.3 Vehicle Suspension | 21 |
| 2.2 Vehicle Instrumentation | 22 |
| 2.3 Manoeuvres..... | 24 |
| 2.4 Validation of Vehicle Simulation Model | 26 |
| 2.4.1 Full Vehicle Model Validation | 26 |
| 2.4.2 Brake Torque vs Brake Pressure Relation..... | 29 |
| Conclusion of experimental setup and validation of vehicle simulation model | 30 |
| Chapter 3 Control Strategy..... | 31 |

| | |
|---|----|
| 3.1 Vehicle Reference Model | 31 |
| 3.2 Linear Quadratic Regulator (LQR) | 35 |
| 3.2.1 Control System Design | 35 |
| 3.3 Model Predictive Control | 37 |
| 3.3.1 Controller Design..... | 38 |
| 3.4 Brake Torque Difference Distribution..... | 40 |
| 3.5 Pressure Control..... | 41 |
| Conclusion of Control Strategy..... | 42 |
| Chapter 4 Results | 43 |
| 4.1 Simulation Results..... | 43 |
| 4.1.1 Sinusoidal Wave Steer Input | 43 |
| 4.1.2 Step Steer Input..... | 46 |
| 4.2 Experimental Results..... | 51 |
| 4.2.1 Severe Double Lane Change ISO3888-1 | 51 |
| 4.2.2 Severe Lane Change ISO3888-2 Obstacle Avoidance | 55 |
| Conclusion of Results..... | 57 |
| Chapter 5 Conclusion and Recommendations | 58 |
| 5.1 Conclusion..... | 58 |
| 5.2 Recommendations..... | 58 |
| Chapter 6 References | 60 |
| Appendix..... | 63 |

List of Figures

| | |
|---|----|
| Figure 1 Handling Characteristics with and without ESP (Wong, 2008) | 3 |
| Figure 2 Left-right torque vectoring concept (Sawase et al., 2006) | 4 |
| Figure 3 Tyre load equalization between left and right wheels (Sawase et al., 2006) | 5 |
| Figure 4 Geometry of a vehicle turning at low speeds (Gillespie, 1992) | 6 |
| Figure 5 2DOF Bicycle Model turning at high speed..... | 6 |
| Figure 6 Tyre cornering force properties (Gillespie, 1992)..... | 7 |
| Figure 7 Examples of Understeer vs Neutral steer vs Oversteer (Gillespie, 1992)..... | 9 |
| Figure 8 Tyre Lateral Force as a function of Vertical Load | 10 |
| Figure 9 Free body diagram of vehicle roll (Gillespie, 1992) | 11 |
| Figure 10 Vehicle Roll Centres and CG heights (Abe, 2009) | 12 |
| Figure 11 Yaw Rate and Side-Slip Angle Schematic | 13 |
| Figure 12 Yaw Rate gain as a function of vehicle speed (Gillespie, 1992) | 14 |
| Figure 13 Visual Demonstration of Side-Slip Angle (Racelogic, 2015)..... | 14 |
| Figure 14 ZMP on a kinematic chain of bodies..... | 17 |
| Figure 15 ZMP on a Rigid Vehicle Model | 18 |
| Figure 16 Land Rover Defender test vehicle..... | 19 |
| Figure 17 Graphical view of vehicle Modelled in ADAMS..... | 20 |
| Figure 18 Experimental and FTire Simulated Tyre Model of Michelin LTX2 tyres (Bosch et al., 2016) . | 20 |
| Figure 19 4S ₄ Suspension Setup | 21 |
| Figure 20 Test vehicle with measurement devices..... | 22 |
| Figure 21 Block diagram of data acquisition and control | 23 |
| Figure 22 ISO3888-1 Severe Double Lane Change Path (Standard, 1999) | 24 |
| Figure 23 Modified ISO 3888-2 Modified Obstacle Avoidance Path (Standard, 2011)..... | 25 |
| Figure 24 DLC Trajectory | 26 |
| Figure 25 Speed and Steering Angle Inputs to Simulation Model through DLC at 52km/h. | 26 |
| Figure 26 Correlation of measured parameters through DLC at 52km/h. | 27 |
| Figure 27 Speed and Steering Angle Inputs to Simulation Model through DLC at 65km/h. | 28 |
| Figure 28 Correlation of measured parameters through DLC at 65km/h. | 28 |
| Figure 29 Brake Torque vs Brake Pressure Linear Fit..... | 30 |
| Figure 30 TWO-DOF Bicycle Model..... | 31 |
| Figure 31 Desired Vehicle Model | 34 |
| Figure 32 Controller with Feedback..... | 34 |
| Figure 33 MPC Weighting..... | 39 |

| | |
|---|----|
| Figure 34 Test Vehicle undergoing Yaw Enhancement | 40 |
| Figure 35 Brake Pressure Control | 42 |
| Figure 36 Steering and Speed Input through Modified DLC | 43 |
| Figure 37 Feedback through Modified DLC of various parameters | 44 |
| Figure 38 Roll Index for Bounded MPC with Sinusoidal Steer Input..... | 45 |
| Figure 39 Feedback for Sinusoidal Steer Input with Bounded Roll Index | 45 |
| Figure 40 Vehicle Trajectory and Speed through Modified DLC with Roll Index Bounds | 46 |
| Figure 41 Step Steer Input along with Direct Yaw Control Moments..... | 46 |
| Figure 42 Feedback through Step Steer of various parameters..... | 47 |
| Figure 43 Roll Index through Step Steer..... | 47 |
| Figure 44 Trajectory and Vehicle Speed through Step Steer | 48 |
| Figure 45 Bounded Roll Index and Direct Yaw Control Moment..... | 49 |
| Figure 46 Yaw Rate and Side-Slip Angle through Step Steer with Roll Index Bound on MPC | 49 |
| Figure 47 Feedback through Step Steer with Roll Index bounded MPC of various parameters | 50 |
| Figure 48 ISO3888-1 Trajectory and DYC Moment..... | 51 |
| Figure 49 Yaw Rate and Side-Slip Angle through ISO3888-1 DLC | 52 |
| Figure 50 Yaw Angle through ISO 3888-1 DLC | 52 |
| Figure 51 Roll Characteristics through ISO 3888-1 DLC..... | 53 |
| Figure 52 Brake Torques through ISO3888-1 DLC..... | 54 |
| Figure 53 Vehicle Exiting ISO3888-1 Manoeuvre, Note Brake Lights..... | 54 |
| Figure 54 ISO3888-2 Trajectory and DYC Moment..... | 55 |
| Figure 55 Yaw Rate and Side-Slip Angle through ISO3888-2 Obstacle Avoidance | 55 |
| Figure 56 Roll Characteristics through ISO 3888-2 Obstacle Avoidance..... | 56 |
| Figure 57 Brake Torques through ISO3888-2 Obstacle Avoidance..... | 57 |

List of Tables

| | |
|--|----|
| Table 1 Vehicle Input Output Devices..... | 22 |
| Table 2 ISO3888-1 Section Descriptions | 24 |
| Table 3 Brake Parameters..... | 29 |
| Table 4 LQR Weighting Values | 36 |
| Table 5 Pressure Control Logic..... | 42 |

List of Symbols and Abbreviations

| Abbreviation | Description |
|-----------------|--|
| 4S ₄ | 4-State Semi-Active Suspension System |
| 4WS | Four Wheel Steering |
| ABS | Anti-Lock Braking System |
| ADAMS | Automatic Dynamic Analysis of Mechanical Systems |
| CAN | Controller Area Network |
| CEP | Circular Error Probable |
| COG | Centre of Gravity |
| DGPS | Differential Global Positioning System |
| DLC | Double Lane Change |
| DOF | Degree of Freedom |
| DYC | Direct Yaw Control Moment |
| ESP | Electronic Stability Program |
| FTire | Flexible Structure Tyre Model |
| GLONASS | Global Navigation Satellite System |
| GPS | Global Positioning Unit |
| I/O | Input/Output |
| IMU | Inertial Measurement Unit |
| ISO | International Organization for Standardization |
| LQR | Linear Quadratic Regulator |
| LSD | Limited Slip Differential |
| LTR | Load Transfer Ratio |
| MABX | Micro Autobox |
| Matlab | MATrix LABoratory |
| MMC | Mitsubishi Motors Corporation |
| MPC | Model Predictive Control |
| MSC | MacNeal-Schwendler Corporation Software |
| NHTSA | National Highway Traffic Safety Administration |
| PID | Proportional Integral Derivative |
| RI | Roll Index |
| RTI | Real Time Interface |

| | |
|---------|----------------------------|
| S-AWC | Super-All Wheel Control |
| SSF | Static Stability Factor |
| SUV | Sports Utility Vehicle |
| VBOX 3i | Velocity BOX 3i |
| VSC | Vehicle Stability Control |
| WABCO | Westinghouse Air Brake Co. |
| ZMP | Zero Moment Point |

| Roman Symbols | Description |
|---------------|--|
| a | Linear Acceleration |
| A_x | Longitudinal Acceleration |
| A_y | Lateral Acceleration |
| A_z | Vertical Acceleration |
| B | Stiffness factor |
| C | Shape factor |
| C | Cornering Force |
| CG | Centre of Gravity |
| C_α | Cornering Stiffness Coefficient |
| D | Peak factor |
| D | Driving Force |
| E | Curvature factor |
| F_x | Tyre longitudinal force |
| F_y | Tyre lateral force |
| F_z | Tyre vertical force |
| g | Acceleration due to Gravity |
| h | Height |
| I_z | Yaw Moment of Inertia |
| K | Stability Factor |
| K_ϕ | Roll Stiffness |
| l_f/l_r | Distance from front/rear axle to centre of gravity |
| L | Vehicle WheelBase |
| m | Mass |
| M | Moment |
| M_z | Yaw Moment |

| | |
|-----------|--|
| M_ϕ | Roll Moment |
| p | Roll Rate |
| p | Brake Pressure |
| q | Pitch Rate |
| r | Brake Disc Radius |
| R | Radius |
| S_h | Horizontal shift |
| S_v | Vertical shift |
| T | Vehicle Track |
| T_b | Brake Torque |
| T_r | Yaw Rate time constant |
| V | Velocity |
| v_y | Lateral Velocity |
| W_f/W_r | Axle weight front/rear |
| w_b | Side-slip angle tuning factor |
| w_r | Yaw rate tuning factor |
| w_u | Controller Effort |
| y_{ZMP} | Lateral Distance between vehicle ZMP Point and centre-line |

| Greek Symbols | Description |
|----------------|--|
| ϕ_r | Roll Angle |
| ϕ_t | Roll angle of terrain |
| α | Tyre Side-Slip Angle |
| β | Vehicle Side-Slip Angle |
| γ | Vehicle Yaw Rate |
| δ | Steering angle of front wheels |
| θ | Pitch Angle |
| θ | Brake Radial Angle |
| μ | Surface friction co-efficient |
| μ_{bp} | Brake pad and disc coefficient of friction |
| ω | Angular velocity |
| $\dot{\omega}$ | Angular acceleration |

| Subscripts | Description |
|------------|----------------------------------|
| <i>cg</i> | Centre of Gravity |
| <i>d</i> | Desired |
| <i>f</i> | Front |
| <i>i</i> | Inner Wheel |
| <i>l</i> | Left |
| <i>o</i> | Outer Wheel |
| <i>r</i> | Rear |
| <i>r</i> | Right |
| <i>rc</i> | Roll Centre |
| <i>s</i> | Centre of Gravity to Roll Centre |
| <i>ss</i> | Steady State |

Chapter 1 Literature Study

This Literature Study will discuss the working principles of Vehicle Dynamics and the benefits it could provide for a Sport Utility Vehicle. “Vehicle Dynamics are vital for optimizing a vehicle’s drivability, efficiency and safety” (Abe, 2015).

1.1 Introduction

Sport Utility Vehicles (SUVs) have become more popular in recent years, mainly due to their higher seating position that improves visibility and perception of safety. A higher centre of gravity however makes a vehicle more prone to rollover, especially if the driver makes a sudden directional input during an emergency manoeuvre. Although rollovers occur in only about 3 percent of all crashes, they account for nearly 30 percent of fatalities in vehicles (Reports, 2014).

The United States National Highway Traffic Safety Administration (NHTSA, 2003) states that approximately one in every seven collisions is due to run-off-road collisions, whereby the vehicle fails to navigate a turn, which contributes to a third of all fatal collisions. Therefore, rollover and run-off-road collisions account for a large portion of fatalities in road vehicles.

The vehicle dynamics of SUVs are more complex due to their high centre of gravity, large suspension displacements and varying terrains that SUVs must negotiate. Therefore, various active control systems such as ABS, 4WS, semi-active/active suspensions systems, active anti-roll bars and Electronic Stability Programs (ESP) were introduced in vehicles one after another since the late 1970s. The aim of the control systems is to improve vehicle safety, performance and comfort over the large range of operating conditions. It has been found that ESP systems made rollover two-thirds less likely in SUVs (Kallan, 2008).

A method to prevent the loss of vehicle directional stability in emergency manoeuvres together with a rollover prevention system is necessary to further lower the current fatality rate. Possible solutions in literature are reviewed, to determine the feasibility of the solutions and the practicality of it.

1.1.1 Four Wheel Steering (4WS)

Four-wheel steering can allow for improved steering response, increased vehicle stability at high speed, and decreased turning radiuses at low speeds. At low speeds, the vehicle’s rear wheels will turn in the opposite direction to the front wheels in order to aid in manoeuvrability, whereas at high speeds, the rear wheels will turn in the same direction as the front wheels but at much smaller angles.

Ackermann (1994) models the steering dynamics based on the front axle side-slip angle and vehicle yaw rate, he thereafter prescribes a desired steering dynamic to be tracked. The total vehicle dynamics are

investigated and the rear axle's side-slip angle is also taken into account, from this he determines for a zero-vehicle side-slip angle the rear steering angle.

No mention is made of roll reduction using this method only, however it is mentioned as an aid in rollover prevention amongst other systems such as Electronic Stability Programs. The cost implication of using a four-wheel steer system is however expensive, due to the addition of components, linkages, etc.

1.1.2 Active Anti-Roll Bars

Anti-roll bars have been part of vehicle suspension systems dating back to 1919, it connects both left and right wheels on an axle through short lever arms and a torsion spring. The anti-roll bars increase a suspension's roll stiffness. In 1994 Citroen introduced the first active anti-roll bar, limiting the vehicle's roll to a maximum of 2 degrees (Marsh, 2007). Thereafter the stabilizer bar stiffness became variable, and in 2006 Toyota introduced its Active Stabilizer Suspension system which reduced body roll during cornering and improved handling and stability.

A previous study at the Vehicle's Dynamic Group by Cronje and Els (2010) simulated, designed, manufactured and implemented an active-anti-roll-bar on the rear of a test vehicle. It showed an 80% improvement in body roll angle on a smooth road during a double-lane-change manoeuvre at 80km/h. It cannot be faulted that an Active-Anti-Roll-Bar will indeed be the best solution to reduce vehicle roll angle, however its benefits with regards to consistent predictable handling haven't been investigated.

1.1.3 Controllable Suspension Systems

Els et al. (2006) designed and implemented a semi-active suspension system on the test vehicle used in this study. The suspension system is termed a Four State Semi-Active Suspension System, or 4S₄. It is a hydro-pneumatic suspension system and is discussed further in Section 2.1.3. It can switch between a ride mode and a handling mode. The test vehicle achieved a decrease in body roll angle between 61 and 78% during a double-lane-change manoeuvre at 70km/h in its handling mode in-comparison to the baseline vehicle.

1.1.4 Limited Slip Differentials (LSD)

A vehicle's conventional open differential allows two wheels on an axle to display uniform distribution of the driving torque and allows different wheel speeds during cornering. However, when the surface conditions vary, torque is sent to the wheel with lower adherence, which results in wheel spin and poor traction of the vehicle. Performance vehicles are equipped with limited slip differentials for this reason, it will always transfer torque to the slower wheel and allows no control over the torque transfer however. This can result in a rear wheel drive vehicle to oversteer and a front wheel drive vehicle to understeer.

Lew et al. (2006) proposes a control scheme using an electronically controlled limited slip differential to prevent vehicle rollover, the downsides of such an electronically controlled differential is the manufacturing and cost implications of such a system.

1.1.5 Electronic Stability Programs

In the early 1980s, Toyota introduced an electronic anti-skid control system on a production car. Other manufacturers shortly followed course introducing their traction control system. It works on the fundamentals of applying brakes asymmetrically without the driver applying brakes, done to exert restoring yaw moments on the vehicle, to allow the driver to gain control. Implemented using a closed loop control of yaw rate, the desired yaw-rate is obtained from extensive vehicle testing.

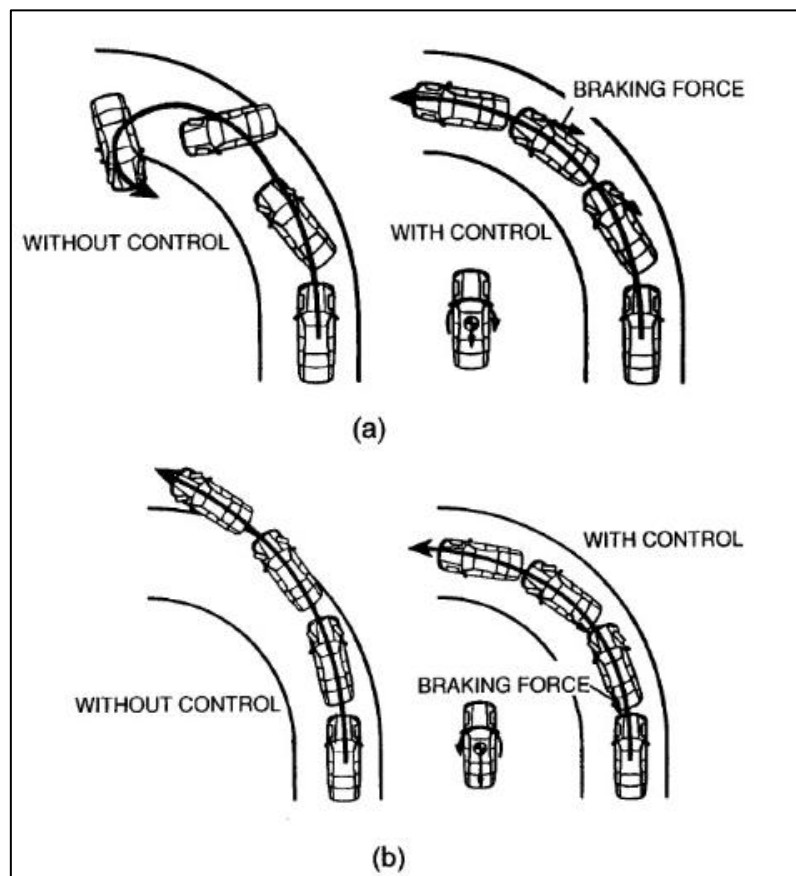


Figure 1 Handling Characteristics with and without ESP (Wong, 2008)

Wong (2008) shows in Figure 1 how ESP can assist the handling characteristics of road vehicles whereby in (a) the vehicle oversteers, a brake force is applied to the outside front wheel to oppose this yaw motion and in (b) where a yaw motion is induced by braking the inside rear wheel to prevent understeer. It should be noted that ESP does not increase traction, nor does it enable predictable consistent handling as it over-rides the driver's command in order to recover vehicle control in a dangerous situation.

1.1.6 Torque Vectoring

Torque Vectoring makes it possible to control both the direction and magnitude of torque transfer, allowing the vehicle to apply a yaw moment on the vehicle. Although more capable on electric vehicles with in-hub motors, the fundamental benefits can be applied on internal combustion vehicles. Torque may be transferred from the slower wheel to the faster wheel and thus create a better compromise between traction and vehicle dynamic performance.

Sawase et al. (2006) mentions that Mitsubishi was at the forefront of the industry by equipping the world's first production vehicle with an active yaw control system in 1996. They thereafter developed a torque vectoring control system named Super-All Wheel Control (S-AWC). S-AWC was aimed at maximizing the capability of all four tyres of a vehicle in a balanced manner and to realize predictable handling along with high marginal performance. The S-AWC was used for three forms of control:

- Control over four tyres' vertical loading, maintaining firm contact with the road surface for consistently maximal grip.
- Control over four tyres' slip ratios and slip angles such that the longitudinal and lateral force produced by each tyre are maximized in a balanced manor.
- Control over the four tyres' force assignments, thus the distribution of longitudinal and lateral forces amongst the four tyres.

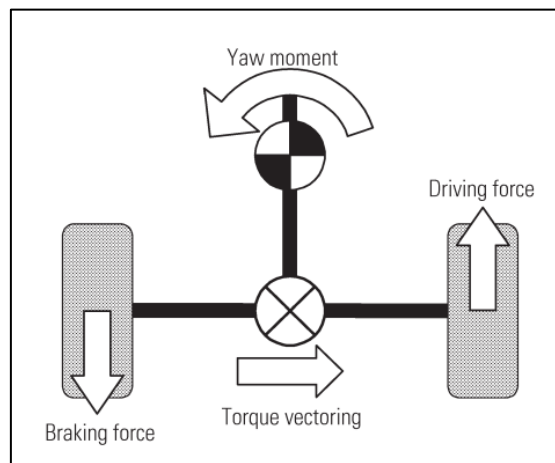


Figure 2 Left-right torque vectoring concept (Sawase et al., 2006)

Mitsubishi Motors Corporation (MMC) devised that an ideal mechanism to track desired cornering be capable of controlling the yaw moment, thus the torque differences between wheels and not the torque distribution. Figure 2 depicts the torque transfer, whereby the left wheel experiences a brake force and the right wheel has a driving force of the same magnitude generated. This allows for the yaw moment to be controlled directly as desired without being dependent on engine torque or the driver's acceleration or deceleration operations. The benefits of torque vectoring are mainly the enhancement of cornering

performance by means of tyre load equalizations between the front and rear as well as left and right of the vehicle.

Figure 3 shows an example of tyre load equalization between left and right wheels when the vehicle is cornering. During the corner, the vertical load on the left tyre decreases and the vertical load on the right tyre increases, a difference is created between the left and right wheels' maximum longitudinal and lateral force capability. In Figure 3(a), an increase in the torque will result in the tyre reaching its grip limit, and starting to slip, thus no cornering improvement is possible. By controlling the drive torque on the left wheel by a longitudinal braking torque, it is possible to increase the lateral force capability of the tyre. It is also mentioned that the lateral force can be increased to a limit, however an excessively large braking force on the left tyre will reduce the benefits.

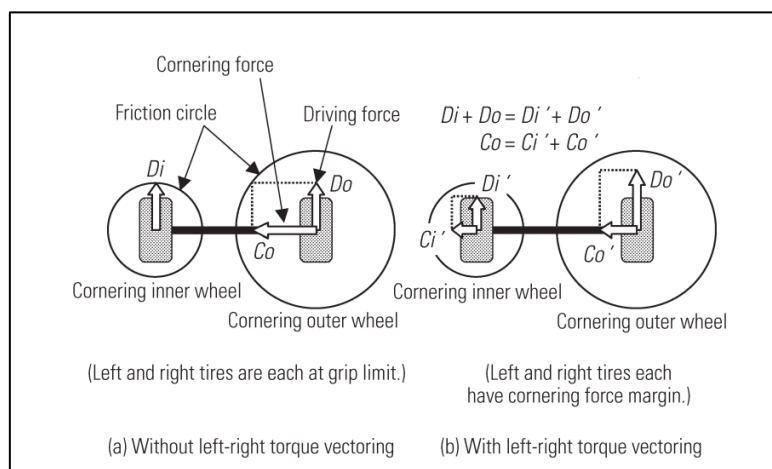


Figure 3 Tyre load equalization between left and right wheels (Sawase et al., 2006)

Conclusion

The methods discussed in this section show that active-anti roll bars and controllable suspension systems can reduce rollover propensity whereas 4WS, LSDs and ESP systems have been mainly introduced over the years to maintain stability. Torque vectoring control shows a possible improvement in both rollover propensity and the stability of a vehicle while offering predictable handling. The study will thus focus on torque vectoring control in the form of differential brake based control, it is noted that it is also readily implementable in most commercial vehicles.

In this study a combined yaw-rate and side-slip angle controller is proposed. The controller tracks the states of a reference linear 2 Degree of Freedom (2DOF) vehicle model with fixed tyre/terrain interface parameters. The system will maintain the actual vehicle states, yaw-rate and side-slip angle, as close as possible to the proposed desired responses without an excessively large external yaw moment and without compromising rollover stability. The rollover stability is based on a zero-moment-point rollover index. The external yaw moment is kept as small as possible in order to let the driver feel supported rather than overruled.

1.2 Vehicle Dynamics

Vehicle dynamics is investigated with regards to inconsistent vehicle handling and rollover propensity.

1.2.1 Vehicle Navigating a Corner at low speed

When a vehicle travels through a curved path at low speeds, such as parking lot speeds, the tyres develop very small lateral forces as the tyres roll without a slip angle. Ackermann (1994) describes the average front steer angle required for a vehicle with wheelbase L to navigate a circle with radius R as seen in Figure 4 as:

$$\delta = \frac{L}{R} \tag{1.1}$$

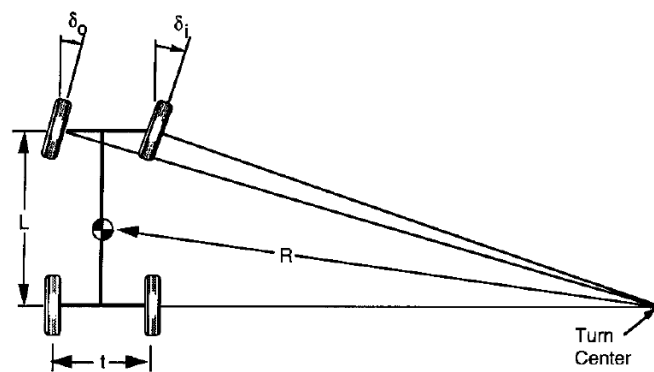


Figure 4 Geometry of a vehicle turning at low speeds (Gillespie, 1992)

1.2.2 Vehicle Navigating a Corner at high speed

At higher speeds however, the vehicle will experience a lateral acceleration which is the centripetal acceleration acting towards the centre of the turn as depicted in Figure 5. For simplicity, a 2DOF bicycle model is used to depict this. The tyres develop lateral forces which results in the centripetal acceleration, so in order to go around a corner, the tyres need to generate forces.

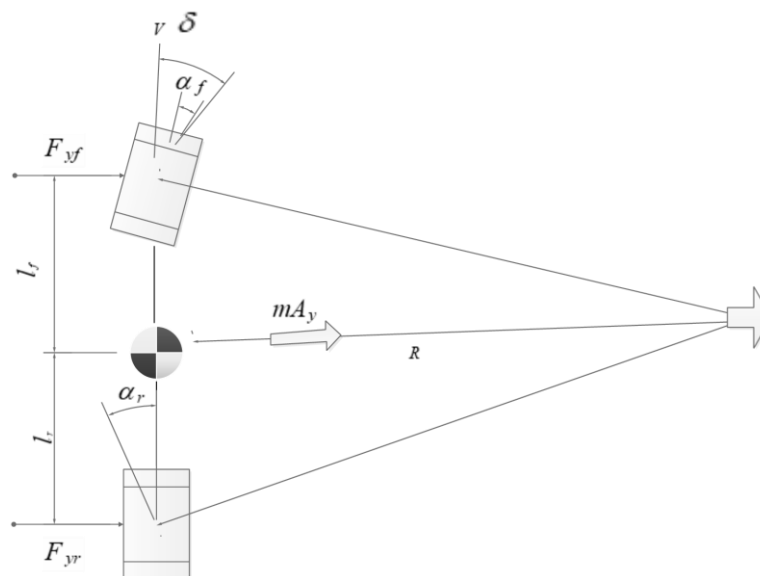


Figure 5 2DOF Bicycle Model turning at high speed

Where Lateral Acceleration can be defined as:

$$A_y = \frac{V^2}{R} \quad (1.2)$$

1.2.2.1 Lateral Force of a Tyre

In order for a tyre to generate a lateral force, the tyre must undergo deformation. For F_y , this deformation is called the tyre side-slip angle as shown in Figure 6. Tyre side-slip angles can also be expressed as the difference between a tyre's direction of heading and its direction of travel during a corner when the tyre develops a lateral force. The tyre experiences different lateral forces for different slip angles and generally an increase in slip angle results in an increase in lateral force within the linear aspect of a tyre.

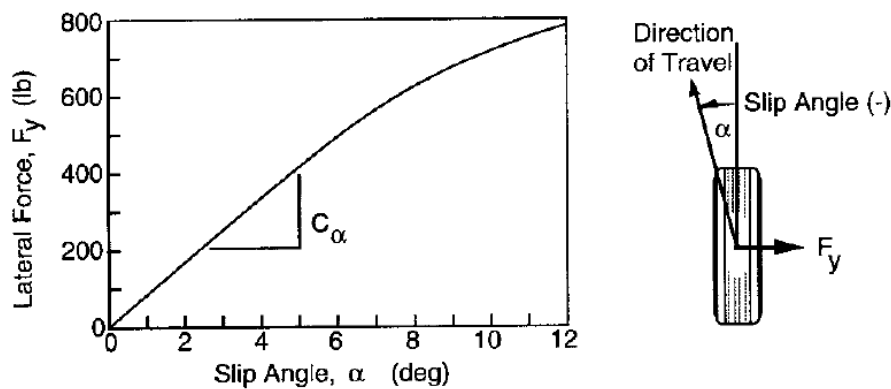


Figure 6 Tyre cornering force properties (Gillespie, 1992)

Figure 6 also shows that at increasing slip angles α , the tyre is capable of developing increased lateral forces F_y , and the slope of the curve C_α is known as the cornering stiffness leading to Equation (1.3). Cornering stiffness fluctuates based on variables such as tyre size, type, width, tread, vertical load and inflation pressure amongst others.

$$F_y = C_\alpha \alpha \quad (1.3)$$

Tyre lateral forces however decrease at even higher slip angles, whereby saturation occurs and (1.3) does not hold anymore, as the tyre displays nonlinear behaviour.

1.2.2.2 Vehicle Dynamic Equations for high speed cornering

The cornering equations at higher speeds are more complex than stated in (1.1). Using the 2DOF bicycle model shown in Figure 5 travelling with a forward velocity of V , cornering around a turn and using Newton's Second Law of motion with the modified tyre's slip-angle conditions, one may analyse steady-state cornering equations of a vehicle. The sum of forces in the lateral direction from the tyres must equal the mass times the centripetal acceleration.

$$\sum F_y = F_{yf} + F_{yr} = M \frac{V^2}{R} \quad (1.4)$$

For the vehicle to be in moment equilibrium about the centre of gravity, the sum of moments from the front and rear lateral forces must be zero.

$$F_{yf}l_f - F_{yr}l_r = 0 \quad (1.5)$$

Therefore

$$F_{yf} = F_{yr} \frac{l_r}{l_f} \quad (1.6)$$

Substituting (1.6) into (1.4) yields:

$$M \frac{V^2}{R} = F_{yr} \left(\frac{l_r}{l_f} + 1 \right) = \frac{F_{yr}(l_r + l_f)}{l_f} = F_{yr} \frac{L}{l_f} \quad (1.7)$$

$$F_{yr} = M \frac{l_f}{L} \left(\frac{V^2}{R} \right) \quad (1.8)$$

But $M \frac{l_f}{L}$ is the portion of the vehicle mass carried on the rear axle thus $\frac{W_r}{g}$, therefore the rear lateral force becomes:

$$F_{yr} = \frac{W_r}{g} A_y \quad (1.9)$$

and solving for the front lateral force is:

$$F_{yf} = \frac{W_f}{g} A_y \quad (1.10)$$

As mentioned, with lateral forces comes tyre slip angles as in (1.3), thus the slip angles can be calculated assuming linear relationships as:

$$\alpha_f = \frac{W_f V^2}{C_{\alpha f} g R} \quad (1.11)$$

$$\alpha_r = \frac{W_r V^2}{C_{\alpha r} g R} \quad (1.12)$$

Ackermann (1994) states that from analysis now the required steer angle in degrees is:

$$\delta = \frac{180}{\pi} \frac{L}{R} + \alpha_f - \alpha_r \quad (1.13)$$

Which can be described as:

$$\delta = \frac{180}{\pi} \frac{L}{R} + \frac{W_f V^2}{C_{\alpha f} g R} - \frac{W_r V^2}{C_{\alpha r} g R} \quad (1.14)$$

$$\delta = \frac{180}{\pi} \frac{L}{R} + \left(\frac{W_f}{C_{\alpha f}} - \frac{W_r}{C_{\alpha r}} \right) \frac{V^2}{g R} \quad (1.15)$$

From (1.15) one can define the stability factor as:

$$K = \left(\frac{W_f}{C_{\alpha f}} - \frac{W_r}{C_{\alpha r}} \right) \quad (1.16)$$

The stability factor shows how the steering angle must be adjusted to maintain the radius of a turn based on lateral acceleration, with regards to the ratio of the load on the front and rear axles. There are three main categories with regards to a vehicle navigating a turn, these are shown in Figure 7 as: (Gillespie, 1992)

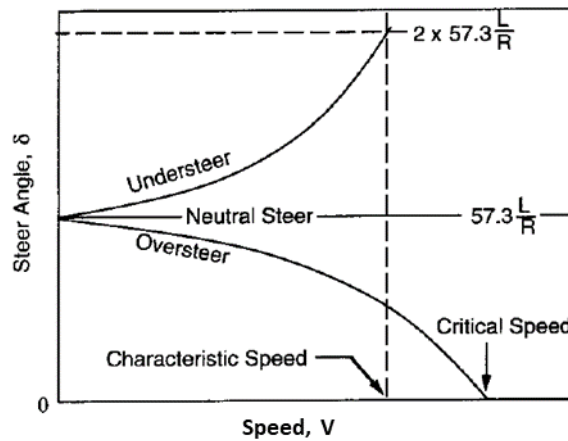


Figure 7 Examples of Understeer vs Neutral steer vs Oversteer (Gillespie, 1992)

Understeer

$$\frac{W_f}{C_{\alpha f}} > \frac{W_r}{C_{\alpha r}} \rightarrow K > 0 \rightarrow \alpha_f > \alpha_r \quad (1.17)$$

This occurs when the steering angle of the vehicle has to increase with speed, the lateral acceleration at the vehicle's centre of gravity causes the front wheels to slip sideways to a greater extent than the rear wheels. Therefore, in order to maintain the radius of the turn, the vehicle will either have to increase its steering angle as seen in Figure 7, or to reduce its longitudinal speed. Most passenger vehicle manufacturers design for this outcome, as it is more natural for a driver who has lost control to steer more into the corner when losing control.

Oversteer

$$\frac{W_f}{C_{\alpha f}} < \frac{W_r}{C_{\alpha r}} \rightarrow K < 0 \rightarrow \alpha_f < \alpha_r \quad (1.18)$$

On a constant radius turn, with increased vehicle speed the steering angle has to be decreased. This is due to the lateral acceleration at the vehicle's centre of gravity, causing the slip angle on the rear wheels to increase more than at the front wheels. The rear of the vehicle thus drifts outwards and the front of the vehicle drifts inwards, requiring corrective steering in the opposite direction as depicted in Figure 7 in order to maintain the radius of the turn or a reduction in vehicle longitudinal speed.

Neutral Steer

$$\frac{W_f}{C_{\alpha_f}} = \frac{W_r}{C_{\alpha_r}} = K = 0 \rightarrow \alpha_f = \alpha_r \quad (1.19)$$

This is where no change in steer angle is required with an increase in speed around a constant radius turn. The Ackerman angle, $\frac{180}{\pi} \frac{L}{R}$ is required at varying speed as shown in Figure 7. The balance on the vehicle is such that the lateral acceleration at the vehicle's centre of gravity causes an equivalent increase in slip angle at both the front and rear of the vehicle.

Taking the different forms of cornering, a controller should be designed to allow for predictable and consistent handling. The most dangerous cornering scenario is oversteer and should be avoided, thus forcing the vehicle to have neutral steer or slight understeer.

1.2.2.3 Effect of Lateral Load Transfer

Figure 8 shows an increase in vertical load on a tyre generally results in larger lateral forces, however as with increased slip angles, there is a point whereby saturation occurs and the relationship between lateral force and vertical load is also non-linear. For an axle with two wheels, the static load on each wheel is generally equal, however when cornering, load transfer occurs between the inner and outer wheel. The outside wheel becomes more loaded ($W + \Delta W$) and the inside wheel load reduces ($W - \Delta W$). The lateral forces at each wheel will have a combined lateral force F' , which is smaller as opposed the lateral force F of the no load transfer case. For a vehicle experiencing load transfer, the net effect on an axle will be reduced lateral force generation.

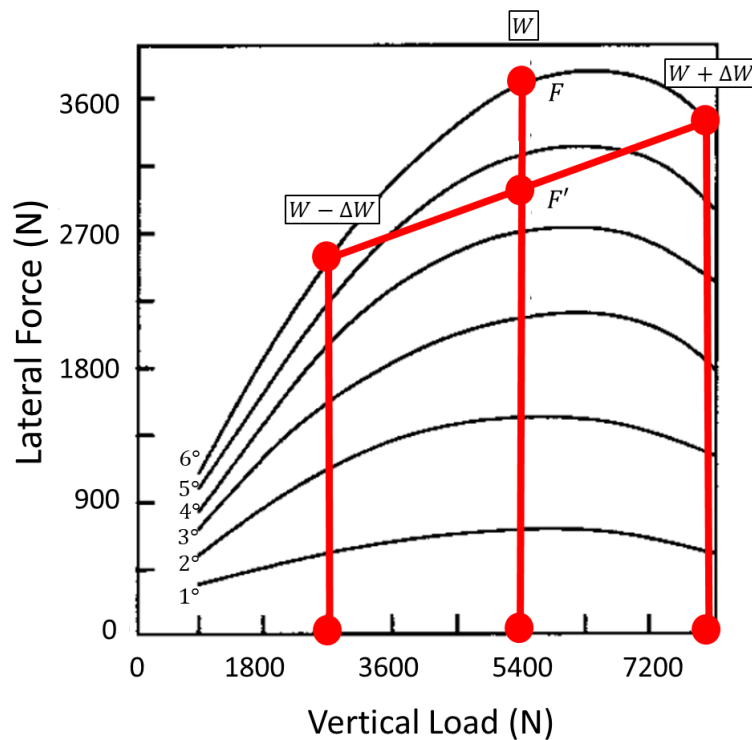


Figure 8 Tyre Lateral Force as a function of Vertical Load

In general, for most cars, the larger the load transfer, the greater the reduction in lateral force, also in most cars, the load transfer is different for the front and rear wheels. During cornering, the tyre road interface is highly non-linear, it is thus crucial to use actual tyre data representative of the vehicle's tyres and not a generic tyre model. A vehicle also experiences body roll during cornering whereby the roll angle of the vehicle increases/decreases according to the corner. This also has an effect on the loading of the tyres.

The free body diagram shown in Figure 9 depicts the forces acting on a vehicle experiencing body roll through a cornering manoeuvre. The load transfer can be obtained by:

$$F_{z_o} - F_{z_i} = 2F_y \frac{h_{rc}}{t} + \frac{2K_\phi \phi}{t} \quad (1.20)$$

Where K_ϕ is the roll stiffness of the suspension, ϕ the roll angle and h_{rc} the roll centre height.

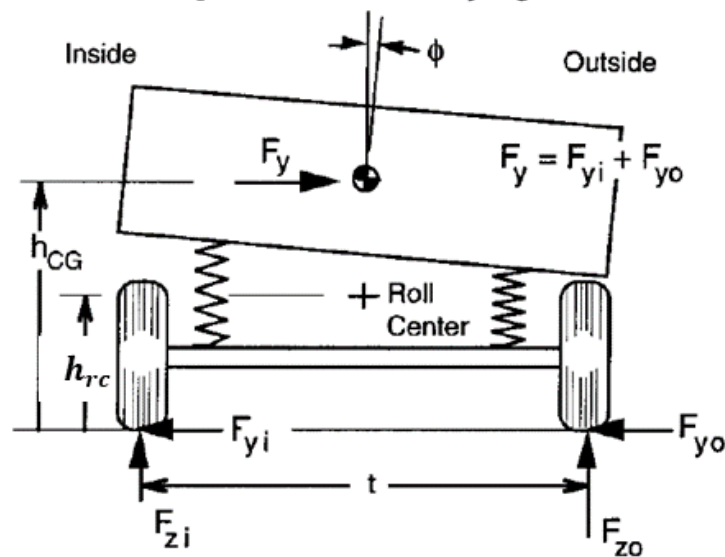


Figure 9 Free body diagram of vehicle roll (Gillespie, 1992)

In equation (1.20), there are two factors that contribute to load transfer, the first being the load transfer due to the cornering forces which arises from the lateral force imposed on the axle and the second being a result of vehicle roll which is dependent on the roll dynamics and the front/rear roll moment distribution.

The front and rear axle load transfer due to cornering forces can be expressed as:

$$\Delta F_{zf} = F_{yf} \frac{h_f}{t} \quad (1.21)$$

$$\Delta F_{zr} = F_{yr} \frac{h_r}{t} \quad (1.22)$$

However, since the load transfer due to vehicle roll is dependent on roll dynamics, the vehicle needs to be considered as a whole.

Figure 10 depicts the roll axis as a line connecting the roll centres of the front and rear.

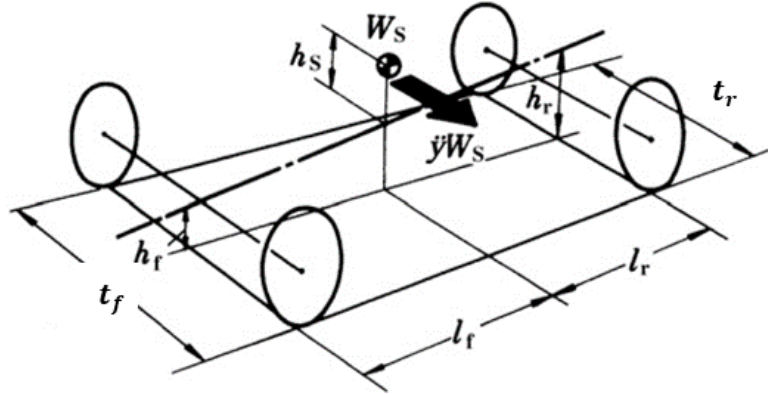


Figure 10 Vehicle Roll Centres and CG heights (Abe, 2009)

The moment about the roll axis is then:

$$M_{\phi} = W_s h_s \sin\phi + m A_y h_s \cos\phi \quad (1.23)$$

The roll moment can also be expressed as:

$$M_{\phi} = M_{\phi f} + M_{\phi r} = (K_{\phi f} + K_{\phi r})\phi \quad (1.24)$$

Substituting (1.24) into (1.23) and assuming small angles, the roll angle can be obtained as:

$$\phi = \frac{m A_y h_s}{K_{\phi f} + K_{\phi r} - W_s h_s} \quad (1.25)$$

From this it follows that the front and rear load transfers can be obtained as:

$$\Delta F_{zf} = \left[K_{\phi f} \frac{m A_y h_s}{K_{\phi f} + K_{\phi r} - W_s h_s} + F_{yf} h_f \right] \frac{1}{t_f} \quad (1.26)$$

$$\Delta F_{zr} = \left[K_{\phi r} \frac{m A_y h_s}{K_{\phi f} + K_{\phi r} - W_s h_s} + F_{yr} h_r \right] \frac{1}{t_r} \quad (1.27)$$

The final vertical load on the wheels can therefore be simply obtained by adding or subtracting the load transfer from the static load on the wheel.

$$F_{zf1} = F_{zf1,static} - \Delta F_{zf} \quad (1.28)$$

$$F_{zf2} = F_{zf2,static} + \Delta F_{zf} \quad (1.29)$$

$$F_{zr1} = F_{zr1,static} - \Delta F_{zr} \quad (1.30)$$

$$F_{zr2} = F_{zr2,static} + \Delta F_{zr} \quad (1.31)$$

The vertical loads on each wheel give the potential to use tyre models such as the Pacejka tyre model to determine non-linear tyre properties and develop a friction circle for each wheel.

1.3 Control Focus

This section describes what variables can be controlled using torque vectoring control to allow for predictable handling and to reduce the rollover propensity.

1.3.1 Yaw Rate and Side Slip Angle

Yaw rate and side-slip angle form a major component of vehicle lateral dynamics. A large increase in these variables is a major cause of vehicle instability. Many algorithms have been proposed in literature assuming the availability of these variables, however in practise these are hardly measured due to sensor costs.

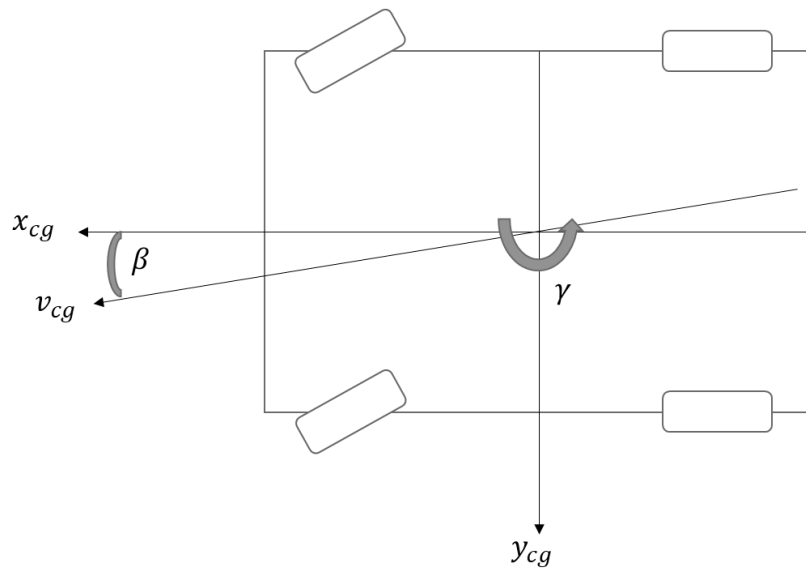


Figure 11 Yaw Rate and Side-Slip Angle Schematic

Figure 11 depicts that a vehicle's yaw rate is the rate of rotation about the z-axis, which is directly related to the lateral acceleration of the vehicle during a cornering manoeuvre.

Gillespie (1992) states the yaw rate of a vehicle in cornering as:

$$\gamma = \frac{180V}{\pi} \frac{R}{L} \quad (1.32)$$

Substituting (1.32) into (1.15) and solving for the ratio of yaw rate to steer angle gain gives the relation:

$$\frac{\gamma}{\delta} = \frac{V/L}{1 + \frac{KV^2}{\frac{180}{\pi} Lg}} \quad (1.33)$$

Figure 12 shows this ratio is directly proportional to velocity in the case of a neutral steer vehicle, however for the oversteer case, the yaw rate gain increases to infinity as the vehicle reaches its critical speed. The vehicle experiencing understeer will experience a yaw rate gain until a characteristic speed, thereafter the yaw rate gain begins to decrease. The vehicle is thus most responsive in yaw at the characteristic speed for an understeering vehicle.

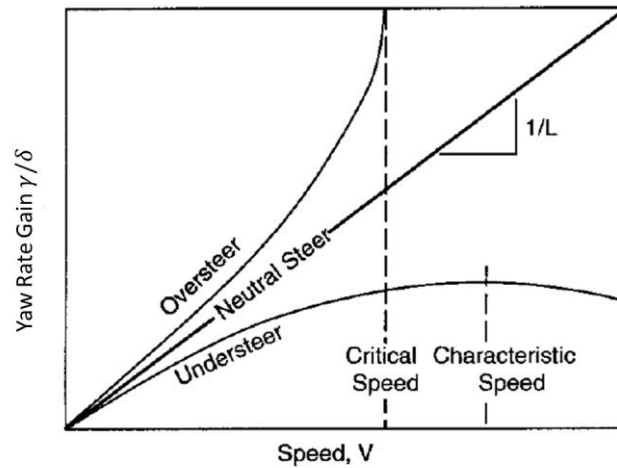


Figure 12 Yaw Rate gain as a function of vehicle speed (Gillespie, 1992)

Side-slip angle is the difference between the direction a vehicle is travelling and the direction that the body of the vehicle is pointing towards. As lateral acceleration becomes present, the rear of the vehicle must drift outwards to develop the necessary slip angles on the rear tyres as in Figure 5. The vehicle side-slip angle can be calculated as:

$$\beta = 57.3 \frac{l_r}{R} - \alpha_r \tag{1.34}$$

$$\beta = 57.3 \frac{l_r}{R} - \frac{W_r V^2}{C_{\alpha_r} g R} \tag{1.35}$$

In Figure 13 it can be seen that the vehicle is in an oversteer position, the vehicle is cornering through a curve in the general direction of the front wheels, however the body of the vehicle is pointing towards the inner radius of the curve, the angle between both is the side-slip angle. When a vehicle’s lateral acceleration is negligible, there exists a small side-slip angle within the linear region, and a steering input will allow for a good yaw rate change, thus good handling performance. In emergency manoeuvres, when the lateral acceleration and side-slip angle are large, a steering input will struggle to give a noticeable yaw rate effect. In this case, torque vectoring direct yaw moment control systems can significantly enhance the handling performance as mentioned in section 1.3.6.

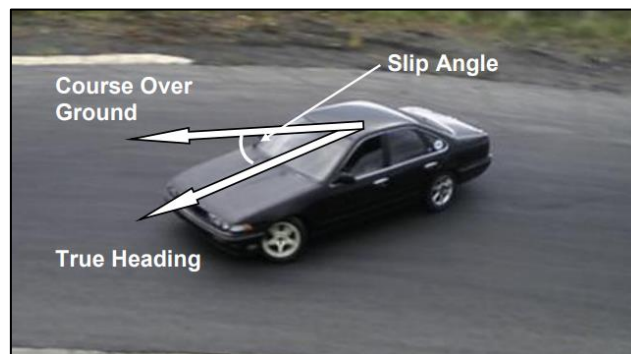


Figure 13 Visual Demonstration of Side-Slip Angle (Racelogic, 2015)

On dry roads, vehicle control is lost at side-slip angles greater than ten degrees, however on snow, vehicle control can be lost at side-slip angles as low as 4 degrees (Van Zanten et al., 1995). Vehicle stability control should take both variables into account for this reason. Van Zanten et al. (1995) mentions that it is necessary to control the side-slip angle together with the yaw motion of a vehicle in order to maintain the stability of the vehicle due to the instability of vehicle motion at the vehicle limits. The instability is brought about by decreased control of the yaw moment at large side-slip angles.

Abe et al. (2001) used experimental validation of side-slip estimation to investigate the effects of side-slip control by using DYC on stabilizing vehicle motion. It was proved that side-slip control by DYC stabilizes a vehicle's motion better than 4WS because the vehicle loses its stability due to the deterioration of rear tyre characteristics. It was also noted that side-slip control is superior to yaw rate control in compensating for loss of stability due to nonlinear tyre characteristics (Abe et al., 2001). This was however proven for a passenger vehicle and not for an SUV type vehicle.

Many conventional systems for vehicle dynamics control operate on the basis of many simplifying assumptions, such as constant longitudinal velocity, small steering angle and a small side-slip angle. However, in this dissertation assumptions are avoided and actual vehicle measurements are taken into account. It should be noted that, by improving vehicle handling, a vehicle can be susceptible to a higher rollover propensity. For this reason, roll prediction methods are investigated.

1.3.2 Types of Roll Prediction

There are various roll prediction methods available, however very few are generally effective measures. Three methods are discussed here, showcasing the benefits and pitfalls, a Roll Index method is selected based on the benefits of such a system.

1.3.2.1 Static Stability Factor (SSF)

The Static Stability Factor is the vehicle's track width divided by twice the height of the centre of mass above the ground (Walz, 2005).

$$SSF = \frac{T}{2h_{cg}} \quad (1.36)$$

This method uses simple experimental measurements. Tests such as the side-pull test, whereby a vehicle is connected to a cable at its centre of gravity and pulled until the vehicle rolls, thereafter wheel force measurements are used to determine when rollover occurs. Other experimental tests include the tilt-table tests and the centrifugal tests. Despite the static stability factor relating well to rollover rates according to the National Crash Databases, there are cases whereby the static stability factor was mimicked to appear better using simple suspension variations (Walz, 2005).

1.3.2.2 Load Transfer Ratio (LTR)

The sum of vertical force on the right side and left side of the vehicle are used to determine the load transfer occurrence. A value of 1 or negative 1 for LTR indicates when all the load is on one side of the vehicle and will represent the vehicle rolling over. This is calculated by:

$$LTR = \frac{F_{Zr} - F_{Zl}}{F_{Zl} + F_{Zr}} \quad (1.37)$$

Other empirical methods include the time to rollover metric, lateral acceleration threshold, threshold roll angle. The downside of these methods is the requirement to calculate measurements which are hard to measure (Tsourapas et al., 2009).

1.3.2.3 Zero Moment Point Roll-Over Index (ZMP)

Lapamong et al. (2012) proposes this method and states it is different to the LTR method. The ZMP does not require the tyre forces to be measured nor estimated but uses the contact polygon of the vehicle to predict wheel lift and can be used on both flat and banked surfaces. The ZMP algorithm has been used to predict skid-before-roll conditions of a vehicle, based on varying vehicle speeds, parameters and environmental conditions.

The zero-moment point is defined as the point on the ground where the summation of all the tipping moments act on an object, from external and internal forces, equal to zero. The object will remain in dynamic equilibrium if the net force vector of the object to the ground acts within the contact polygon of the object to the ground. The force contact point is simply the location where the net moment on the object from the ground is zero, thus it is named zero moment point. Unlike previous methods, contact reaction forces are not necessary, the Lagrange-d' Almer principle is used to estimate the kinematic motion of all objects in a kinematic chain of bodies. This means it is possible to calculate the net moment contribution of each body to the ZMP. If the vehicle's zero moment point extends outside the vehicle's polygon, the vehicle will roll over.

In terms of rollover propensity, the ZMP to the edge of the vehicle's support polygon is a dynamic metric. If the lateral position of the ZMP is outside of the vehicle's track width, then the vehicle will experience wheel lift and is considered unsteady. The distance between the vehicle's ZMP and centreline, called y_{ZMP} is a direct relation to wheel lift.

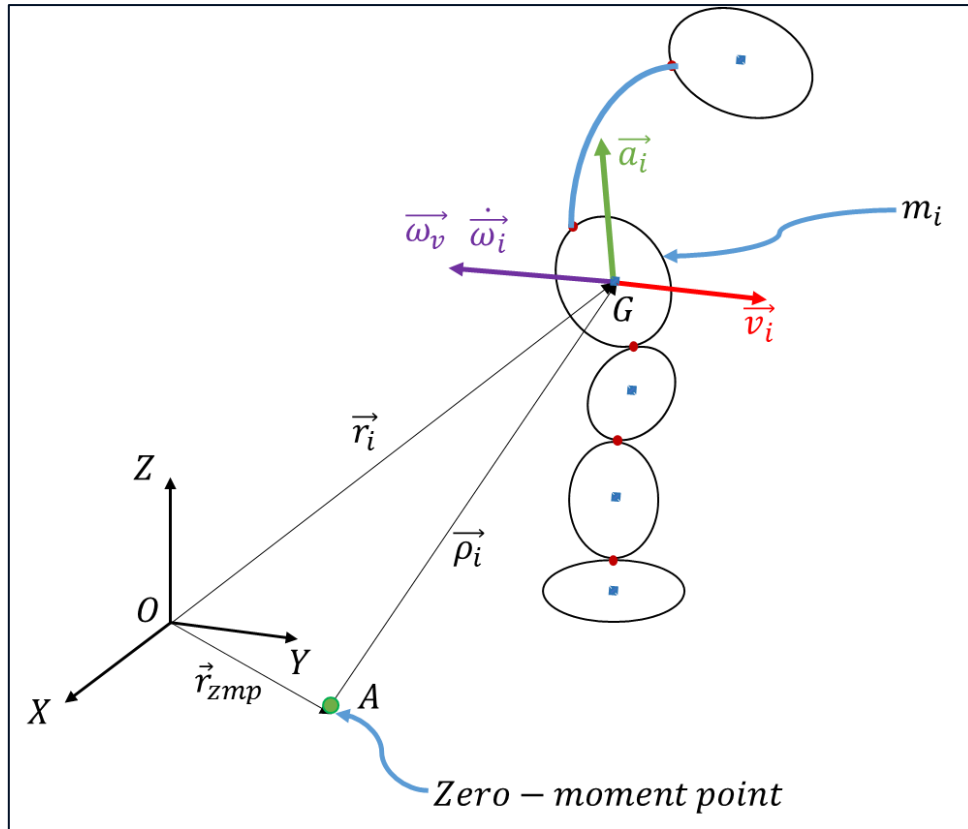


Figure 14 ZMP on a kinematic chain of bodies

As depicted in Figure 14, the centre of mass of the i th body relative to an inertial frame (OXYZ) is located by r_i , assuming that the i th body of the kinematic chain has a mass m_i , an inertia tensor I_i about its centre of mass, and moves with a linear velocity of v_i , linear acceleration a_i , rotates at an angular velocity ω_i and angular acceleration of $\dot{\omega}_i$. D'Alembert's principle states that the moment equation about point A is

$$M_A = \sum_i (\vec{p}_i \times m_i \vec{a}_i) + \sum_i (I_i \vec{\omega}_i + \vec{\omega}_i \times I_i \vec{\omega}_i) - \sum_i (\vec{p}_i \times m_i \vec{g}) \quad (1.38)$$

Vector $p_i = r_i - r_{ZMP}$, with r_{ZMP} being the position vector of the ZMP. If the \vec{i} and \vec{j} components of the moment equate to zero, then point A becomes the ZMP. When applying the ZMP to a vehicle however, the sprung and un-sprung mass are considered using equation 1.39.

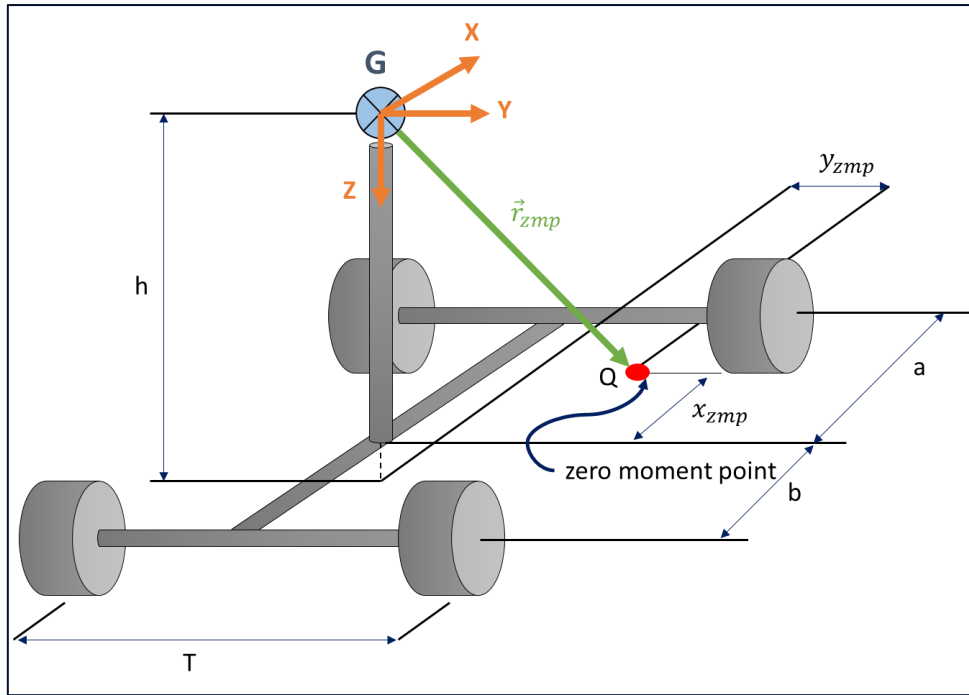


Figure 15 ZMP on a Rigid Vehicle Model

The lateral location of a vehicle's Zero Moment Point can be expressed as:

$$\begin{aligned}
 y_{ZMP} = & \{mg\cos(\theta) \sin(\phi_r)[T|\tan(\phi_r - \phi_t)| + 2h] \\
 & - ma_{Gy}[T|\tan(\phi_r - \phi_t)| + 2h] - 2I_{xx}\dot{\omega}_x + 2I_{xz}\dot{\omega}_z \\
 & + 2I_{yz}(q^2 - \gamma^2) \\
 & + 2(I_{xz} + I_{yy} - I_{zz})q\gamma\}/\{2m[g\cos(\theta) \cos(\phi_t) \sec(\phi_r - \phi_t) \\
 & - a_{Gy} \tan(\phi_r - \phi_t) - a_{Gz}]\}.
 \end{aligned} \tag{1.39}$$

This method is computed as the vehicle's rollover index due to its real time implementation readiness in simulation and experimental work. Yoon et al. (2007) proposes a roll-over index as a controller input to a Vehicle Stability Control (VSC) scheme. The VSC scheme sets a desired roll-over index, from which a desired yaw rate can be determined in relation to a desired lateral acceleration. A similar scheme is used however as a soft constraint in Section 3.3.

Conclusion from Literature Study

This literature study discussed a vehicle navigating a turn with the focus on the vehicle dynamics along with tyre characteristics. It is noted that a tyre should be used within its linear region for good lateral force generation and to provide stability. The relatively new torque vectoring control method has been identified as the most beneficial to allow for predictable consistent handling while reducing rollover propensity. The yaw rate and side-slip angle are important measures that can be controlled from exceeding tyre-road thresholds. Roll detection models are discussed and their implementation on a stability system appears promising.

Chapter 2 Experimental Setup and Validation of Vehicle Simulation Model

This chapter describes the vehicle platform used for this study. A detailed description and validation simulation model is provided, as well as the experimental setup used.

2.1 Vehicle

The vehicle platform used for this study is a Land Rover Defender 110 as seen in Figure 16.

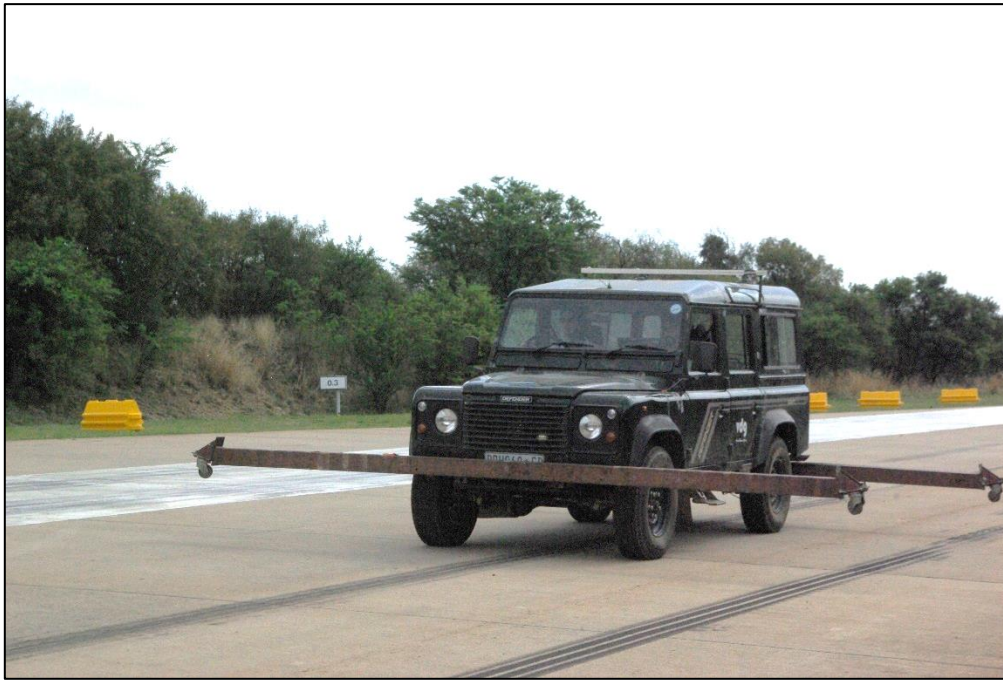


Figure 16 Land Rover Defender test vehicle

2.1.1 Simulation Model

Parameters of the vehicle model have been experimentally determined by Uys (2006). The vehicle has also been the subject of numerous research projects at the University of Pretoria.

The full vehicle model is developed in Automatic Dynamic Analysis of Mechanical Systems (ADAMS) software. The tyres vertical dynamics and load dependent lateral dynamics are considered in this model, thus it is possible to verify the load transfer during a cornering manoeuvre as mentioned in Section 1.2.2.3. The vehicle body has been modelled as two rigid bodies connected along the roll axis at chassis height by a revolute joint and a torsional spring. This was done in order to better capture the vehicle dynamics due to body torsion in roll. Bump and rebound stops are modelled with non-linear splines as force elements between the axles and the vehicle body. Suspension bushings are modelled as kinematic joints with torsional spring characteristics that are representative of the actual vehicle's suspension joint characteristics.

Figure 17 presents a graphical view of the simulation model, it consists of 15 unconstrained degrees of freedom, 16 moving parts, 6 spherical joints, 8 revolute joints, 7 Hooke's joints, and one motion defined by the steering driver. The vertical tyre force is measured on all tyres at all times. If a tyre loses contact with the ground, the driving force applied to the vehicle will be diminished until tyre contact is made again. The MSC ADAMS model is used in co-simulation with Simulink. Inputs to the ADAMS model from Simulink are the steering angle, velocity and drive torques. This allows control over the MSC ADAMS model.

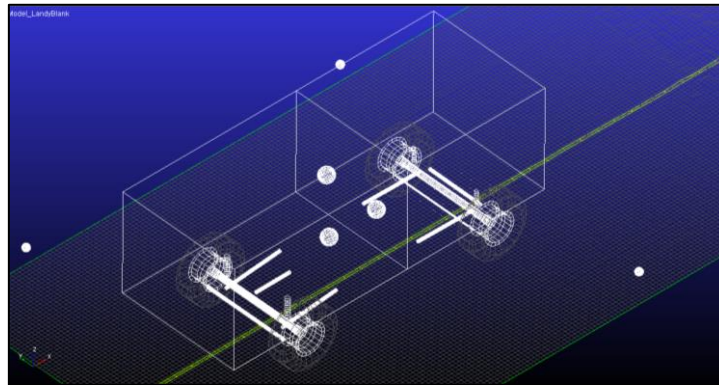


Figure 17 Graphical view of vehicle Modelled in ADAMS

2.1.2 Vehicle Tyre

The tyre-road interaction is complex as mentioned in Section 1.2.2.1 with various non-linear relationships. The tyre used in this study, namely a Michelin LTX² All Terrain Tyre has been parameterized and validated at the Vehicles Dynamic Group by Bosch et al. (2016). Using FTire, the non-linear lateral force is plotted against the tyre's side-slip angle, it can be seen that there in-fact exists a linear region where the lateral force has a directly proportional relationship to the side-slip angle in Figure 18.

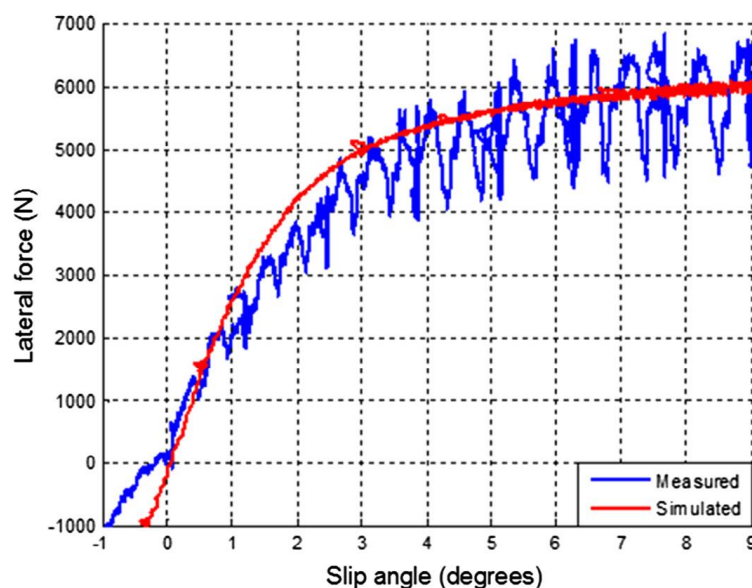


Figure 18 Experimental and FTire Simulated Tyre Model of Michelin LTX2 tyres (Bosch et al., 2016)

The simulation model makes use of the FTire (Flexible Structure Tyre Model) model which is a structural dynamic approach at a tyre model, and is represented by a full 3D non-linear in-plane and out-of-plane tyre model. It is superior in terms of realizing tyre forces on roads with short wave-length obstacles, thus it is better for off-road tyre dynamics. It was initially developed for vehicle comfort in mind, however performs just as well as other tyre models in handling scenarios. A flexible ring is used to describe the tyre belt, that can flex and extend in the radial, tangential and lateral directions whilst the cornering force is determined from the interaction of both the road and the belt (Stallmann and Els, 2014). This tyre model is used for validation purposes and to see a correlation between simulation and experimental work. FTire has high computational requirements and thus cannot be used in real time for control purposes.

2.1.3 Vehicle Suspension

Four State-Semi-Active Suspension System 4S₄

The Test Vehicle is fitted with a semi active suspension system developed and implemented by Els et al. (2006). The system is a 4 state semi active hydro-pneumatic suspension system as mentioned in Section 1.1.3. The suspension system has spring and damper characteristics that can be varied allowing the vehicle to switch between ride comfort and handling, its setup is shown in Figure 19.

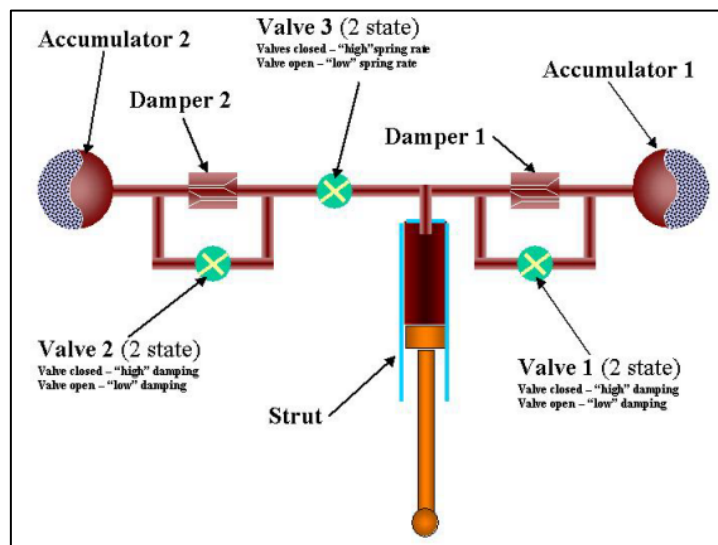


Figure 19 4S₄ Suspension Setup

High performance vehicles are known to be uncomfortable yet possess impressive handling dynamics. This dilemma is solved using the 4S₄ suspension system which can adjust to the driver’s requirements and be automatically controlled. Models of the suspension have been created which can be used to predict vertical forces using suspension deflections and velocities.

Lateral displacement of a vehicle’s centre of gravity due to an induced roll angle is a major contributor to lateral load transfer as mentioned in Section 1.2.2.3, thus a stiff suspension setup will be used for testing to prevent rollover during any manoeuvres.

2.2 Vehicle Instrumentation

The vehicle is connected to numerous sensors as seen in Figure 20. Devices used for measurement and Torque Vectoring Control implementation are mentioned here.

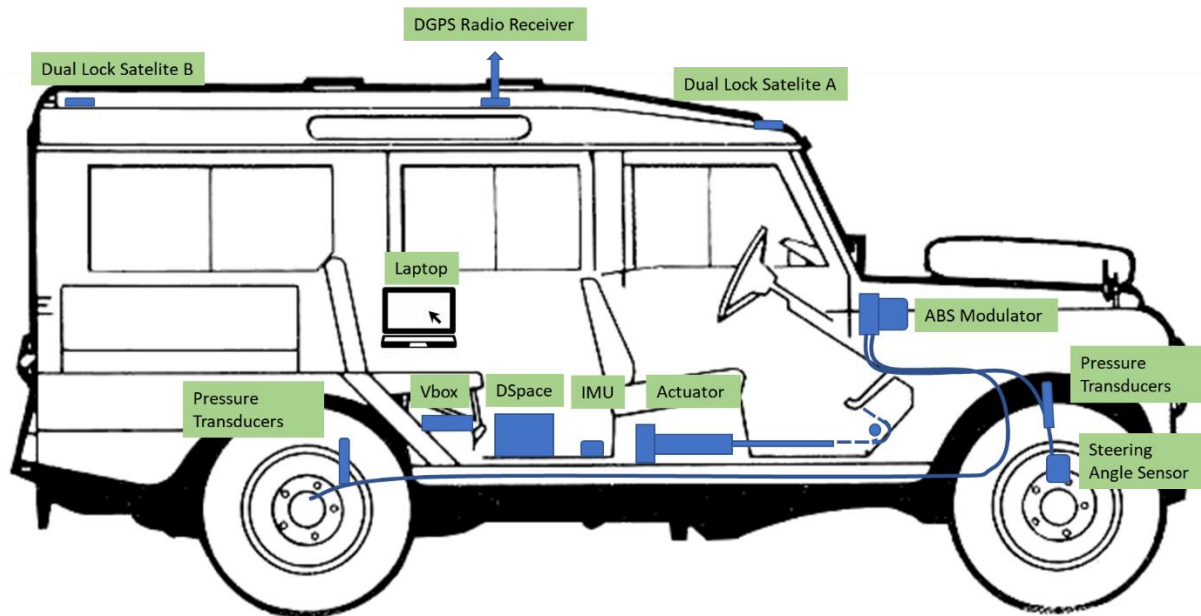


Figure 20 Test vehicle with measurement devices

The vehicle parameters used for Torque Vectoring control and validation purposes are summarised in Table 1.

Table 1 Vehicle Input Output Devices

| Parameter | Sensor | Purpose |
|--|-----------------------------|------------------------|
| Vehicle Position | VBox 3i | Validation |
| Vehicle Speed | | Validation and Control |
| Longitudinal, Lateral, Vertical Acceleration | | Validation and Control |
| Pitch Angle, Rate | | Validation and Control |
| Roll Angle, Rate | | Validation and Control |
| Yaw Angle, Rate | | Validation and Control |
| Side-Slip Angle | | Validation and Control |
| Steering Angle | | Celesco Potentiometer |
| Brake Pressure | Wenkei Pressure Transducers | Validation and Control |
| Brake Force | Dunkermotoren Actuator | Control |
| Pressure Control | WABCO ABS Modulator | Control |

2.2.1 DSpace MicroAutoBox

The MicroAutoBox (MABX) is a real-time system for performing fast function prototyping. It can operate without user intervention, just like an electronic control unit (dSpace, 2017). For this reason, it is used in industry for many different rapid control prototyping applications. The VBox3i data is sampled through a CAN interface whereas other sensor measured data such as steering angle and pressure transducers are measured using analogue channels.

The advantage of using the MABX is that the same Simulink programs can be used in simulation and experimental tests by simply replacing the ADAMS simulation block with the sensor inputs and outputs.

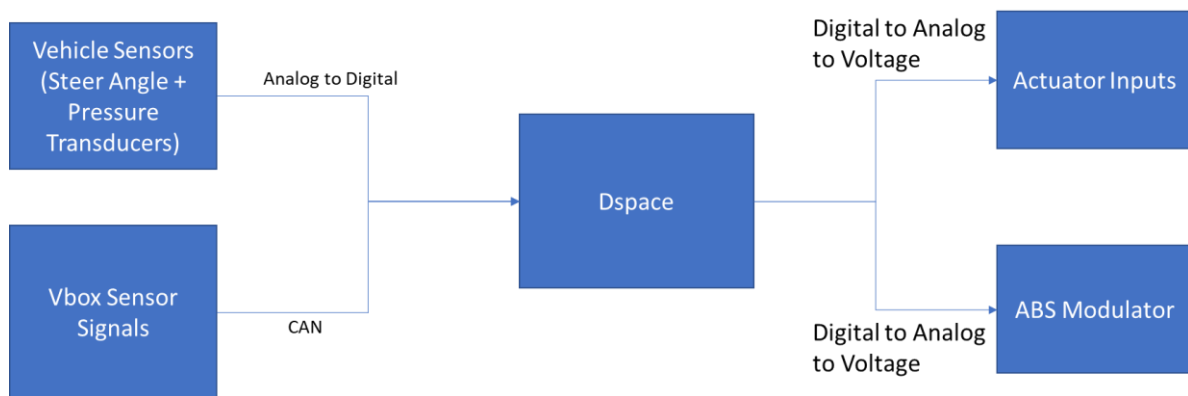


Figure 21 Block diagram of data acquisition and control

2.2.2 VBox 3i

The VBox3i is a high accuracy high sampling frequency GPS system using both GPS and GLONASS. The VBox3i can be integrated with an IMU providing 40cm, 95% CEP positional accuracy and providing additional measurements such as vehicle acceleration. The VBox3i can also be used in combination with a DGPS base station to provide better positional accuracy down to 2cm and additional measurements such as roll, pitch and yaw. It is used in combination with the DGPS base station for this study for optimum accuracy (Racelogic, 2017). The sample rate of data transfer is however limited to 100Hz whereas the analogue sensors can reach 1000Hz. This effects the control aspect as any predictive controllers need to take this delay into consideration.

2.3 Manoeuvres

In order to evaluate whether the system provides improvements, standard test manoeuvres are used.

2.3.1 ISO3888-1 Severe Double Lane Change

The ISO3888-1 Severe Double Lane Change can determine vehicle manoeuvrability, especially due to its sudden change of direction, this will show vehicle loading behaviour as the load transfers from one side of the vehicle to another. The vehicle returns to steady state in the middle of the manoeuvre and consists of multiple changes in direction. It is therefore an ideal test to evaluate the path following capability at the limit of rollover. The specifications of the double lane-change track are shown in Figure 22 and given in Table 2, where the widths are a function of the vehicle width and the lengths are fixed and total 125 meters (Standard, 1999).

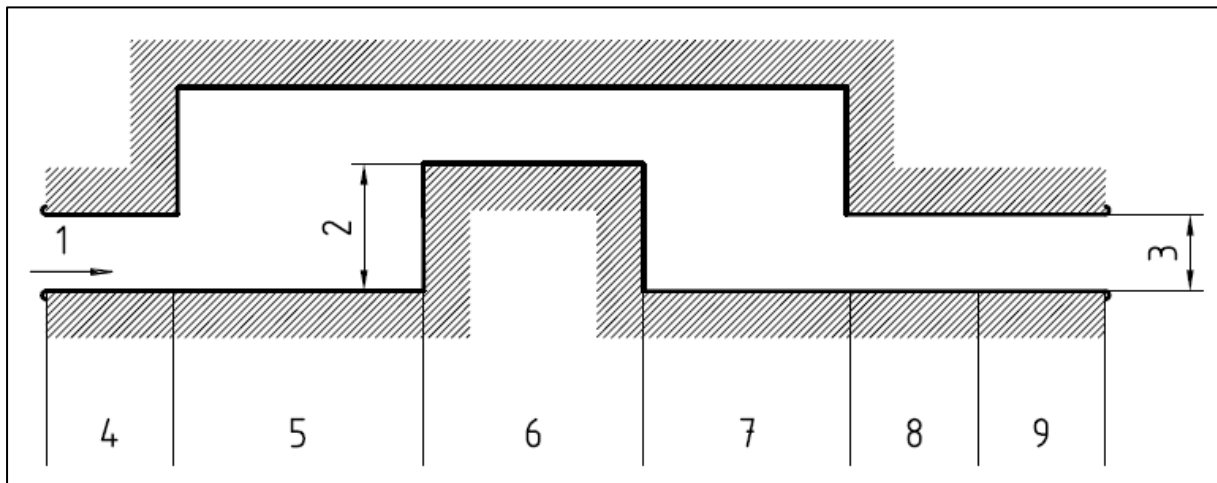


Figure 22 ISO3888-1 Severe Double Lane Change Path (Standard, 1999)

In Figure 22, 1 is the driving direction, 2 is the lane offset, and 3 is the width, the dimensions are tabulated below in meters.

Table 2 ISO3888-1 Section Descriptions

| Section | Length | Lane offset | Width |
|---------|--------|-------------|----------------------------|
| 4 | 15 | - | 1.1 x vehicle width + 0.25 |
| 5 | 30 | - | - |
| 6 | 25 | 3.5 | 1.2 x vehicle width + 0.25 |
| 7 | 25 | - | - |
| 8 | 15 | - | 1.3 x vehicle width + 0.25 |
| 9 | 15 | - | 1.3 x vehicle width + 0.25 |

The test will be computed at increasing speeds to determine when the vehicle requires an active system to intervene and regain vehicle control.

2.3.2 ISO 3888-2 Severe Lane Change/Moose/Obstacle Avoidance Test

The Obstacle avoidance test is designed to provide a criterion to prove the tilt stability of a vehicle. The vehicle enters the manoeuvre at an entrance speed, thereafter the accelerator pedal is released, and the vehicle travels through the manoeuvre in power-off mode. The test is used to avoid sudden overreactions of the vehicle (swerving) (Standard, 2011). In this study, the test is slightly modified and the vehicle will navigate the path at wide open throttle in comparison to power-off mode.

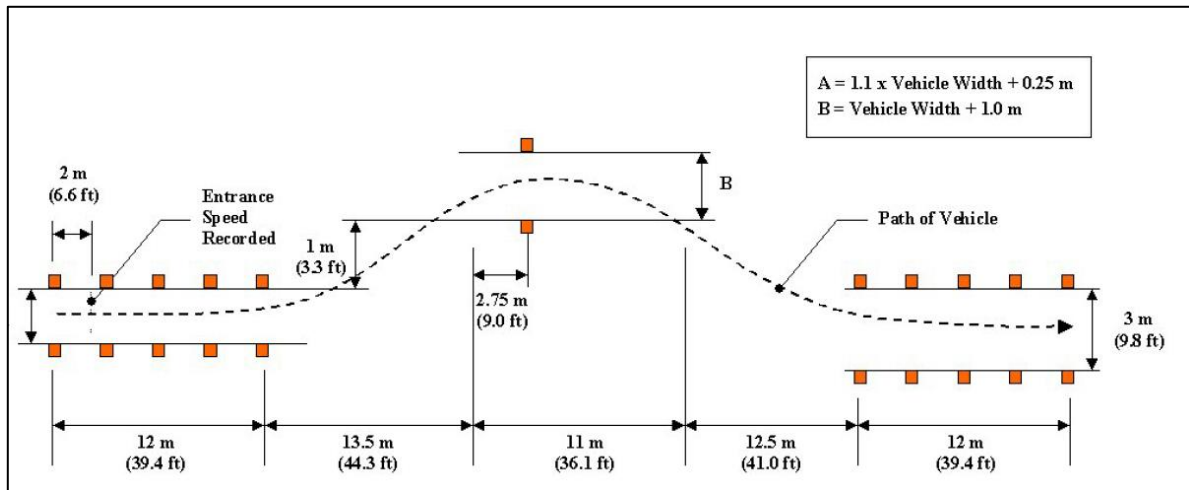


Figure 23 Modified ISO 3888-2 Modified Obstacle Avoidance Path (Standard, 2011)

The test is shorter in comparison to the Double Lane Change ISO 3888-1, the vehicle stays in continuous transition, and the vehicle does not return to a steady state cornering state in the middle of the transition. The benefit of this test is that lower vehicle speeds are required to unsettle the vehicle.

2.3.3 Constant Radius Test

The constant radius test evaluates the steady state cornering of the vehicle often found in normal driving conditions. The constant radius test can be used to determine the stability factor of the vehicle, which will determine whether the vehicle undergoes neutral steer, understeer or oversteer. The measurement of the vehicle's lateral acceleration, steering angle and side-slip angle together with the vehicle's yaw rate will help develop a good understanding of vehicle behaviour. An active system such as torque vectoring should allow the vehicle to follow the constant radius without reducing or increasing the steering angle significantly by forcing the vehicle to possess neutral or slight understeer.

2.4 Validation of Vehicle Simulation Model

2.4.1 Full Vehicle Model Validation

This study is primarily concerned with vehicle lateral dynamics, therefore the model will only be validated for lateral motions including body roll. Experimental results are compared to simulation results during a Double Lane Change (DLC) manoeuvre in accordance to ISO 3888-1 for validation.

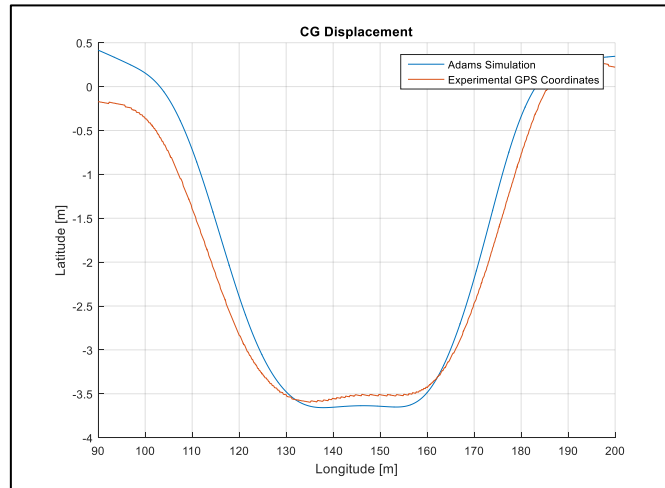


Figure 24 DLC Trajectory

2.4.1.1 Procedure

The DLC is performed at various entry speeds experimentally, the vehicle is driven at wide open throttle against the governor to ensure minimum loss of speed through the manoeuvre. The measured steering angle and vehicle speed are used as inputs into the ADAMS model. The simulation results are compared to the experimentally measured parameters to determine the validity.

2.4.1.2 Validation at 52km/h through DLC

Validation inputs in Figure 25 indicate an entry speed of 52km/h. The vehicle speed is filtered to remove high frequency noise and thereafter inputted into the simulation model.

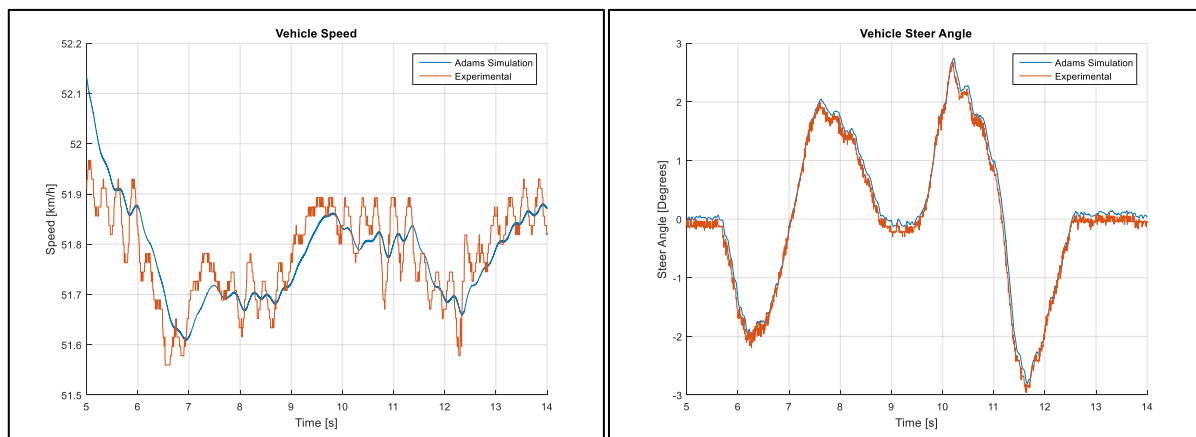


Figure 25 Speed and Steering Angle Inputs to Simulation Model through DLC at 52km/h.

Correlation between experimental and simulated measurements for displacements, velocities and accelerations are shown in Figure 26. Overall a good correlation is observed.

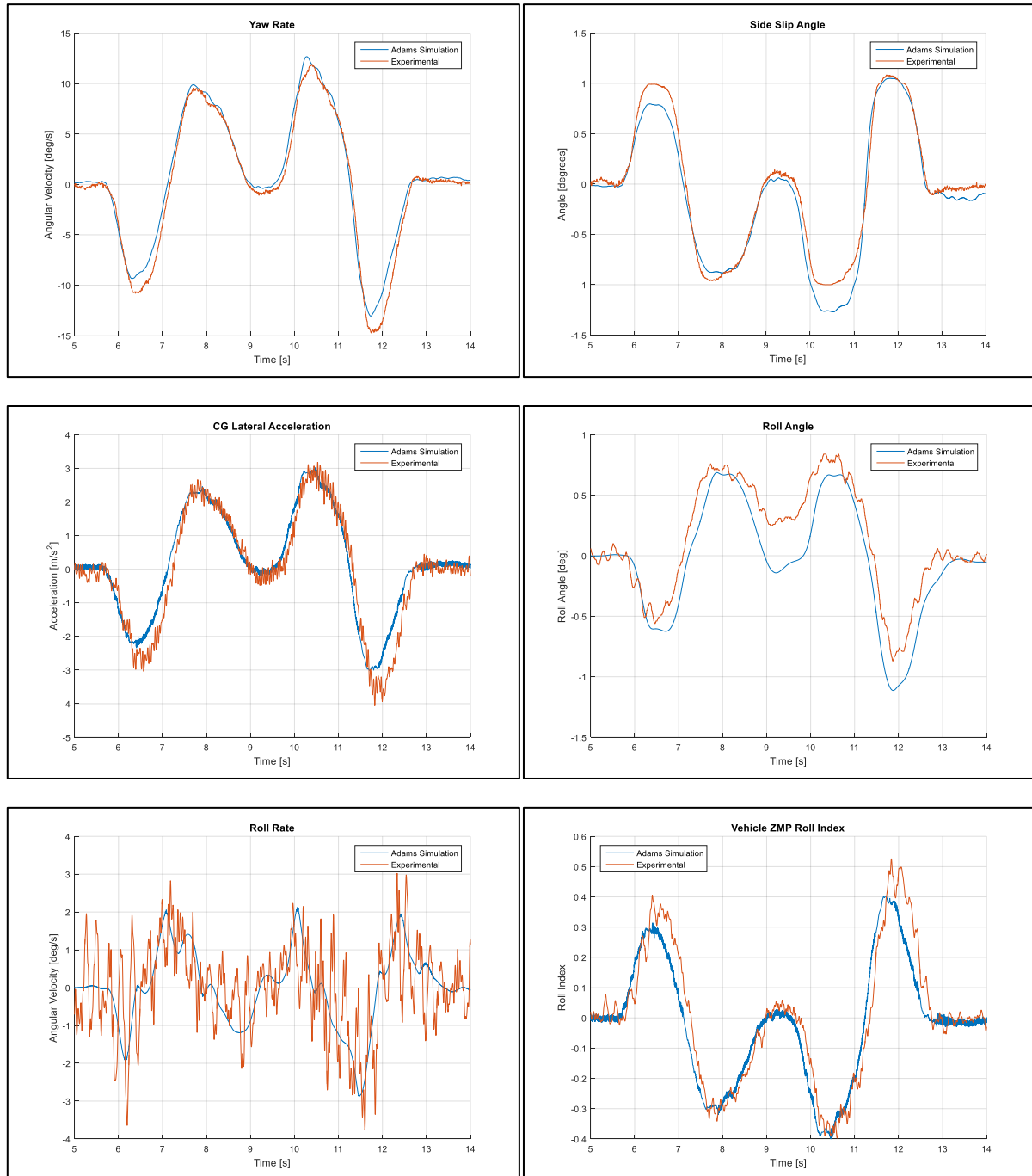


Figure 26 Correlation of measured parameters through DLC at 52km/h.

2.4.1.3 Validation at 65km/h through DLC

Figure 27 shows the vehicle speed and steering input, which was obtained from measurements at 65km/h and inputted to the simulation model. Figure 28 shows the measured vehicle parameters correlation to the simulation model.

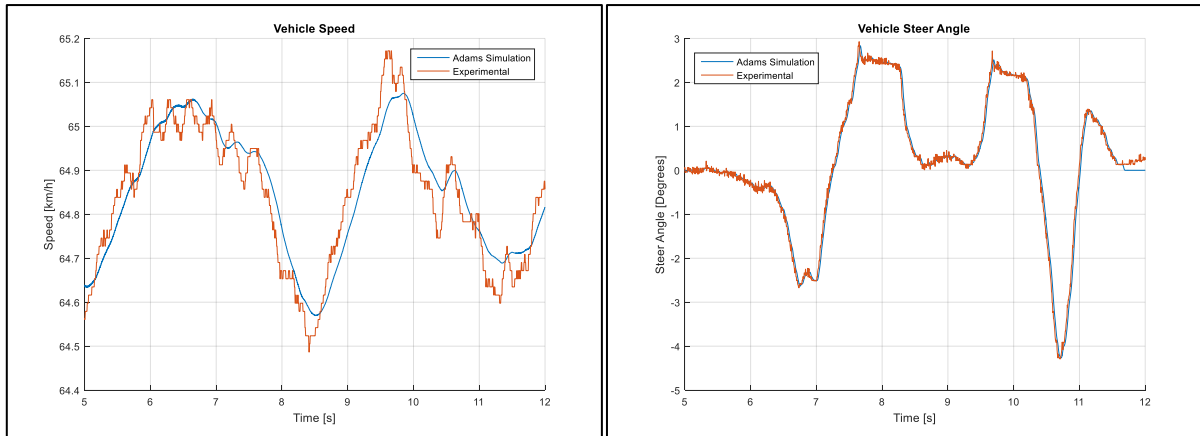


Figure 27 Speed and Steering Angle Inputs to Simulation Model through DLC at 65km/h.

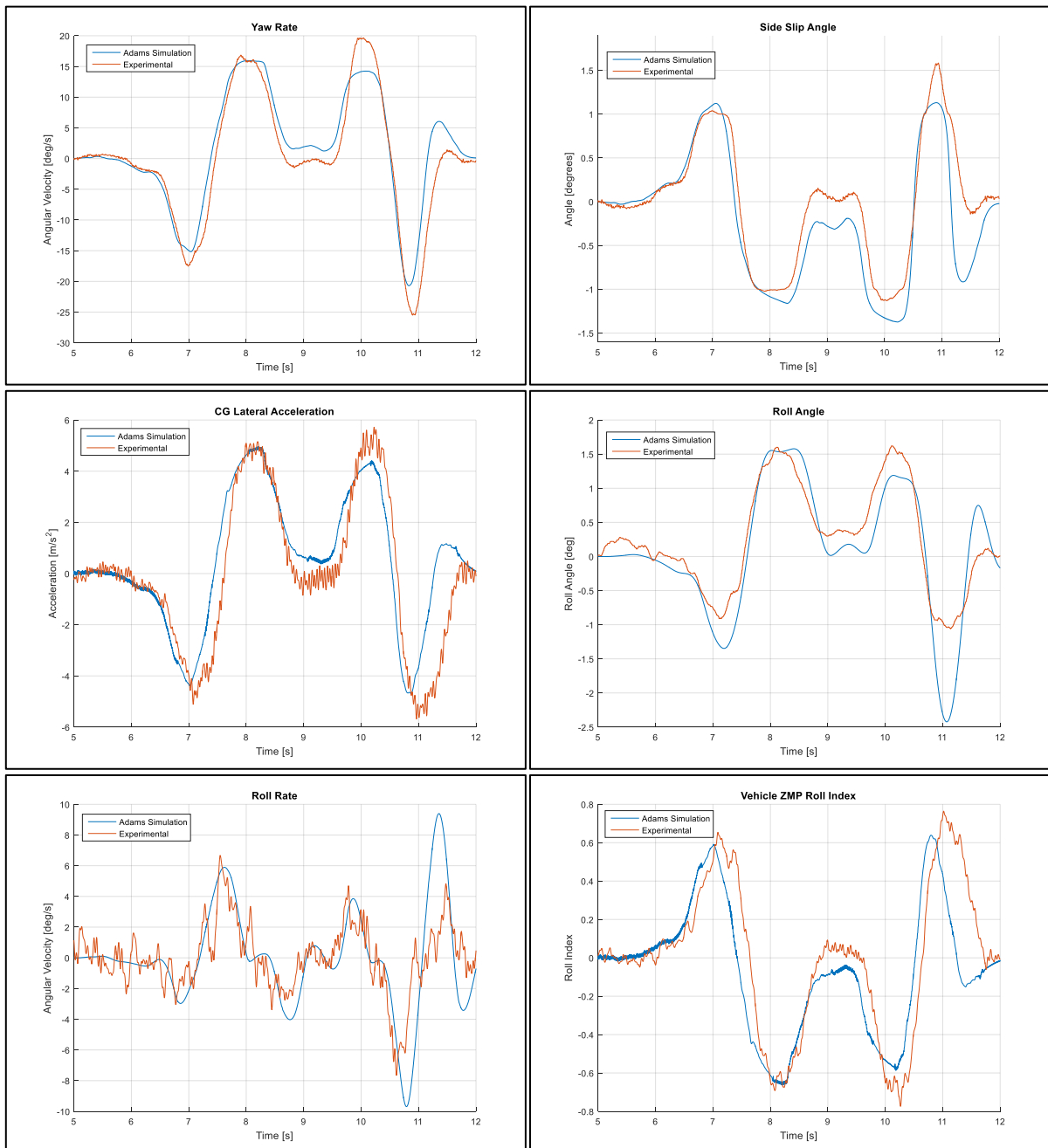


Figure 28 Correlation of measured parameters through DLC at 65km/h.

Good correlation is found, however it is noticed that the body of the simulated vehicle rolls more easily than the body of the test vehicle. This is due to friction at the joints, connection points and seals that are not modelled in the simulation model, because the characteristics of these joints and connections points are unknown. It can be seen that there exists large amounts of high frequency noise on the experimental measurements obtained from VBox3i. The VBox3i was setup for side-slip angle measurement, thus the roll angle measurement will be clearer if setup for roll angle measurement as seen in (Botha, 2011).

2.4.2 Brake Torque vs Brake Pressure Relation

A relation is required for experimental brake pressure to brake torque, this is because in simulation the vehicle receives a brake torque whereas in reality, the brake torque is applied via a brake pressure input. The test vehicle is fitted with Disc Brakes on all four wheels, a typical manner in which to determine the relationship between Brake Pressure and Brake Torque is described by Budynas and Nisbett (2008) as:

$$T_b = \int_{\theta_1}^{\theta_2} \int_{r_i}^{r_o} \mu_{bp} p r^2 dr d\theta \quad (2.1)$$

Where the parameters θ and r represent the radial angle and radius respectively. The maximum allowable pressure on the inner radius is represented as p and μ_{bp} is the coefficient of friction between the brake pads and disk brakes. Table 3 indicates known brake disc parameters.

Table 3 Brake Parameters

| | Inner Diameter | Outer Diameter | Radial Angle |
|---------------------|----------------|----------------|--------------|
| Front Brakes | 0.1m | 0.149m | 65° |
| Rear Brakes | 0.1m | 0.149m | 35° |

In order to determine the relationship between brake pressure and brake torque, a Wheel Force Transducer (WFT) was instrumented on the vehicle and brake tests were performed. Figure 29 shows a linear fit applied to the Brake Torques Vs Brake Pressure.

A linear fit was found of the form:

$$T_b = 26.2p \quad (2.2)$$

Assuming uniform wear or uniform pressure and solving for the coefficient of friction between the brake pads and brake discs, a value of 0.378 was achieved. This falls within the average range of 0.35 to 0.42 for standard brake pads (Orłowicz et al., 2016) and serves as validation of the result achieved.

Figure 29 shows the brake torque linear fit plotted against actual brake torque values achieved.

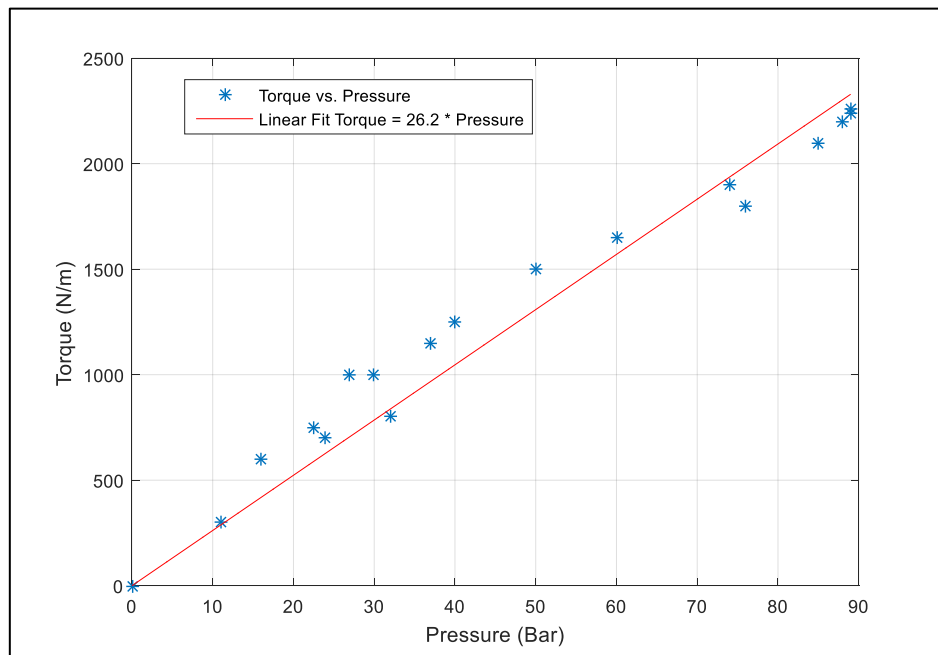


Figure 29 Brake Torque vs Brake Pressure Linear Fit

Conclusion of experimental setup and validation of vehicle simulation model

In this chapter the test vehicle is setup and the simulation model is validated against experimental data. Despite small discrepancies in the simulation model, it can overall be trusted to mimic the dynamics of the test vehicle. Manoeuvres are also mentioned which can determine the benefits of a potential torque vectoring active control system. The main input of torque vectoring is validated by means of a WFT to determine the relationship between brake torque and brake pressure.

Chapter 3 Control Strategy

This chapter will discuss two methods commonly used in yaw rate and side-slip angle control, namely a Linear Quadratic Regulator (LQR) developed by Mirzaei (2009) as a reference controller and a Model Predictive Controller (MPC) developed here. Park et al. (2001) and Zheng et al. (2006) proposed that a LQR approach could be used in order to improve vehicle stability as well as handling. This led to a predictive optimal yaw stability controller based on a linearized vehicle model being developed by Anwar (2005). The drawback was that these solutions worked well in a simulation environment, however were not suitable for experimental testing due to excessive computational processing requirements such that online numerical computation was needed. It was noted that an analytical solution was presented for a similar optimization problem by Esmailzadeh et al. (2003). This allowed for experimental validation of an optimization-based controller because it was solvable in real time.

Yaw rate and side-slip angle control is investigated here with the aim of experimental implementation on the test vehicle by using an analytical solution to an optimization problem.

3.1 Vehicle Reference Model

As previously discussed, vehicle handling is not consistent and due to the effect of load transfer gets even worse. In order to have a more consistent and better handling vehicle, a simple vehicle model is used for the model design, in this case a conventional linear 2DOF bicycle model is selected shown in Figure 30. The controller will track the responses of this bicycle model in order to maintain consistent handling.

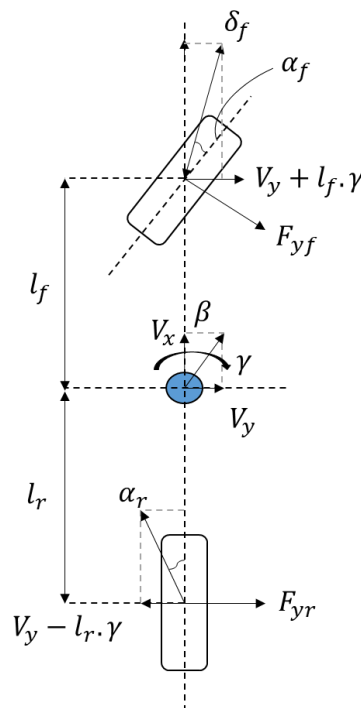


Figure 30 TWO-DOF Bicycle Model

Using abbreviated notation, in state space form, governing equations relating the side-slip angle and yaw rate as a function of steering angle for a linear vehicle model are defined by (Wong, 2008) as:

$$\begin{bmatrix} \dot{\beta} \\ \dot{\gamma} \end{bmatrix} = \begin{bmatrix} a_{11} & a_{12} \\ a_{21} & a_{22} \end{bmatrix} \begin{bmatrix} \beta \\ \gamma \end{bmatrix} + \begin{bmatrix} e_1 \\ e_2 \end{bmatrix} \delta \quad (3.1)$$

where

$$a_{11} = -2 \frac{C_{\alpha f} + C_{\alpha r}}{mv}, a_{12} = 2 \frac{L_r C_{\alpha r} - L_f C_{\alpha f}}{mv^2} - 1, a_{21} = 2 \frac{L_r C_{\alpha r} - L_f C_{\alpha f}}{I_z}, a_{22} = -2 \frac{L_r^2 C_{\alpha r} + L_f^2 C_{\alpha f}}{I_z v}$$

$$e_1 = \frac{2C_{\alpha f}}{mv}, e_2 = \frac{2L_f C_{\alpha f}}{I_z}$$

The transfer function from steering input to the side-slip angle and yaw rate is derived from the state equations as:

$$\frac{\beta(s)}{\delta(s)} = G_B \frac{1 + T_B s}{1 - \left(\frac{T_A}{D_A}\right) s + \left(\frac{1}{D_A}\right) s^2} \quad (3.2)$$

$$\frac{\gamma(s)}{\delta(s)} = G_R \frac{1 + T_R s}{1 - \left(\frac{T_A}{D_A}\right) s + \left(\frac{1}{D_A}\right) s^2} \quad (3.3)$$

where

$$G_B = \frac{e_2 a_{12} - e_1 a_{22}}{D_A}, T_B = \frac{e_1}{e_2 a_{12} - e_1 a_{22}}, G_R = \frac{e_1 a_{21} - e_2 a_{11}}{D_A}, T_R = \frac{e_2}{e_1 a_{21} - e_2 a_{11}}$$

$$T_A = a_{11} + a_{22}, D_A = a_{11} a_{22} - a_{12} a_{21}$$

The linear vehicle model is considered stable if the value of D_A is positive as T_A is always negative. This means that

$$l + K v^2 \geq 0 \quad (3.4)$$

Where K is the stability factor as mentioned in section 1.2.2.2 given as:

$$K = \frac{m}{2l} \left(\frac{L_r}{C_{\alpha f}} - \frac{L_f}{C_{\alpha r}} \right) \quad (3.5)$$

A positive value of K shows an understeer behaviour, generally a more stable vehicle and a zero K value shows neutral steer. This is how the vehicle is controlled to depict consistent predictable handling and avoid the oversteer scenario.

In order to increase vehicle stability, Mokhiemar and Abe (2002) proposed a modification to the yaw rate response, changing it from a second order to a first order model. The reasoning behind this was that when side-slip angle converges to zero, the yaw rate response can be reduced to just a first order lag. This is expressed in Equation (3.6).

$$\frac{\gamma(s)}{\delta(s)} = G_R \frac{1}{1 + T_r s} \quad (3.6)$$

Equation (3.6) explains the transfer function between yaw rate and steer angle where G_R is the gain and T_r is the yaw rate time constant delay whereby when T_r is small it represents a fast response and when T_r is large it represents a slow response.

In order to take different surfaces into account, a coefficient of friction of the surface is introduced. This allows limitations on the linear vehicle model and is derived from the relationship to lateral accelerations.

$$a_y = \dot{v}_y + v\gamma \quad (3.7)$$

v_y is the lateral velocity, thus this results in the steady-state yaw rate during constant cornering as:

$$\gamma_{ss} = \frac{a_{yu}}{v} \quad (3.8)$$

Limiting the steady state yaw rate from exceeding the maximum road coefficient of friction, the steady-state yaw rate should satisfy:

$$|\gamma_{ss}| \leq \frac{\mu g}{v} \quad (3.9)$$

The steady state yaw rate can thus be expressed as:

$$\gamma_{ss} = G_R \delta = \frac{v\delta}{l + k_{us}v^2} \quad (3.10)$$

The desired steady state yaw rate is limited to a value abiding to the tyre/road conditions by:

$$\gamma_{ss} = \begin{cases} G_R \delta & \text{if } |G_R \delta| < \frac{\mu g}{v} \\ \frac{\mu g}{v} \text{sign}(G_R \delta) & \text{otherwise} \end{cases} \quad (3.11)$$

The steady-state vehicle side-slip angle is obtained by:

$$\beta_{ss} = G_B \delta \quad (3.12)$$

There is a linear relationship between the steady-state side-slip angle and steady-state yaw rate

$$\beta_{ss} = \gamma_{ss} f_u \quad (3.13)$$

Where

$$f_u = \frac{L_r}{v} - \frac{L_f m v}{2l C_{ar}} \quad (3.14)$$

Where f_u is the ratio of the steady-state values of side-slip angle to yaw rate.

The desired responses depicted in Figure 31 show that the model could work on rough/lower surface coefficient terrain despite only being used for smooth terrain in this study. The vehicle reference model received a step steer input, this results in a positive desired yaw rate, the maximum road coefficient of friction is manipulated to show the outcome for a μ of 0.4 and 0.8. The desired yaw rate is similarly halved for the lower μ . From (3.13) the desired side slip angle is a function of the desired yaw rate and shows a negative yet smaller magnitude to the desired yaw rate, however sharing a similar shape. Due to their state dependency, the desired side-slip angle is thus limited by the tyre/road interaction as the desired yaw rate is.

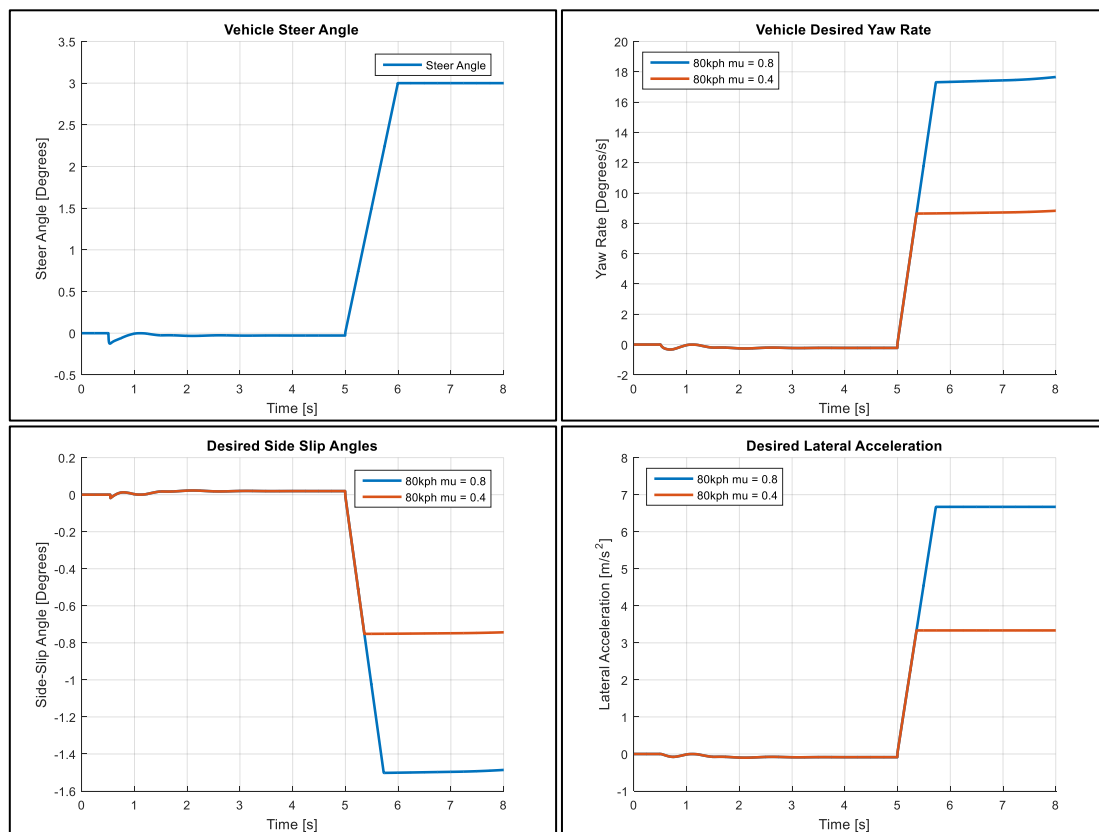


Figure 31 Desired Vehicle Model

These desired responses ensure the vehicle will depict neutral or slight understeer based on vehicle parameters and are used as the reference model to be tracked. The structure of the vehicle closed loop system is shown in Figure 32. Vehicle states are sent from the simulation model or actual vehicle to the controller. The controller sends a control signal to the vehicle to obtain the desired vehicle behaviour.

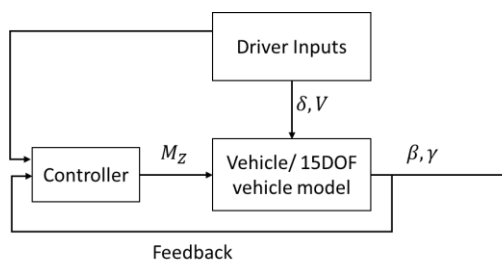


Figure 32 Controller with Feedback

3.2 Linear Quadratic Regulator (LQR)

A yaw rate controller was developed by a predictive optimal approach (Mirzaei et al., 2008). The same approach was used to develop a side-slip control type of DYC (Eslamian et al., 2007). A complete LQ optimal problem is formulated to track the proposed desired models for both yaw rate and side-slip angle (Mirzaei, 2009). In this study, the work of (Mirzaei, 2009) is implemented as suggested without further modification as a baseline stability control system.

3.2.1 Control System Design

A performance index is formulated which penalizes the tracking errors, in this case side-slip angle, yaw rate and control effort.

$$J = \frac{1}{2} \int_0^{t_f} [w_b(\beta - \beta_d)^2 + w_r(\gamma - \gamma_d)^2 + w_u M_z^2] dt \quad (3.15)$$

Where w_b , w_r and w_u are weighting factors and must be tuned accordingly for the side-slip angle error, yaw rate error and controller effort respectively. β_d and γ_d represent the desired side-slip and yaw rate responses to be tracked as formulated in Section 3.1 and the subscript d represents desired response. It is desired to have a performance index as small as possible. A small performance index means the vehicle tracks the desired states as close as possible with a small control effort input.

The linear 2DOF vehicle model discussed earlier is used to design the yaw moment controller as:

$$\dot{X} = AX + E\delta + BU \quad (3.16)$$

where

$$X = \begin{bmatrix} \beta \\ \gamma \end{bmatrix}, A = \begin{bmatrix} a_{11} & a_{12} \\ a_{21} & a_{22} \end{bmatrix}, E = \begin{bmatrix} e_1 \\ e_2 \end{bmatrix}, B = \begin{bmatrix} 0 \\ 1/I_z \end{bmatrix}, U = [M_z]$$

With the yaw moment (M_z) considered as the control input and the steer angle being an external disturbance to the system. The performance index in (3.15) is rewritten based on (3.16) matrix form as:

$$J = \frac{1}{2} \int_0^{t_f} [(X - X_d)^T Q (X - X_d) + U^T R U] dt \quad (3.17)$$

where

$$Q = \begin{bmatrix} w_b & 0 \\ 0 & w_r \end{bmatrix}, R = [w_u]$$

The Hamiltonian function is given by:

$$\mathcal{H} = \frac{1}{2} (X - X_d)^T Q (X - X_d) + \frac{1}{2} U^T R U + P^T (AX + E\delta + BU) \quad (3.18)$$

where $P = [p_1 \ p_2]^T$ are the Lagrangian multipliers.

The co-state equations are

$$\dot{P} = -\frac{\partial \mathcal{H}}{\partial X} = -Q(X - X_d) - A^T P \quad (3.19)$$

The relation that needs to be satisfied algebraically is:

$$0 = \frac{\partial \mathcal{H}}{\partial U} = RU + B^T P \quad (3.20)$$

Thus,

$$U = -R^{-1}B^T P \quad (3.21)$$

Substituting (3.21) into the state equation (3.16) results in the state and co-state equations

$$\begin{bmatrix} \dot{X} \\ \dot{P} \end{bmatrix} = \begin{bmatrix} A & -BR^{-1}B^T \\ -Q & -A^T \end{bmatrix} \begin{bmatrix} X \\ P \end{bmatrix} + \begin{bmatrix} E\delta \\ QX_d \end{bmatrix} \quad (3.22)$$

Instead of determining the transition matrix to solve these linear differential equations, the matrix P can be written in the form:

$$P = KX + S \quad (3.23)$$

Whereby the matrix $K_{2 \times 2}$ is symmetric and satisfies the Ricatti equation

$$\dot{K} = -KA - A^T K - Q + KBR^{-1}B^T K \quad (3.24)$$

and

$$\dot{S} = -(A^T - KBR^{-1}B^T)S + QX_d - KE\delta \quad (3.25)$$

With the boundary conditions being $K(t_f) = 0$ and $S(t_f) = 0$. Substituting (3.23) into (3.21), the control input is obtained as:

$$U = -R^{-1}B^T(KX + S) \quad (3.26)$$

This equates to the control input M_z being:

$$M_z = -\frac{1}{w_u J_z} (k_{12}\beta + k_{22}\gamma + s_2) \quad (3.27)$$

The first order differential equations (3.24) and (3.25) are numerically solved backward in time to determine the control law gains. For an infinite horizon problem, $t_f = \infty$ and considering it as steady state the derivatives of K and S vanish thus $\dot{K} = 0$ and $\dot{S} = 0$. Therefore, non-linear algebraic equations can now be obtained. Expanding these equations, independent equations are obtained to determine the elements of the symmetric matrix K . The equations can be solved analytically to determine the values of k_{11} , k_{12} and k_{22} with the weighting factors w_r , w_b and w_u for the yaw-rate error, side-slip angle error and controller effort respectively. The different control types of DYC are examined by changing the weighting factors on the control system. The weights used in this study are shown in Table 4. It should be noted that only independent control of each variable was suggested by Mirzaei (2009).

Table 4 LQR Weighting Values

| | w_r | w_b | w_u |
|-------------------------------|-------|--------|-----------|
| Yaw rate Control Type | 1 | 0 | 10^{-9} |
| Side-slip Control Type | 0 | 10^3 | 10^{-7} |

3.3 Model Predictive Control

A Model Predictive Controller (MPC) was chosen based on its ease of implementation, systematic handling of constraints, multiple variable control potential and feed forward ability to make good use of future target information implicitly such as the ability to incorporate constraints explicitly to determine optimum solutions. The corrective yaw moment is determined by MPC based on two variables, namely the yaw rate and side-slip angle however the roll index provides a bounded desired yaw rate which the controller adheres to by transitioning to the new desired value.

Taking the side-slip angle and yaw rate as state vectors, the state equations for the model may be written in standard state space form as:

$$\dot{x} = Ax + Bu \quad (3.28)$$

where

$$x = \begin{bmatrix} \beta \\ \gamma \end{bmatrix}, A = \begin{bmatrix} a_{11} & a_{12} \\ a_{21} & a_{22} \end{bmatrix}, B = \begin{bmatrix} 0 \\ 1/I_z \end{bmatrix}, u = M_z$$

The control input u is the yaw moment (M_z). The state space equation can be transformed to discretize state space equations for digital control as:

$$x(k+1) = A_f x(k) + B_f u(k) \quad (3.29)$$

The subscript f is used to highlight discretized values. Taking the disturbance into consideration, namely the steering angle, equation 3.28 becomes

$$x(k+1) = A_f x(k) + B_f u(k) + E_f \delta(k) \quad (3.30)$$

where

$$A_f = A, B_f = B, E_f = \begin{bmatrix} e_1 \\ e_2 \end{bmatrix}$$

In order to enforce the rollover index, the yaw rate limit corresponding to a desired rollover index is determined. From Section 1.4.2.3, Equation (1.39) is rewritten using Matlab's symbolic toolbox for the corresponding yaw rate limit. It is not written here due to its complexity.

This yaw rate limit is then added as a soft constraint on the yaw rate state as an exponential decay approach such that

$$\gamma(k) \leq \gamma_{max} + e^{-\alpha k} m \quad (3.31)$$

where m represents the margin of error allowed. This approach was used to prevent the controller from settling to the unbounded solution but to adhere to the soft constraint as much as possible.

The steering angle disturbance provided to the system can potentially be predicted using machine learning based on GPS path tracking, or neurologic response theory. However, for the purpose of this study, it is assumed to have a zero-order hold for the preview horizon i.e. constant.

The state error vectors on the tracking error for time steps 0, 1 and 2 appear as:

$$\begin{aligned}
 \Delta x(0) &= x_0 - x_{ref} \\
 \Delta x(1) &= A_f x(0) + B_f u(0) + E_f \delta(0) - x_{ref} \\
 \Delta x(2) &= A_f x(1) + B_f u(1) + E_f \delta(0) - x_{ref} \\
 \Delta x(2) &= A_f^2 x(0) + A_f B_f u(0) + B_f u(1) + A_f E_f \delta(0) + E_f \delta(0) - x_{ref}
 \end{aligned} \tag{3.32}$$

This results in the following recursive pattern state error vectors for the prediction horizon of N steps:

$$\begin{aligned}
 X = \begin{pmatrix} \Delta x_0 \\ \Delta x_1 \\ \Delta x_2 \\ \vdots \\ \Delta x_N \end{pmatrix} &= \begin{pmatrix} I \\ A_f \\ A_f^2 \\ \vdots \\ A_f^N \end{pmatrix} x_0 + \begin{pmatrix} 0 & \cdots & \cdots & \cdots & 0 \\ B_f & 0 & \vdots & \vdots & \vdots \\ A_f B_f & B_f & 0 & \vdots & \vdots \\ \vdots & \vdots & \vdots & 0 & \vdots \\ A_f^{N-1} B_f & A_f^{N-2} B_f & \cdots & A_f B_f & B_f \end{pmatrix} \begin{pmatrix} u(0) \\ u(1) \\ u(2) \\ \vdots \\ u(N-1) \end{pmatrix} \\
 &+ \begin{pmatrix} 0 \\ E_f \\ (A_f + I)E_f \\ \vdots \\ \sum_{i=0}^{N-1} A_f^i E_f \end{pmatrix} \delta_0 - \begin{pmatrix} x_{ref} \\ \vdots \\ \vdots \\ x_{ref} \end{pmatrix}
 \end{aligned} \tag{3.33}$$

This is represented in matrix form as:

$$X = \mathbf{A}x_0 + \mathbf{B}U + \mathbf{E}\delta_0 - X_{ref} \tag{3.34}$$

3.3.1 Controller Design

Formulation of the optimization problem for $x - x_{ref} = 0$. The cost function is chosen to be of the form:

$$\begin{aligned}
 J &= \sum_{k=0}^{N-1} [(x(k) - x_{ref})^T Q (x(k) - x_{ref}) + u(k)^T R u(k)] \\
 &+ (x(N) - x_{ref})^T P_f (x(N) - x_{ref})
 \end{aligned} \tag{3.35}$$

Where J represents the cost function and must be strictly positive, and is subject to minimization. In order to assure a positive cost, Q and R are symmetric and positive definite matrices, used as weighting functions in relation with input efforts.

$$J = X^T \begin{pmatrix} Q & 0 & \cdots & \vdots \\ 0 & \ddots & \ddots & \vdots \\ \vdots & \ddots & Q & \vdots \\ \vdots & \cdots & \vdots & P_f \end{pmatrix} X + U^T \begin{pmatrix} R & 0 & \cdots & \vdots \\ 0 & \ddots & \ddots & \vdots \\ \vdots & \ddots & \ddots & \vdots \\ \vdots & \cdots & \ddots & R \end{pmatrix} U \tag{3.36}$$

thus

$$J = X^T \mathbf{Q}X + U^T \mathbf{R}U \tag{3.37}$$

In order to solve the optimization problem, a quadratic program shall be formulated which can be solved efficiently using convex optimization. The required quadratic structure of the problem is:

$$J = \frac{1}{2}U^T\mathbf{H}U + \mathbf{F}U + C \quad (3.38)$$

Where the sequence of inputs U is the optimization variable, namely the yaw moment M_z . The constant term C is not relevant to the optimization problem as it cannot be varied. For implementation purposes, the Matrixes H and F have to be found from the prediction model. Solving for the Matrixes is as follows:

Substituting (3.34) into (3.37) and expanding until achieving the form of (3.38)

$$\begin{aligned} J = & x_0^T A^T Q A x_0 + x_0^T A^T Q B U + x_0^T A^T Q E \delta_0 + x_0^T A^T Q B U + U^T B^T Q B U + \delta_0^T E^T Q B U \\ & + \delta_0^T E^T Q A x_0 + \delta_0^T E^T Q B U + \delta_0^T E^T Q E \delta_0 + U^T R U + X_{ref}^T Q X_{ref} \\ & - 2X_{ref}^T Q A x_0 - 2X_{ref}^T Q B U - 2X_{ref}^T Q E \delta_0 \end{aligned} \quad (3.39)$$

From equation (3.39) using coefficient comparison, it can be seen that

$$\mathbf{H} = 2B^T Q B + 2R \quad (3.40)$$

$$\mathbf{F} = 2x_0^T A^T Q B + 2\delta_0^T E^T Q B - 2X_{ref}^T Q B \quad (3.41)$$

The optimisation problem was initially solved using a quadratic programming function (interior point method), however it was found to be prohibitively computationally expensive. Thus, a simpler linear gradient method was chosen as the solver. The gradient method is implemented in the iterative form as:

$$U_{i+1}^* = U_i^* - h\nabla_U J(U_i^*) \quad (3.42)$$

This iterative method is used until the following condition is met:

$$|U_j^* - U_{j-1}^*| < \varepsilon \quad (3.43)$$

The optimal yaw moment sequence over the prediction horizon will be $U_{opt} = U_j^*$ and as the current control action, $u = U_{opt}(1)$ is applied. The system is implemented using weight scheduling as follows in Figure 33. The vehicle is always in yaw rate control, however when the side-slip angle surpasses the desired side-slip angle, the side-slip angle weighting is increased based on a side-slip angle error gain schedule. This is referred to as MPC Combined in the results section of this study.

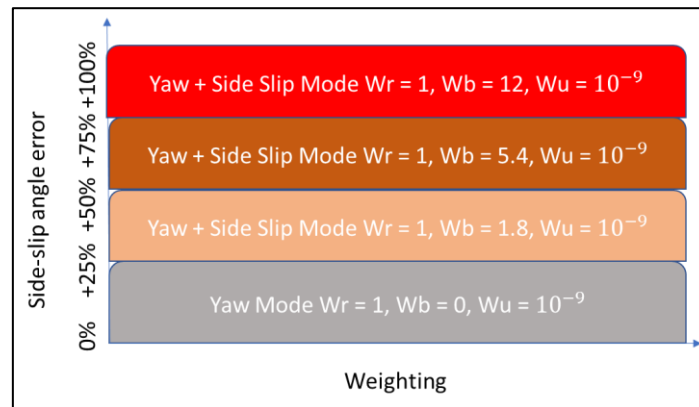


Figure 33 MPC Weighting

This Model Predictive Controller is setup for multivariable control, namely the yaw rate and side-slip angle control. It also has a soft constraint on the yaw rate from the ZMP roll index in the form of an exponential decaying approach which is referred to as MPC Bound in the results section of this study. A fail-safe limitation is also made on the optimal yaw moment such that it does not exceed 4000Nm as this is undesirable.

3.4 Brake Torque Difference Distribution

The optimal yaw moment acts on the vehicle via the brakes. A yaw enhancing moment in the direction of yaw rate will act on the wheels closest to the radius of the turn, whereas a yaw opposing moment opposite to the yaw rate will act on the wheels further away from the radius of the turn. Figure 34 shows a yaw enhancing moment being applied to the vehicle turning to the right, whereby the wheels being braked are circled in red and the wheels not being braked are circled in green.



Figure 34 Test Vehicle undergoing Yaw Enhancement

The optimal yaw moment is designated to the brakes of the vehicle, the brake force on either side of the vehicle is determined as:

$$Brake\ Force_{xl} = \frac{M_z}{T/2}, Brake\ Force_{xr} = -\frac{M_z}{T/2} \quad (3.44)$$

In order to prevent wheel lockup, the vehicle's load transfer mentioned in Section 1.2.2.3 is taken into account, thus each wheel's individual loading is determined. A friction circle is devised for each individual wheel based on the vertical loading, and together with an estimated tyre side-slip angle, the lateral force F_y is determined using a Pacejka fit of the Michelin LTX² parameterised data.

The Pacejka tyre model is used for this purpose due to real time implementation as it has low computation requirements. The Magic Formula was proposed by (Bakker et al., 1989) to describe the tyre's handling characteristics in just one formula. The Magic Formula relates the tyre's lateral force vs. slip angle relationship, which directly affects the vehicle's handling and steering response. The Magic-

Formula is used where the terms are dependent on the vertical tyre load, and camber angle. The vehicle used in this study is equipped with solid axles, thus the influence of camber is neglected due to the tyres remaining mainly vertical. The tyre is able to experience a camber angle due to tyre deflection, this is however assumed to be small and is neglected.

The tyre's maximum longitudinal brake force is now calculated based on the friction circle and the assumed surface coefficient.

$$\text{Tyre Maximum Brake Force} = \sqrt{\mu F_z^2 - F_y^2} \quad (3.45)$$

The brake force distribution on the right side of the vehicle between the front and rear tyre is determined:

$$\text{Distribution Ratio}_r = \frac{\text{Max Brake Force Rear Right}}{\text{Max Brake Force Front Right}} \quad (3.46)$$

$$\text{Desired Brake Force FR} = \frac{\text{Brake Force}_{xr}}{1 + \text{Distribution Ratio}_r} \quad (3.47)$$

$$\text{Desired Brake Force RR} = \text{Brake Force}_{xr} - \text{Desired Brake Force FR} \quad (3.48)$$

The desired brake force is calculated in the same manor for the left-hand side of the vehicle. If the desired brake force is larger than the maximum brake force, the maximum brake force is used. However, due to limitations on the optimal moment, the vehicle should never run into the limitation. It is merely a fail-safe feature. The desired brake torque is a function of the brake force and tyre's rolling radius.

$$T_b = \text{Brake Force} * \text{Rolling Radius} \quad (3.49)$$

3.5 Pressure Control

The test vehicle is fitted with a standard 1997 model year WABCO ABS modulator, the drawbacks of an ABS modulator in comparison to an ESP modulator is that the system requires brake pedal actuation. An ESP Modulator can create hydraulic pressure because the pump can draw fluid independently from the master cylinder. In order to get around this drawback, an actuator was fitted in order to preload the modulator's accumulator prior to each run. The modulator is left in the dump phase whereby fluid from the master cylinder will flow straight to the accumulator and remain there until either the ABS pump or the pump phase is activated and the brake pedal is actuated.

Table 5 shows the logic used whereby the ABS pump is only switched on when the error between the desired pressure and actual pressure is larger than 10Bar. Within the 10Bar region, controlled switching between the pump and hold settings are used together with an error based pedal actuation until the value is within 3Bar of the desired pressure. The dump phase is similar with controlled switching and error based pedal release when the error is within the negative 10Bar region and just the dump phase is selected when the error is smaller than 10Bar.

Table 5 Pressure Control Logic

| Error (Desired Pressure – Actual Pressure) | ABS Pump Status | Actuator Status | Valve Status |
|---|-----------------|--------------------|------------------------|
| Error > 10 Bar | ON | Engage | Pump |
| Error < 10 Bar Error > 3 Bar | OFF | Error gain engage | Synchronised Pump-Hold |
| Error < 3 Bar Error > –3 Bar | OFF | Hold | Hold |
| Error > –10 Bar Error < –3 Bar | OFF | Error gain release | Synchronised Dump-Hold |
| Error < –10 Bar | OFF | Release | Dump |

Figure 35 shows experimental testing of the system and indicates that the ABS pump displayed a delay of 100ms. It should be noted that the ABS modulator is not designed for ESP usage and is limited to 10Hz valve switching. Better results can be obtained with modern ESP modulators.

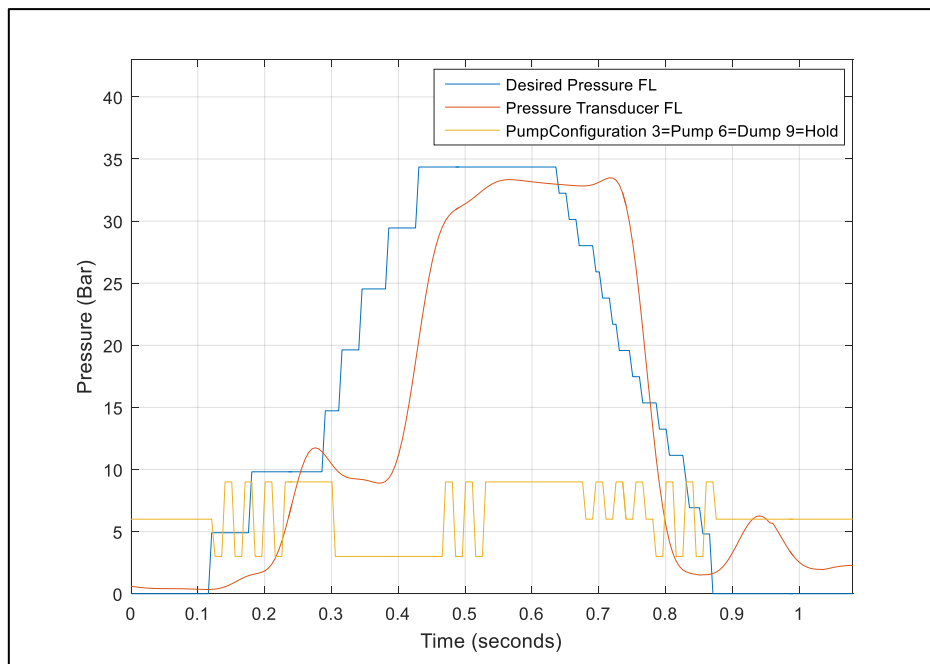


Figure 35 Brake Pressure Control

Conclusion of Control Strategy

This chapter shows that there are numerous mathematical methods available to solve the problem at hand, however some controllers have their advantages and it shall be seen in the following section. The MPC was implemented such that the roll index yaw rate could be added as a boundary on the yaw rate and scheduled weighting is used to include side-slip control when necessary. The controllers appear similar so far but the added weighting functionality and boundaries on MPC allow it more flexibility. The old ABS modulator is not ideal and shows overshoot and slow response, there are newer more responsive ESP modulators available that will be investigated in future work.

Chapter 4 Results

This chapter summarises the results obtained from simulation and experimental tests. The analysis will show how the controllers react to various inputs under different conditions and determine at what point a loss of control occurs.

4.1 Simulation Results

Open loop steering input manoeuvres are used to test the performance of the stability control program without a driver model. This is done to prevent the driver model from altering the yaw moment and results in easier comparison. The first 5 seconds are however conducted with a driver model. The driver model is used to ensure that prior to the actual manoeuvre, where the vehicle is brought up to speed, the vehicle is in the correct entry position to the manoeuvre. The vehicle is accelerated up-to a predefined speed using a large drive force which is thereafter switched over to a PI speed controller before the manoeuvre. The PI speed controller attempts to maintain the vehicle speed by equal wheel torque distribution. The speed controller is limited by the vehicle's achievable longitudinal acceleration.

4.1.1 Sinusoidal Wave Steer Input

A three-degree sinusoidal steer input is used to mimic a scenario similar to a double lane change. The vehicle should ideally return to its original heading direction prior to the start of the manoeuvre. The manoeuvre tests whether the controller successfully improves stability and roll. The vehicle enters the manoeuvre at 80km/h.

4.1.1.1 Controller Comparison with no roll index limit

No rollover index limit is used at this time in order to compare both LQR and MPC with one another.

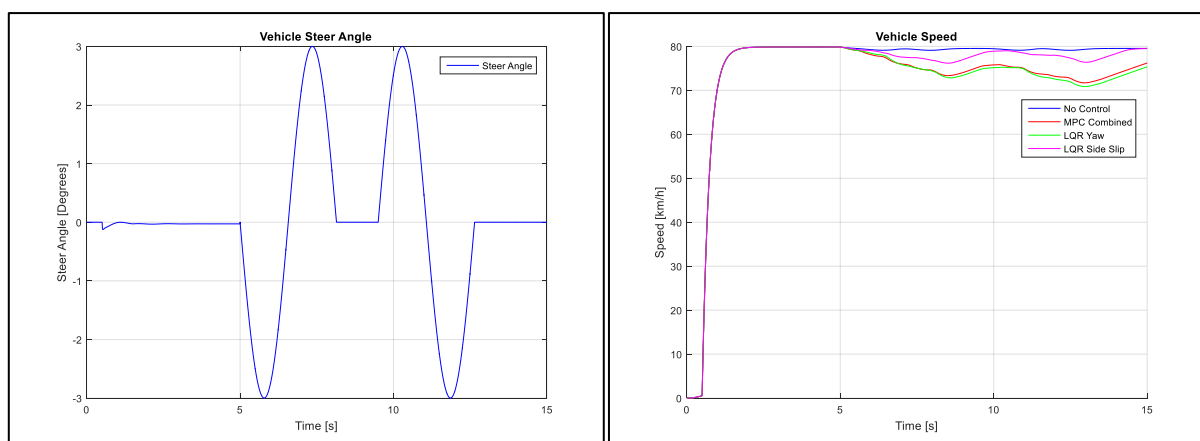


Figure 36 Steering and Speed Input through Modified DLC

Figure 36 shows the steer input (left) and the vehicle speed (right). The vehicle speed decreases with control through the manoeuvre as the vehicle applies brakes. The comparison between vehicle states for the LQR and MPC is shown in Figure 37. The vehicle returns to its original heading direction and the

controlled states namely yaw rate and side-slip angle are better controlled with less overshoot for the MPC controller. The MPC corrective moment is also larger due to the combined control of both yaw rate and side-slip angle. The roll index of the vehicle is slightly smaller using MPC however it is noted that the roll index exceeds 0.9 which is undesirable. Section 4.1.1.2 introduces the roll index bound on the desired yaw response.

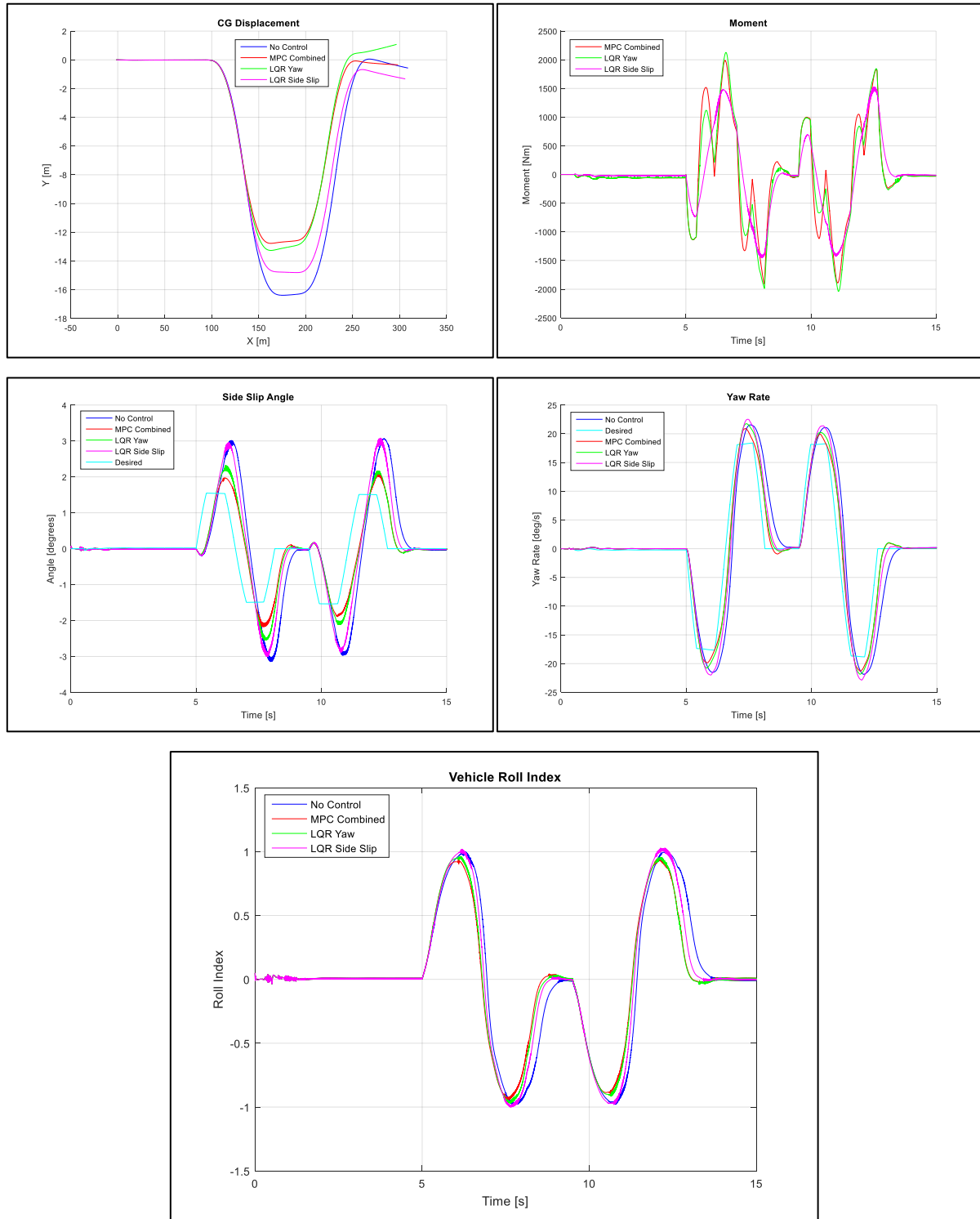


Figure 37 Feedback through Modified DLC of various parameters

4.1.1.2 MPC Controller with and without roll index bound

The previous tests showed an undesired roll index of 0.9 is reached, to limit this a desired roll index of 0.6 is chosen with a 0.08 margin of error allowed. The desired yaw response is now varied based on this roll index and the tests are redone to determine the feasibility of the MPC roll index yaw rate bounded solution. The same steering input as in Figure 36 is used.

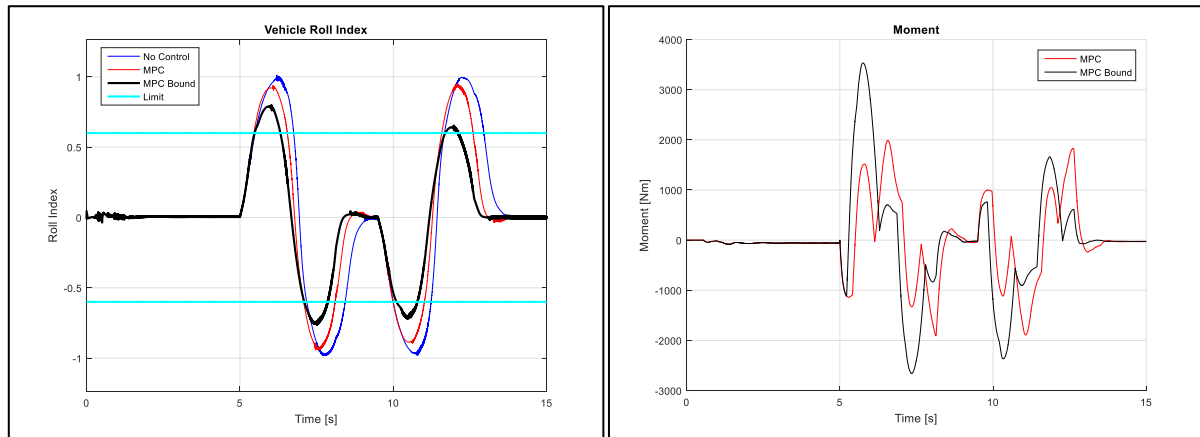


Figure 38 Roll Index for Bounded MPC with Sinusoidal Steer Input

The roll index is drastically decreased as seen in Figure 38, the index still overshoots the 0.6 limit in the first turn, but eventually stays within the desired roll index margin. Overall the roll index is reduced with the bound. It can also be seen that the corrective direct yaw moment is significantly larger in-comparison to the unbounded moment. Transition from an enhancing to an opposing yaw moment also occurs much faster as the vehicle reaches the desired roll index of 0.6.

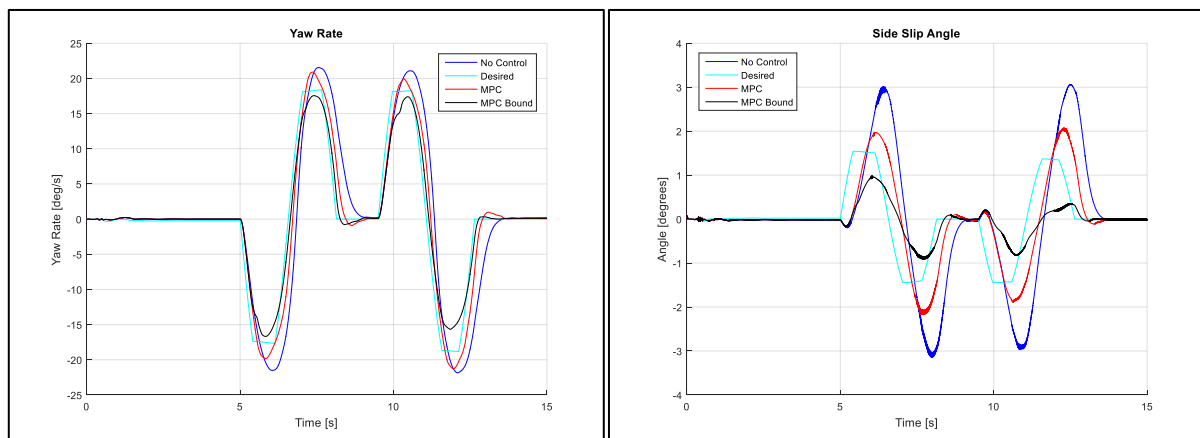


Figure 39 Feedback for Sinusoidal Steer Input with Bounded Roll Index

Both the yaw rate and side-slip angle track their desired responses better with the bounded solution. This shows how the roll index acts on the lateral dynamics of the vehicle.

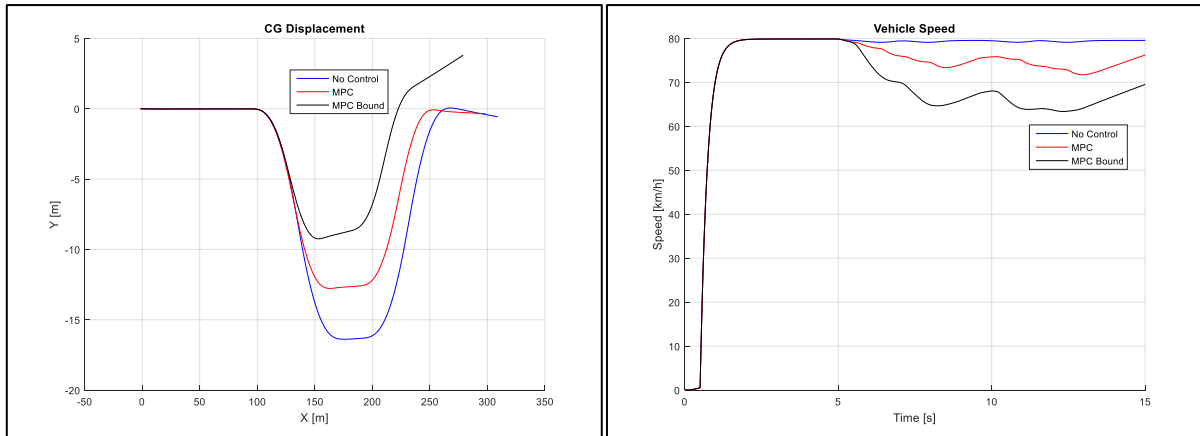


Figure 40 Vehicle Trajectory and Speed through Modified DLC with Roll Index Bounds

The vehicle’s trajectory shows over-compensation during turning, this shows that the tyres created a larger cornering force and more equal cornering load. The vehicle loses speed through the manoeuvre due to the larger moment experienced. This loss of speed adds to the roll index being significantly reduced.

4.1.2 Step Steer Input

This test shows how long it takes for the vehicle to stabilize itself by reaching a steady yaw rate and side-slip angle. The vehicle enters the manoeuvre at 80km/h. This test is similar to a constant radius test, however without path tracking, thus a fixed step steer input is used.

4.1.2.1 Controller Comparison with no roll index limit

Figure 41 shows the steer input (left) and controller moments (right). The MPC moment is only in yaw control mode for the beginning of the manoeuvre, thereafter an inclusion of the side-slip angle weighting results in a slightly larger moment.

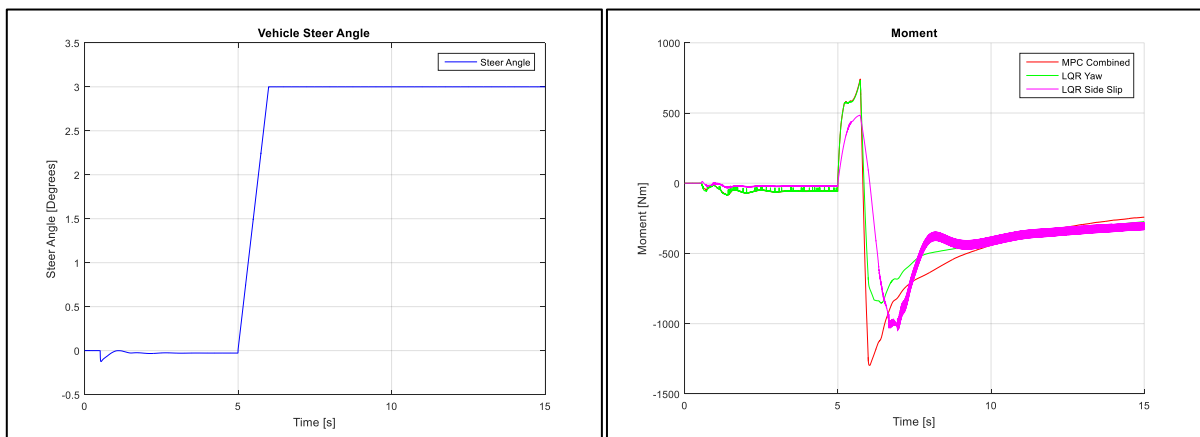


Figure 41 Step Steer Input along with Direct Yaw Control Moments

Without control the vehicle loses control and spins out, wheel lift is also experienced. The side-slip angle and yaw rate of the vehicle are controlled well using MPC and smaller overshoots of the yaw rate and side-slip angle are experienced in Figure 42.

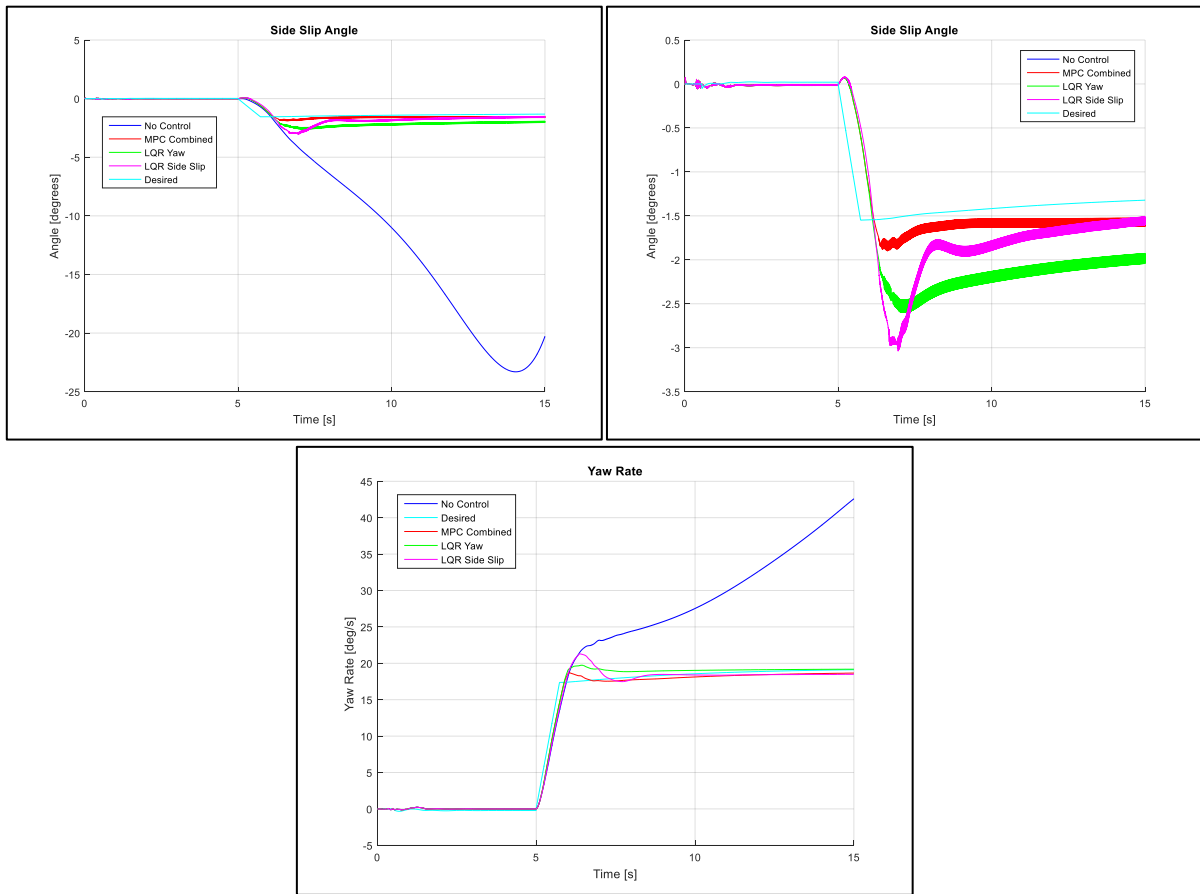


Figure 42 Feedback through Step Steer of various parameters

Figure 43 shows that the vehicle's roll index returns to a steady state with LQR yaw control and MPC faster. The side-slip control weighting using LQR doesn't appear to suit a SUV as there is a long delay before the system retains control. The roll index of all the controllers settle around 0.9, which shows that the desired response of the yaw rate and side-slip angle is too large and can result in vehicle rollover.

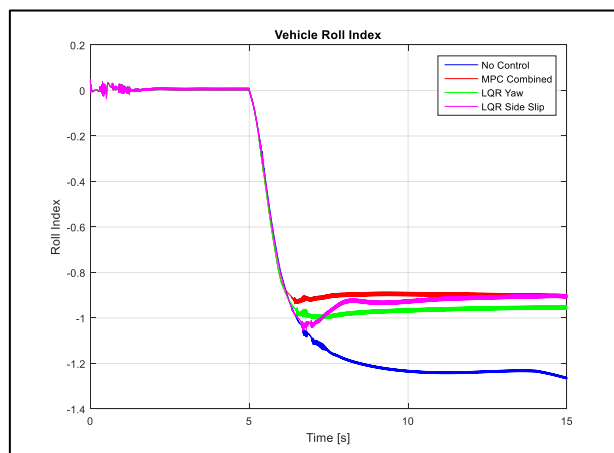


Figure 43 Roll Index through Step Steer

The vehicle path is shown in Figure 44, whereby the vehicle with no control results in oversteer followed by a spin off, any form of control shows a half circle path with a radius of roughly 65 metres. A small decrease in vehicle speed is seen with control. The decrease in lateral acceleration, which is a function of both the radius of curvature and vehicle speed, shows that the increase in radius and slight decrease in vehicle speed, allowed for a more neutral/understeer behaviour that improved vehicle stability.

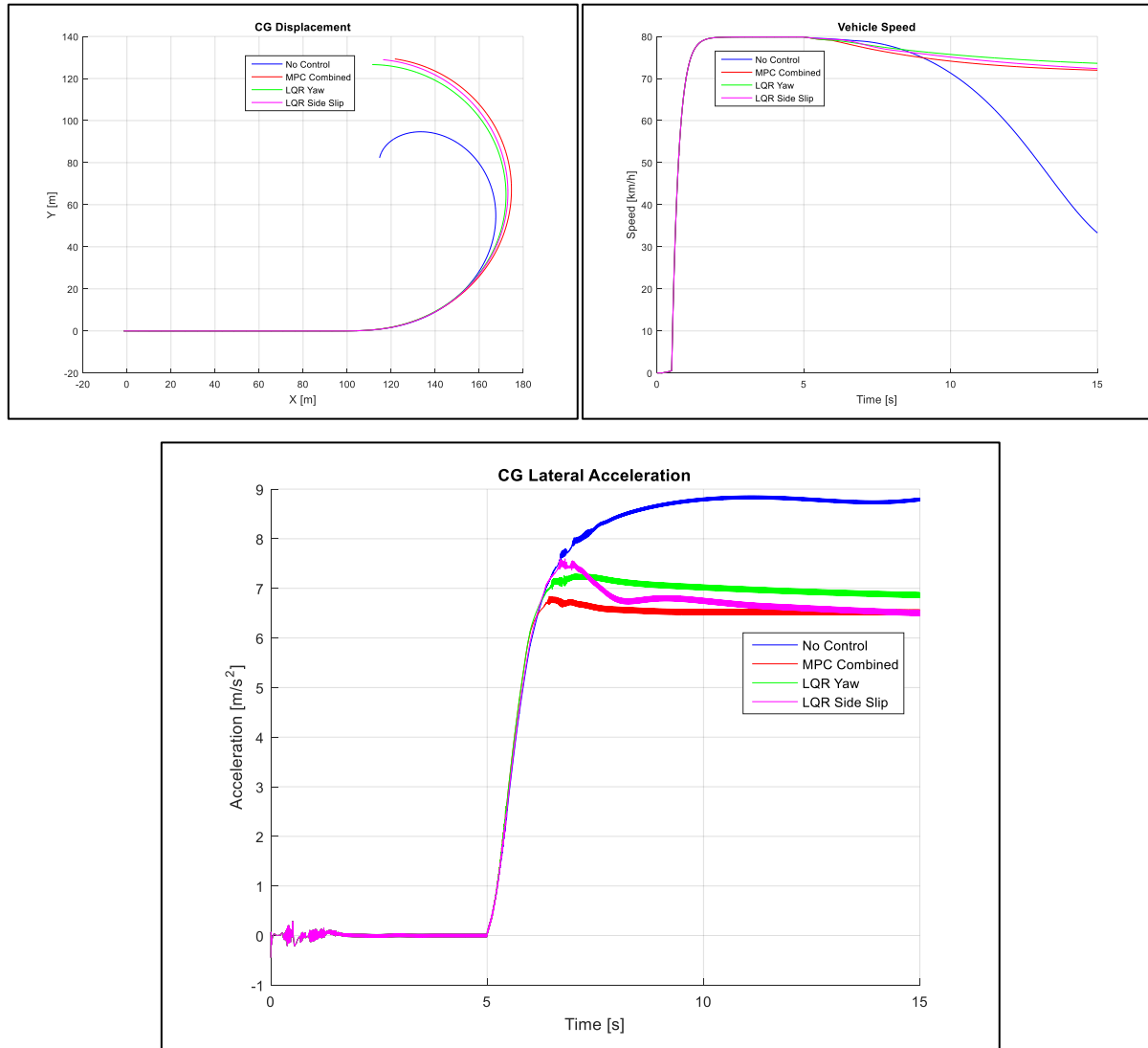


Figure 44 Trajectory and Vehicle Speed through Step Steer

The test is done with roll index bounds on the desired yaw rate response again in Section 4.1.2.2 for the MPC controller.

4.1.2.2 MPC Controller with and without roll index bound

The step steer test is redone with a roll index bound of 0.6 to determine the feasibility of the bounded solution. A margin of error of 0.08 is used on the bound, the desired yaw response is now varied based on the roll index accordingly. The steer input is as used in Figure 41 again.

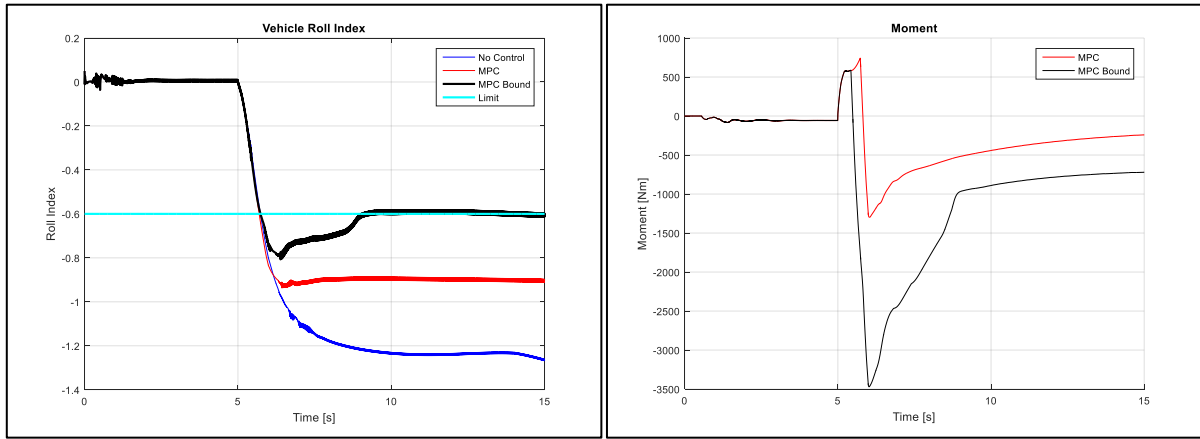


Figure 45 Bounded Roll Index and Direct Yaw Control Moment

A faster transition is seen on the roll index bounded MPC moment, from enhancing to opposing as the vehicle reaches the soft constraint roll index of 0.6, the roll index overshoots and there exists a delay before the system can decrease the roll index. Figure 46 indicates that the yaw rate and side-slip angle are within the desired responses due to the roll index bound requiring smaller desired responses.

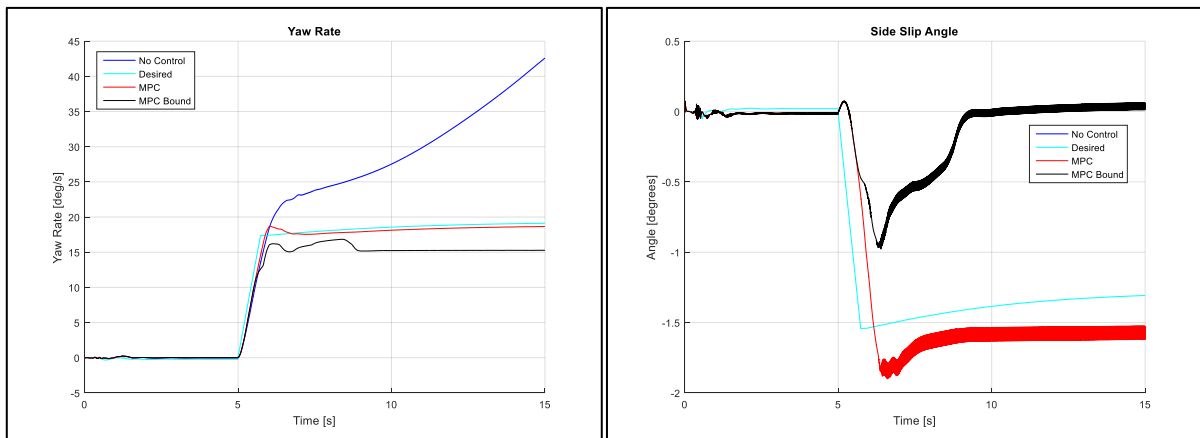


Figure 46 Yaw Rate and Side-Slip Angle through Step Steer with Roll Index Bound on MPC

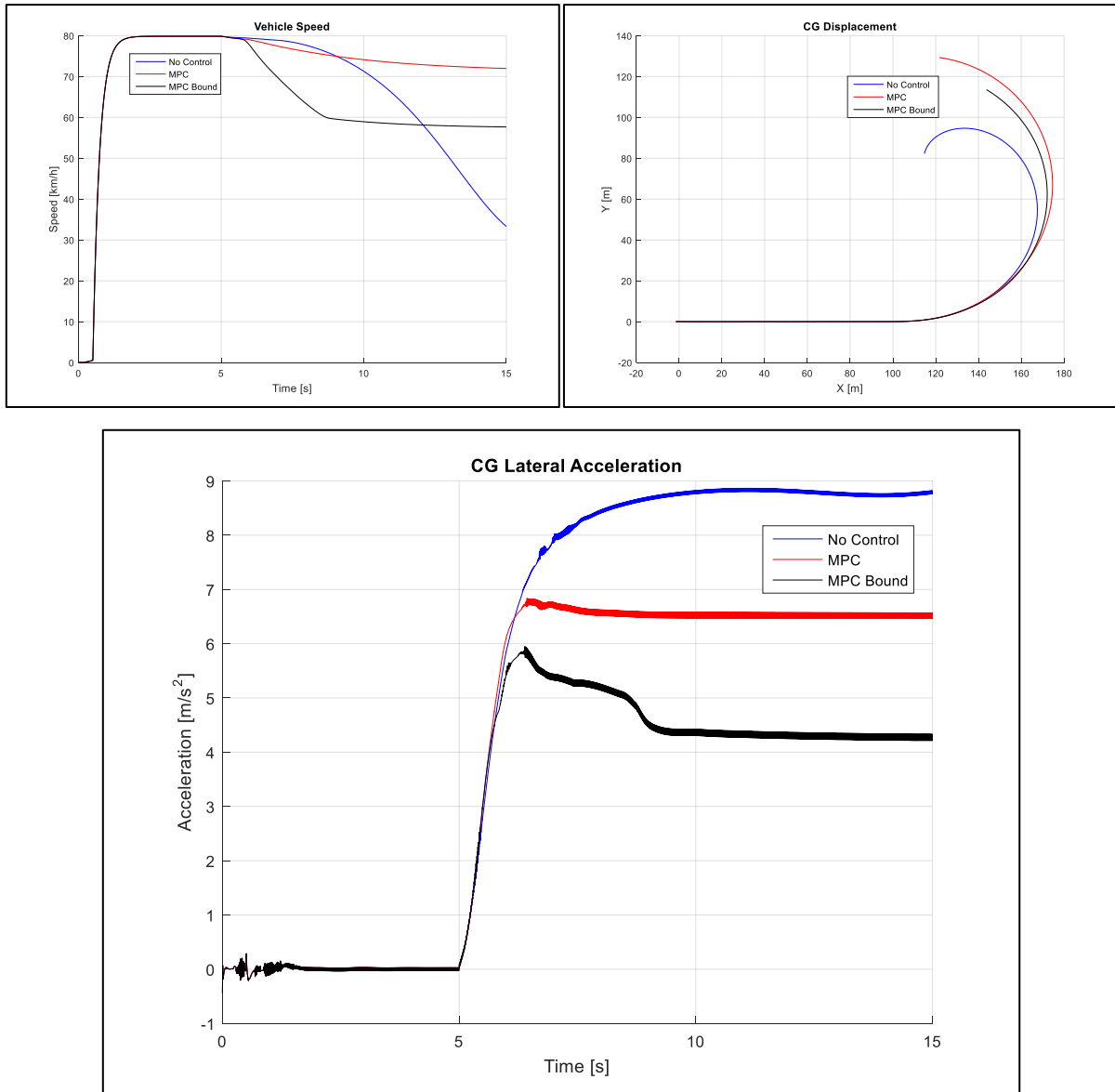


Figure 47 Feedback through Step Steer with Roll Index bounded MPC of various parameters

It can be seen that the vehicle speed is further reduced, whereby the roll index bound can only be satisfied at 60kph, this is quite a significant reduction in speed and lateral acceleration, thus to satisfy the bound, a reduction in speed is the most important. The vehicle follows a tighter path, whereby the radius of curvature decreases to 60 metres with the bounded MPC controller.

4.2 Experimental Results

After tuning the controller in the simulation environment, the control strategies were implemented on the actual vehicle discussed in Chapter 2 to evaluate the performance of the controllers. From early experimental testing, it was decided that MPC had a clear advantage over LQR and that MPC allowed more control over the perturbations arising from noise and other dynamic effects that are ever present and generally not modelled. MPC was implemented with a dead-band during transition, such that corrective moments less than 100Nm were neglected. Experimental validation is hardly done and almost no experimentally published results are available, thus experimental validation of the controller is preferred.

4.2.1 Severe Double Lane Change ISO3888-1

The vehicle was tested with a limit on the roll index value at 0.8 and a limitation of 4000Nm on the magnitude of the direct yaw moment as mentioned in Section 3.3.1. The limit will result in the driver feeling aided instead of overruled. Tests were started at entry speeds of 40km/h increasing as testing progressed. The higher the speed, the more notable the difference.

ISO3888-1 Vehicle Speed 85kph

Figure 48 shows tests at 85km/h where the vehicle could be successfully manoeuvred through the double lane change with the control system active. The Direct Yaw Moment exceeded 3000Nm but never reached its limit of 4000Nm, the driver of the test vehicle could noticeably feel the vehicle braking but not too dramatically. The controller was modified in order to not be susceptible to noise, thus the transition between enhancing and opposing moments, where the controller remains at the zero point before transitioning can be seen due to the 100Nm dead-band.

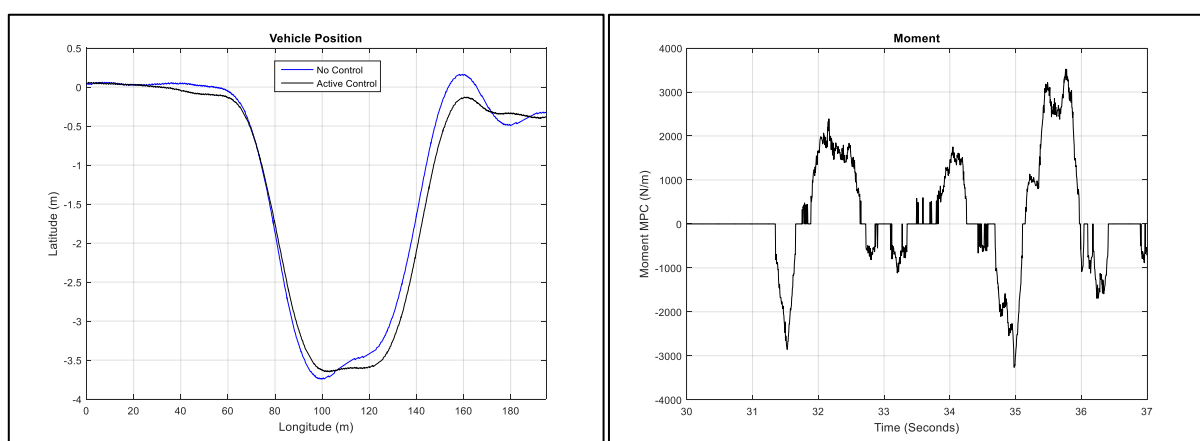


Figure 48 ISO3888-1 Trajectory and DYC Moment

From Figure 48(right) one can see the vehicle experiences a yaw enhancing moment in the first turn between 31.4 and 31.6 seconds, the vehicle's yaw rate in Figure 49 is slightly larger in-comparison to the vehicle without any active systems. The enhancing moment helps the vehicle change direction from 31.9

seconds onwards, however the moment becomes an opposing moment as the vehicle begins to steer away and the yaw rate is larger than the desired response. The yaw rate response is closer to the desired response than without any active-control and exits the manoeuvre without requiring a large yaw rotation. The side-slip angle does not surpass the desired response limit until the transition of the turns around 33.5 seconds. It appears mostly within the same range as the vehicle without any active control however a much smaller side-slip angle is experienced on the exit of the manoeuvre.

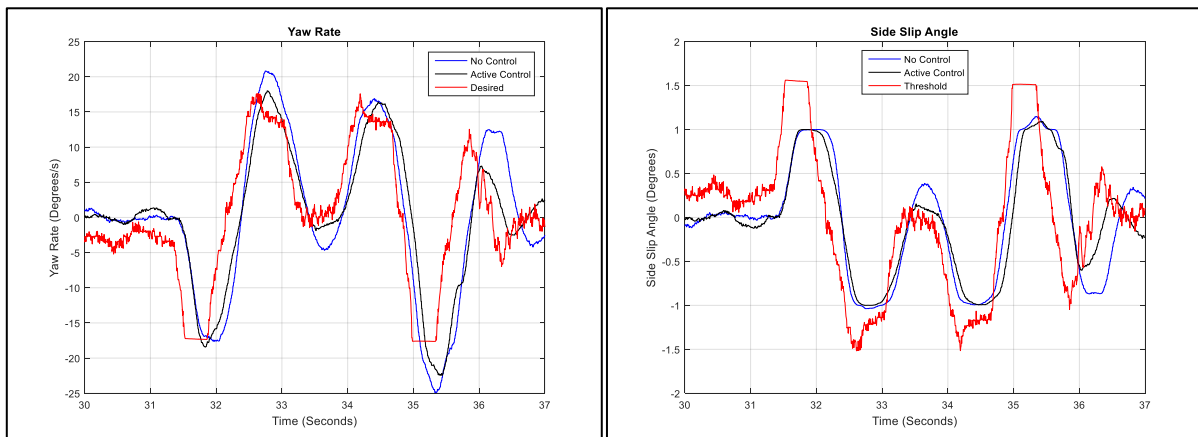


Figure 49 Yaw Rate and Side-Slip Angle through ISO3888-1 DLC

The vehicle's yaw angle in Figure 50 shows the vehicle with active control displaying a much smoother change of heading, with smaller overshoots such that the driver does not need to apply large corrections through the manoeuvre.

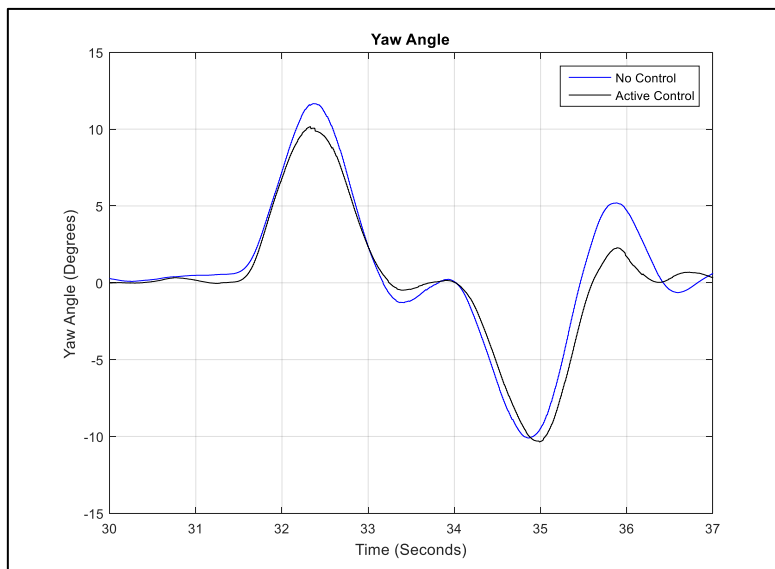


Figure 50 Yaw Angle through ISO 3888-1 DLC

In Figure 51 a notable difference is seen in the roll angle of the vehicle, slightly smaller peaks are experienced in the roll rate as well. The vehicle's Roll Index slightly exceeds the limit of 0.8, however up to an 20% improvement on peaks in-comparison to the vehicle without any active-control.

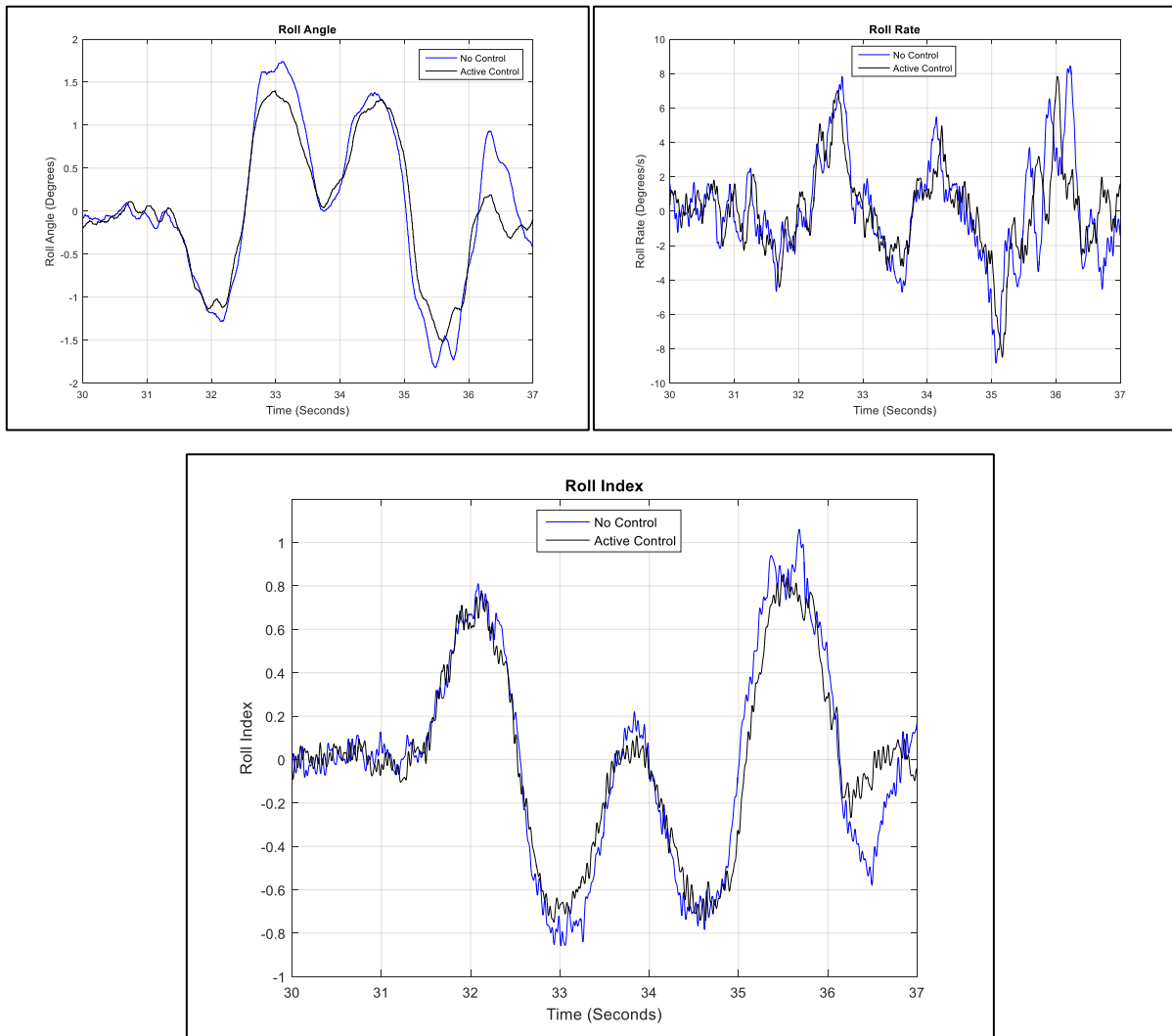


Figure 51 Roll Characteristics through ISO 3888-1 DLC

The Brake Torques delays in Figure 52 is notably visible, there also appears to be large variances in some instances. The ABS modulator refused to dump pressure all the time and in some cases a dump in pressure on one wheel resulted in a burst of pressure on another. Better control of the modulator is necessary for further enhancement due to the crude fuzzy logic scheme used. The modulator is old and not designed for continuous use, thus a newer one may work better. There exists even larger possibilities of improvement with an ESP modulator in-comparison to an ABS modulator.

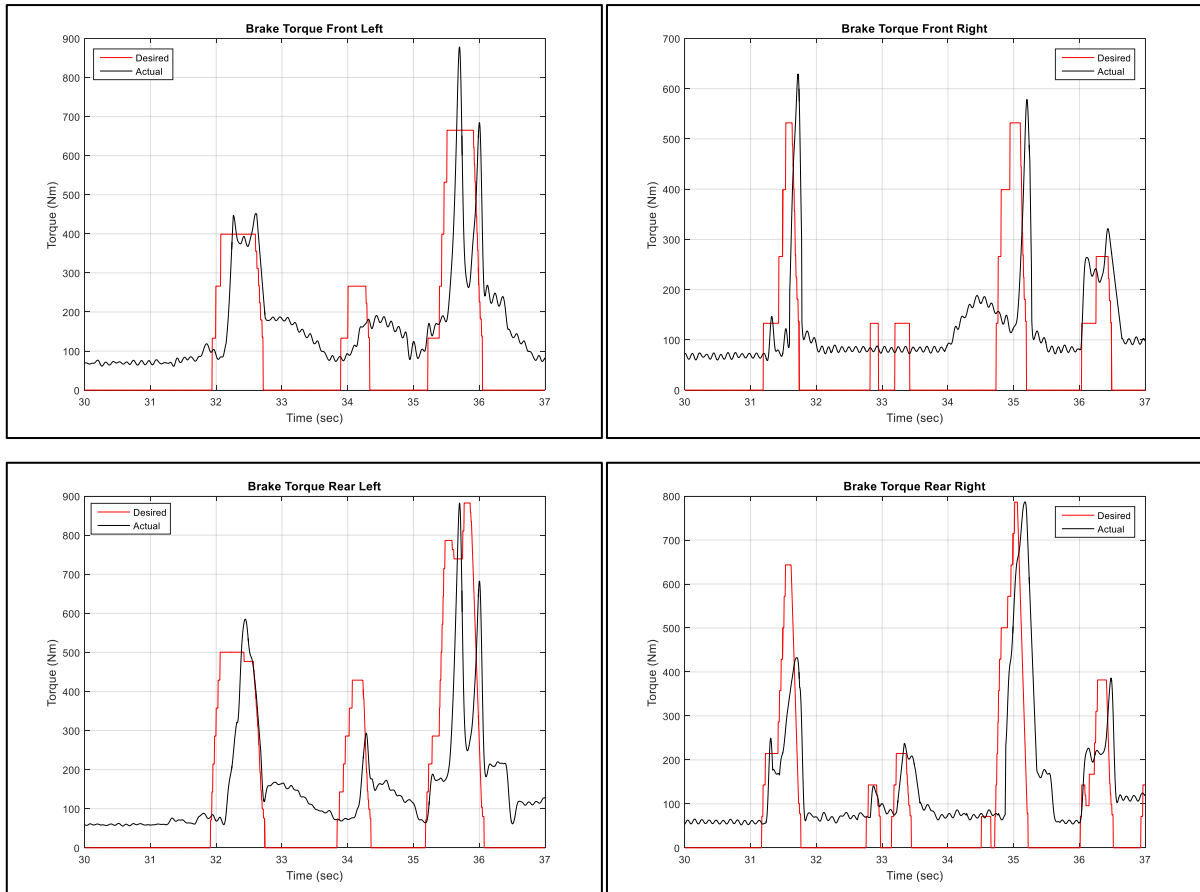


Figure 52 Brake Torques through ISO3888-1 DLC

Figure 53 shows the vehicle exiting the Double Lane Change Manoeuvre with its brake lights on.



Figure 53 Vehicle Exiting ISO3888-1 Manoeuvre, Note Brake Lights

4.2.2 Severe Lane Change ISO3888-2 Obstacle Avoidance

The vehicle was tested with a limit on the roll index of 0.6 for this test. Tests commenced at entry speeds of 30km/h, increasing as testing progressed.

ISO3888-2 Vehicle Speed 53kph

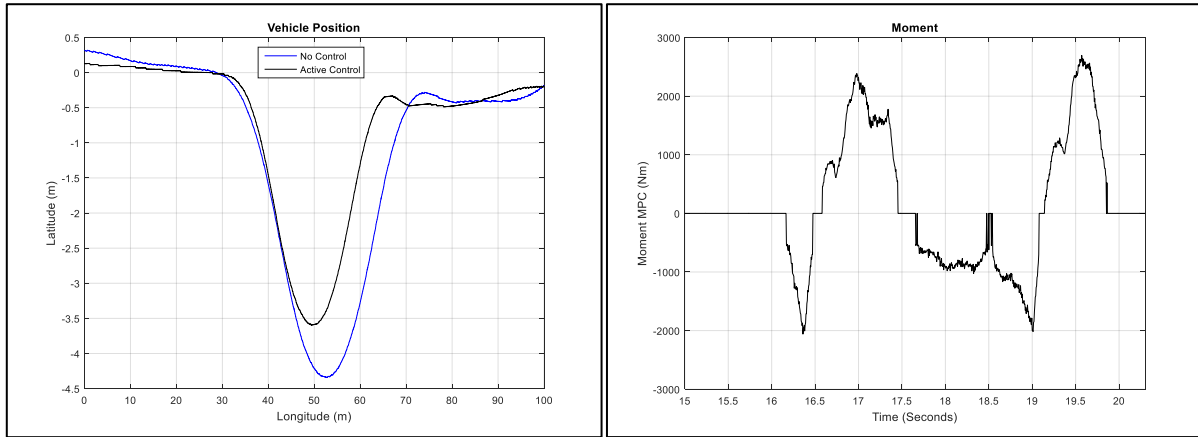


Figure 54 ISO3888-2 Trajectory and DYC Moment

The vehicle followed a much tighter line through this manoeuvre with active control as seen in Figure 54, the enhancing moment was experienced at the beginning of all the turns, thereafter an opposing moment was applied, the increase in brake force resulted in the vehicle slowing down and completing the manoeuvre successfully without hitting any cones.

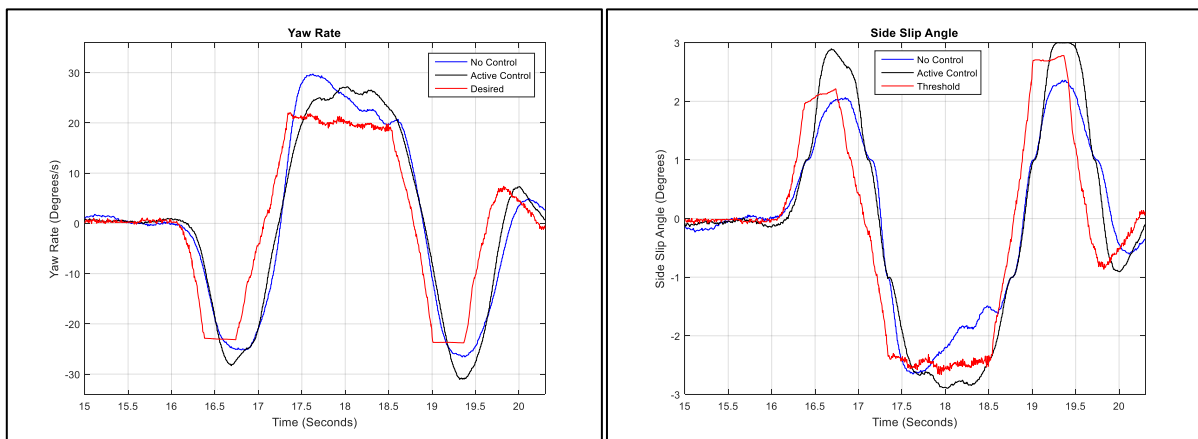


Figure 55 Yaw Rate and Side-Slip Angle through ISO3888-2 Obstacle Avoidance

The yaw response showed a more distributed yaw rotation and an increase in side-slip angle, this allowed the vehicle to rotate more through the manoeuvre. It can be seen that the points where the yaw rate and side-slip angle cross the desired responses is where the moment changes from enhancing to opposing.

The roll characteristics in Figure 56 show that a smaller roll angle was experienced mid-manoevre. The roll rate fluctuated severely with active control as the system intervened. The opposing moments also helped reduce the roll index throughout the manoeuvre. The roll index oscillated about the desired index of 0.6 however never settled. There is however an overall decrease in the rollover propensity.

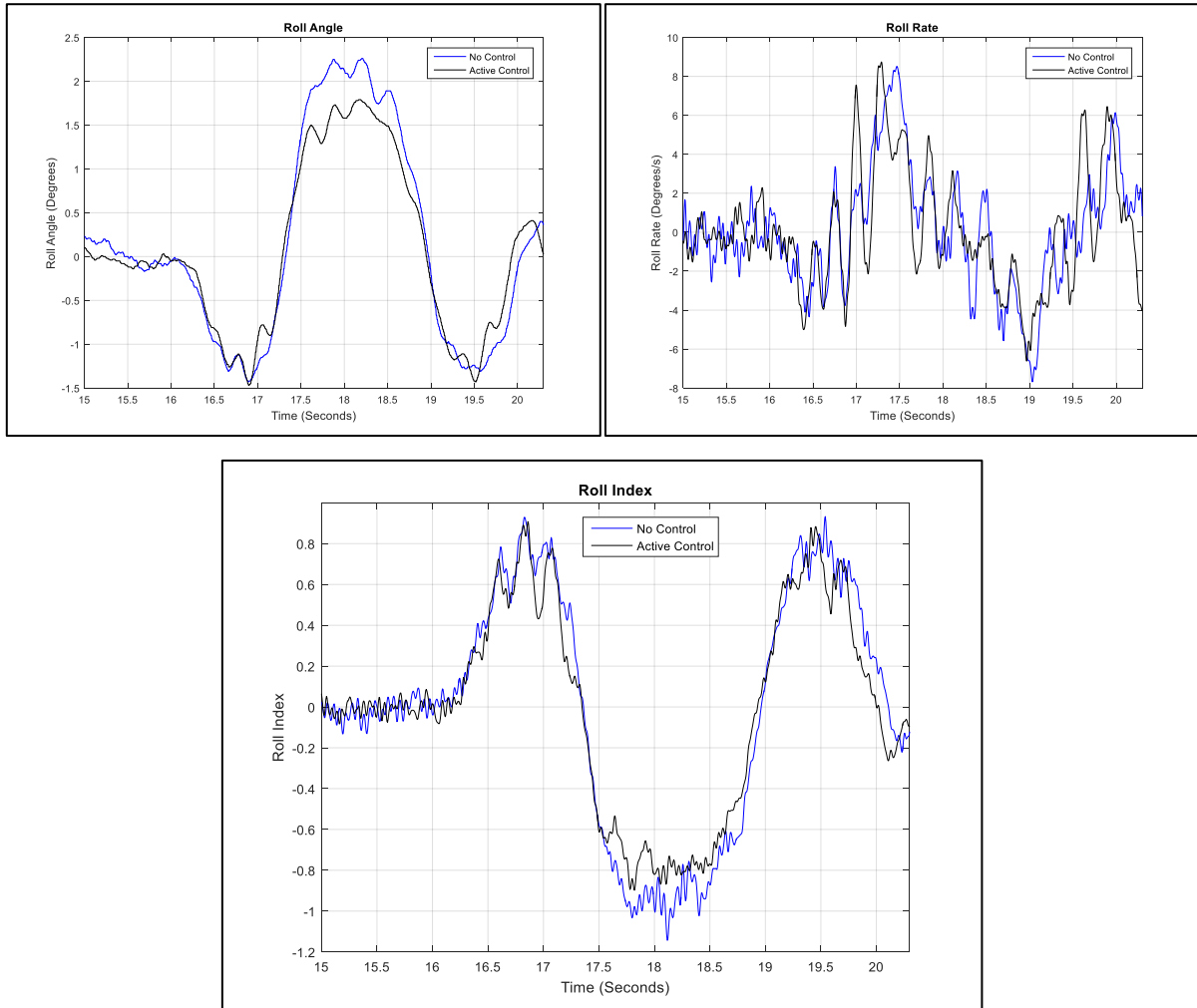


Figure 56 Roll Characteristics through ISO 3888-2 Obstacle Avoidance

In Figure 57 the brake torques applied generally represent that of the desired values, however the front brakes refused to release pressure. It can be seen at 17.5 seconds, the Brake Torque on the left wheels is transferred to the front right wheel. There also exists a slow build-up of torque on the rear right wheel and unfavourable torque around the 19.5 second mark.

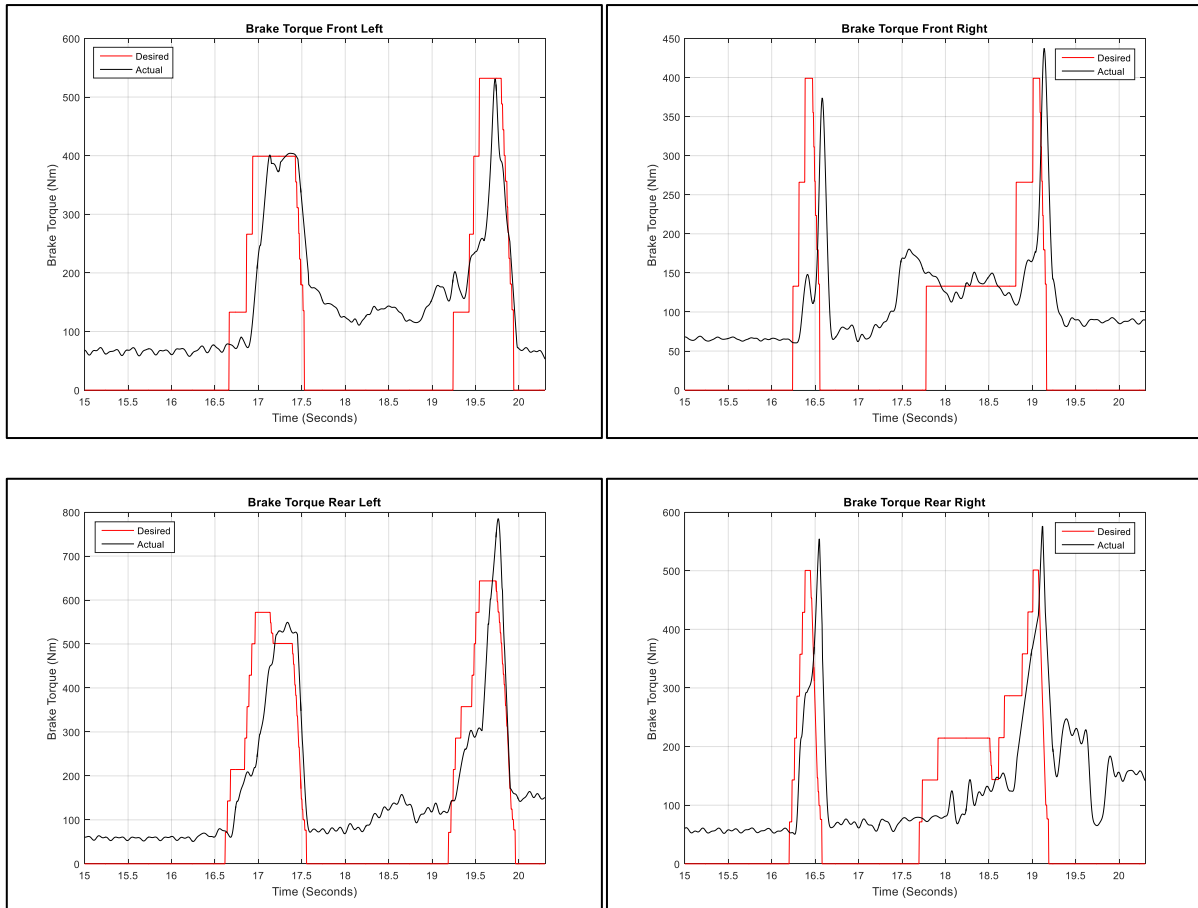


Figure 57 Brake Torques through ISO3888-2 Obstacle Avoidance

Conclusion of Results

Roll index limitations on the desired yaw rate and side-slip angle provided stable results with lower rollover propensity through both simulation and experimental tests. It can be concluded that torque vectoring control is a feasible method at implementing a direct yaw control moment and it worked well. The vehicle was stable through the ISO3888-1 Double Lane Change at 85km/h without hitting any cones and the vehicle managed to successfully complete the ISO3888-2 manoeuvre at 53km/h whereas the vehicle failed to do so without active control. The vehicle was not tested experimentally on a constant radius test due to the lack of such an enclosed space to do so safely.

Chapter 5 Conclusion and Recommendations

5.1 Conclusion

This study aimed to improve SUV handling yet reduce rollover propensity, due to the high number of fatalities caused by run-off road and rollover collisions. Numerous methods were discussed and torque vectoring control had the potential to improve both handling and rollover propensity.

A Land Rover Defender 110 at the University of Pretoria's Vehicle Dynamics Group was chosen as the platform to perform experimental tests and evaluate torque vectoring control. The vehicle was instrumented and validated using a full ADAMS simulation model previously developed.

Two types of mathematical controllers were identified and implemented in the simulation environment. A LQR method formulated by Mirzaei (2009) was used as a foundation, whereby yaw rate and side-slip angle were controlled independently of one another. A linear MPC method was developed in this study with combined yaw rate and side-slip angle control. A limit on the rollover index was added as a soft constraint on the MPC to reduce rollover propensity. A relation between the rollover index and yaw rate was used to limit the yaw of the vehicle whenever the roll index reached a desired threshold.

Simulation results showed an improvement in the vehicle trajectory and roll characteristics using the MPC method with both yaw rate and side-slip angle control. Further improvement was achieved using the MPC method with a rollover index threshold, it was noted that there existed some tracking errors on the yaw-rate however. The tracking errors were discarded due to the vehicle appearing more agile and over compensating for the turn, thus the driver would have to turn less and it aided driveability. Experimental tests were conducted using only the MPC method due to its advantages shown from the simulation results. The vehicle managed to follow paths not possible prior to active control.

5.2 Recommendations

Numerous aspects of this study can be improved upon, these include:

- Non-linear model predictive control, this would allow for the vehicle to be tested in the non-linear regime, taking into account the tyre's non-linear region and controlling how the vehicle behaves once the vehicle exceeds its limits and begins to slide.
- Combination with active suspension control could result in better cornering, as the vehicle's height/damping/stiffness can be adjusted according to the corner and vehicle behaviour. Less roll will result in more even vertical loading on each tyre, thus more lateral force generation would be possible from each tyre.
- Steering robot and speed controller to eradicate the driver from the system for experimental tests, this will help determine the controller effects without the uncertainty of driver error.

- A more modern ESP modulator with a faster response that allows for some sort of PID Control. Immediate effects could be had as this hardware component did not provide good repeatability.
- Brake temperature estimation would be required if this system is permanently connected to a vehicle, with increased brake temperature comes decreased brake power which should be monitored.
- Use of wheel force transducer on all four wheels will allow for determination of the actual brake torques applied on the vehicle amongst vertical loading and lateral force. Real time implementation of the wheel force transducer could be used for control purposes as well.
- Constant radius experimental tests would be beneficial to show the delay that the controller requires in order to reach desired thresholds and how it can be more finely tuned for predictive handling.

Chapter 6 References

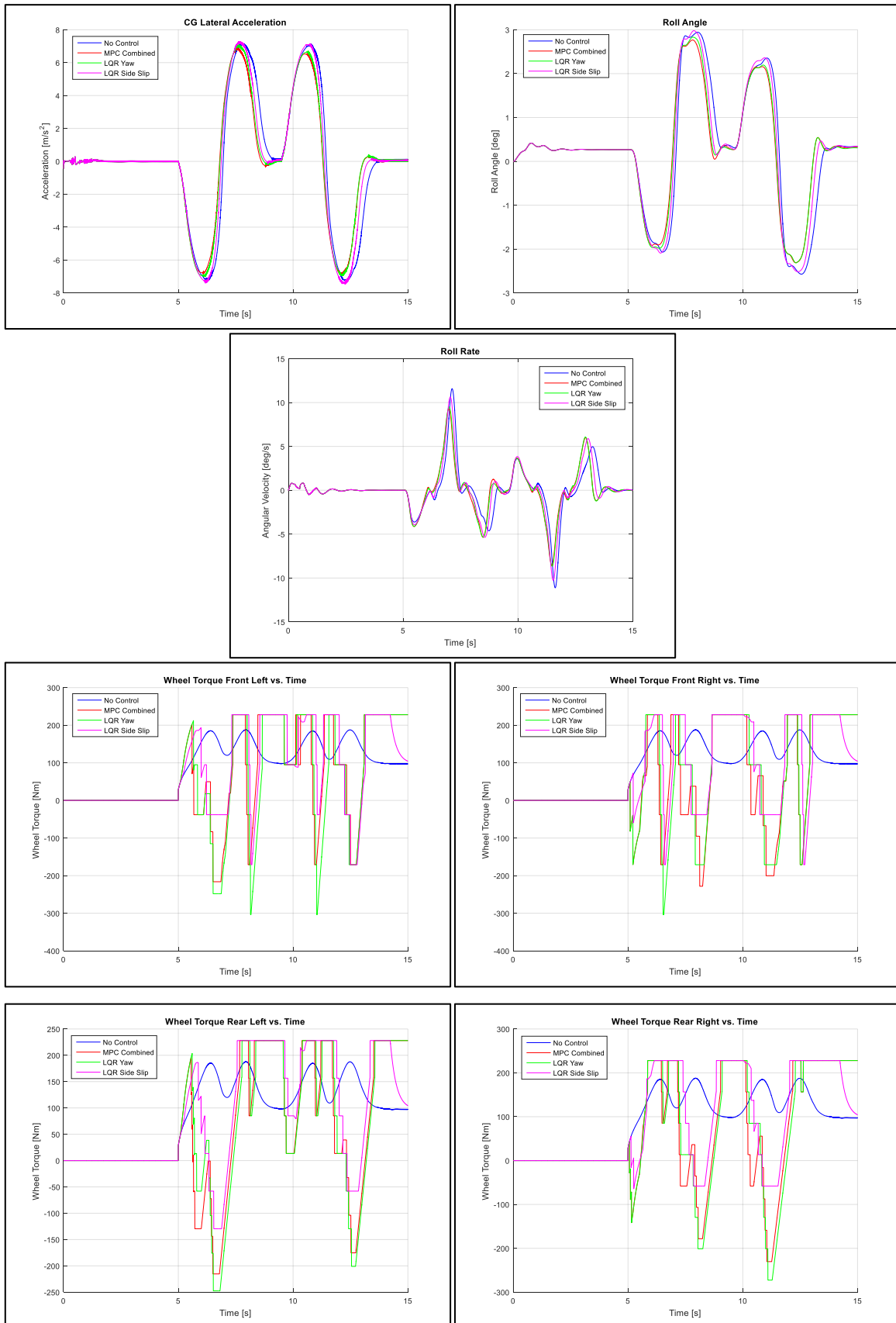
- ABE, M. 2015. *Vehicle handling dynamics: theory and application*, Butterworth-Heinemann.
- ABE, M., KANO, Y., SUZUKI, K., SHIBAHATA, Y. & FURUKAWA, Y. 2001. Side-slip control to stabilize vehicle lateral motion by direct yaw moment. *JSAE review*, 22, 413-419.
- ABE, M. A. W. M. 2009. *Vehicle Handling Dynamics*, Great Britain, Elsevier Ltd.
- ACKERMANN, J. 1994. Robust decoupling, ideal steering dynamics and yaw stabilization of 4WS cars. *Automatica*, 30, 1761-1768.
- ANWAR, S. 2005. Generalized predictive control of yaw dynamics of a hybrid brake-by-wire equipped vehicle. *Mechatronics*, 15, 1089-1108.
- BAKKER, E., PACEJKA, H. B. & LIDNER, L. 1989. A new tire model with an application in vehicle dynamics studies. *SAE technical paper*.
- BOSCH, H.-R. B., HAMERSMA, H. A. & ELS, P. S. 2016. Parameterisation, validation and implementation of an all-terrain SUV FTire tyre model. *Journal of Terramechanics*, 67, 11-23.
- BOTHA, T. R. 2011. *High speed autonomous off-road vehicle steering*.
- BUDYNAS, R. G. & NISBETT, J. K. 2008. *Shigley's mechanical engineering design*, McGraw-Hill New York.
- CRONJE, P. H. & ELS, P. S. 2010. Improving off-road vehicle handling using an active anti-roll bar. *Journal of Terramechanics*, 47, 179-189.
- DSPACE. 2017. *MicroAutoBox II* [Online]. Available: <https://www.dspace.com/en/inc/home/products/hw/micautob.cfm> [Accessed 16 August 2017].
- ELS, P. S., THERON, N. J., UYS, P. E. & THORESSON, M. J. 2006. The ride comfort vs. handling compromise for off-road vehicles. *Journal of Terramechanics*, 44, 303-317.
- ESLAMIAN, M., ALIZADEH, G. & MIRZAEI, M. 2007. Optimization-based non-linear yaw moment control law for stabilizing vehicle lateral dynamics. *Proceedings of the Institution of Mechanical Engineers, Part D: Journal of Automobile Engineering*, 221, 1513-1523.
- ESMAILZADEH, E., GOODARZI, A. & VOSSOUGH, G. 2003. Optimal yaw moment control law for improved vehicle handling. *Mechatronics*, 13, 659-675.
- GILLESPIE, T. D. 1992. *Vehicle Dynamics*. Warren dale.
- KALLAN, M. J. SUV Rollover in Single Vehicle Crashes and the Influence of ESC and SSF. In: MEDICINE, A. F. T. A. O. A., ed. *Advances in Automotive Medicine/ Annual Scientific Conference*, 2008 2008. *Ann Adv Automotive Med*.
- LAPAPONG, S., BROWN, A., SWANSON, K. & BRENNAN, S. 2012. Zero-moment point determination of worst-case manoeuvres leading to vehicle wheel lift. *Vehicle system dynamics*, 50, 191-214.
- LEW, J., PIYABONGKARN, D. & GROGG, J. 2006. Minimizing dynamic rollover propensity with electronic limited slip differentials. *SAE Technical Paper*.
- MARSH, J. 2007. *Hydropneumatique* [Online]. Available: <http://www.citroenet.org.uk/miscellaneous/hydraulics/hydraulics-11.html> [Accessed 19 April 2017].

- MIRZAEI, M. 2009. *A new strategy for minimum usage of external yaw moment in vehicle dynamic control system*. *Transportation Research Part C: Emerging Technologies*, 18, 213-224.
- MIRZAEI, M., ALIZADEH, G., ESLAMIAN, M. & AZADI, S. 2008. *An optimal approach to non-linear control of vehicle yaw dynamics*. *Proceedings of the Institution of Mechanical Engineers, Part I: Journal of Systems and Control Engineering*, 222, 217-229.
- MOKHIAMAR, O. & ABE, M. 2002. *Effects of model response on model following type of combined lateral force and yaw moment control performance for active vehicle handling safety*. *JSAE review*, 23, 473-480.
- NHTSA 2003. *Consumer information, new car assessment program, rollover resistance*, Docket No. NHTSA-2001-9663; Notice 3.
- ORŁOWICZ, A., MRÓZ, M., WNUK, G., MARKOWSKA, O., HOMIK, W. & KOLBUSZ, B. 2016. *Coefficient of Friction of a Brake Disc-Brake Pad Friction Couple*. *Archives of Foundry Engineering*, 16, 196-200.
- PARK, K., HEO, S.-J. & BAEK, I. 2001. *Controller design for improving lateral vehicle dynamic stability*. *JSAE review*, 22, 481-486.
- RACELOGIC 2015. *Slip Angle Explained*.
- RACELOGIC. 2017. *VBOX 3i* [Online]. Available: <https://www.vboxautomotive.co.uk/index.php/en/products/data-loggers/vbox-3i> [Accessed 18 August 2017].
- REPORTS, C. 2014. *How rollovers happen and what you can do to avoid one* [Online]. *Consumer Reports*. Available: <https://www.consumerreports.org/cro/2012/02/rollover-101/index.htm> [Accessed 19 November 2016].
- SAWASE, K., USHIRODA, Y. & MIURA, T. 2006. *Left-right torque vectoring technology as the core of super all wheel control (S-AWC)*. *Mitsubishi Motors Technical Review*, 18, 16-23.
- STALLMANN, M. J. & ELS, P. S. 2014. *Parameterization and modelling of large off-road tyres for ride analyses: Part 2-Parameterization and validation of tyre models*. *Journal of Terramechanics*, 55, 85-94.
- STANDARD, I. 1999. *Passenger cars - Test track for severe lane change manoeuver. Part 1: Double lane-change ISO 3888-1*. *International Organization for Standardization*.
- STANDARD, I. 2011. *Passenger cars - Test track for severe lane-change manoeuver. Part 2: Obstacle avoidance ISO 3888-2*. *International Organization for Standardization*.
- TSOURAPAS, V., PIYABONGKARN, D., WILLIAMS, A. C. & RAJAMANI, R. *New method of identifying real-time predictive lateral load transfer ratio for rollover prevention systems*. *American Control Conference, 2009. ACC'09., 2009. IEEE*, 439-444.
- UYS, P. E., ELS, P.S., THORESSON, M.J., VIGHT, K.G., COMBRINCK, W.C. 2006. *Experimental Determination of Moments of Inertia for an Off-Road Vehicle in a Regular Engineering Laboratory*. *International Journal of Mechanical Engineering Education* 34/4: Univeristy of Pretoria.
- VAN ZANTEN, A. T., ERHARDT, R. & PFAFF, G. 1995. *VDC, the vehicle dynamics control system of Bosch*. *SAE Technical Paper*.
- WALZ, M. C. 2005. *Trends in the static stability factor of passenger cars, light trucks, and vans*.

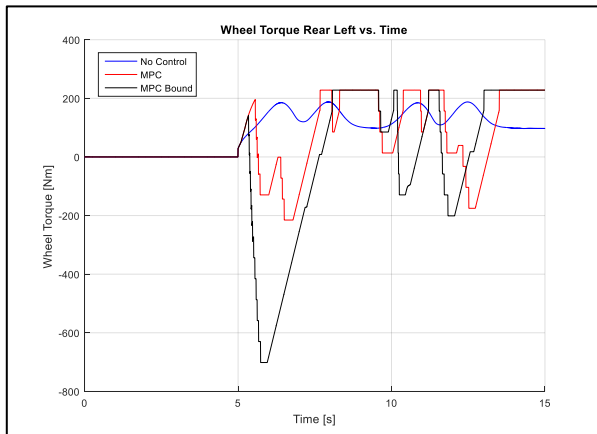
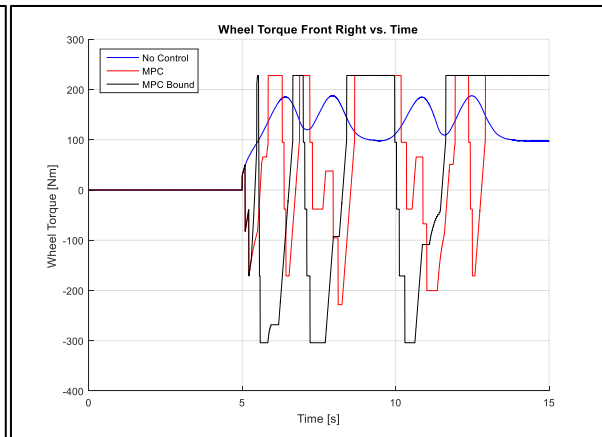
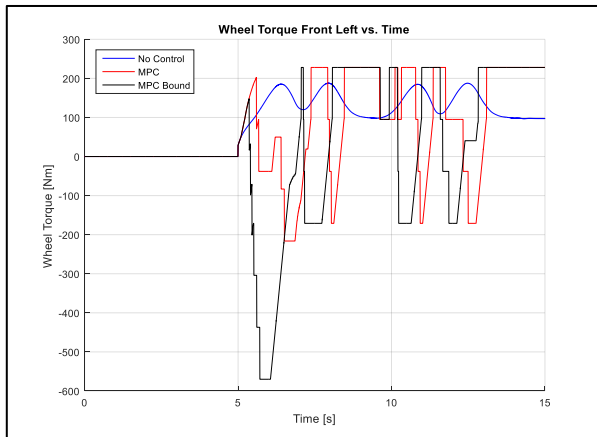
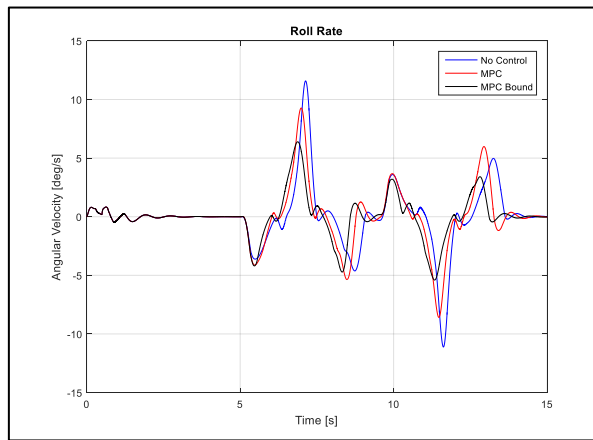
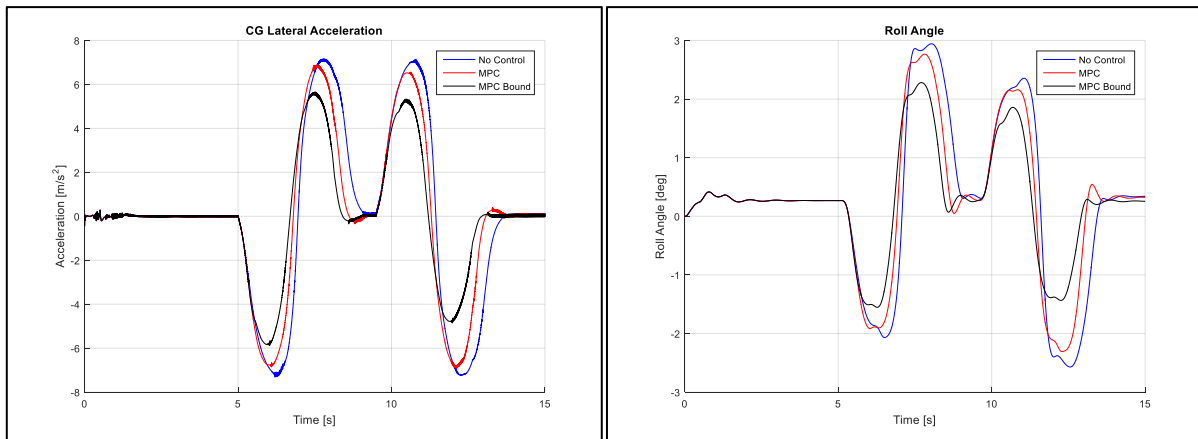
- WONG, J. Y. 2008. *Theory of ground vehicles*, John Wiley & Sons.
- YOON, J., KIM, D. & YI, K. 2007. Design of a rollover index-based vehicle stability control scheme. *Vehicle system dynamics*, 45, 459-475.
- ZHENG, S., TANG, H., HAN, Z. & ZHANG, Y. 2006. Controller design for vehicle stability enhancement. *Control Engineering Practice*, 14, 1413-1421.

Appendix

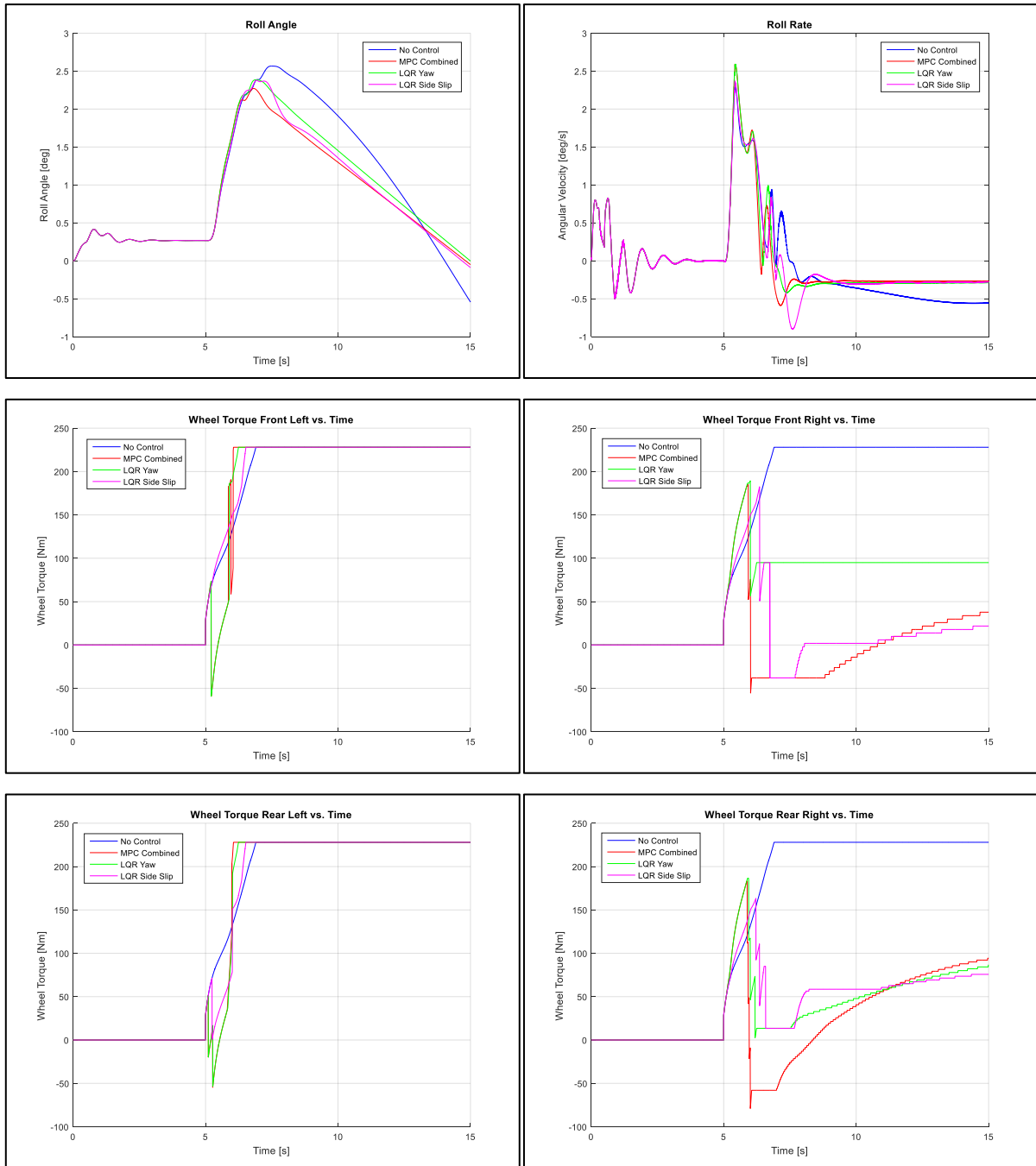
A.1 Sinusoidal Wave Steer Input without Roll Index Bounds



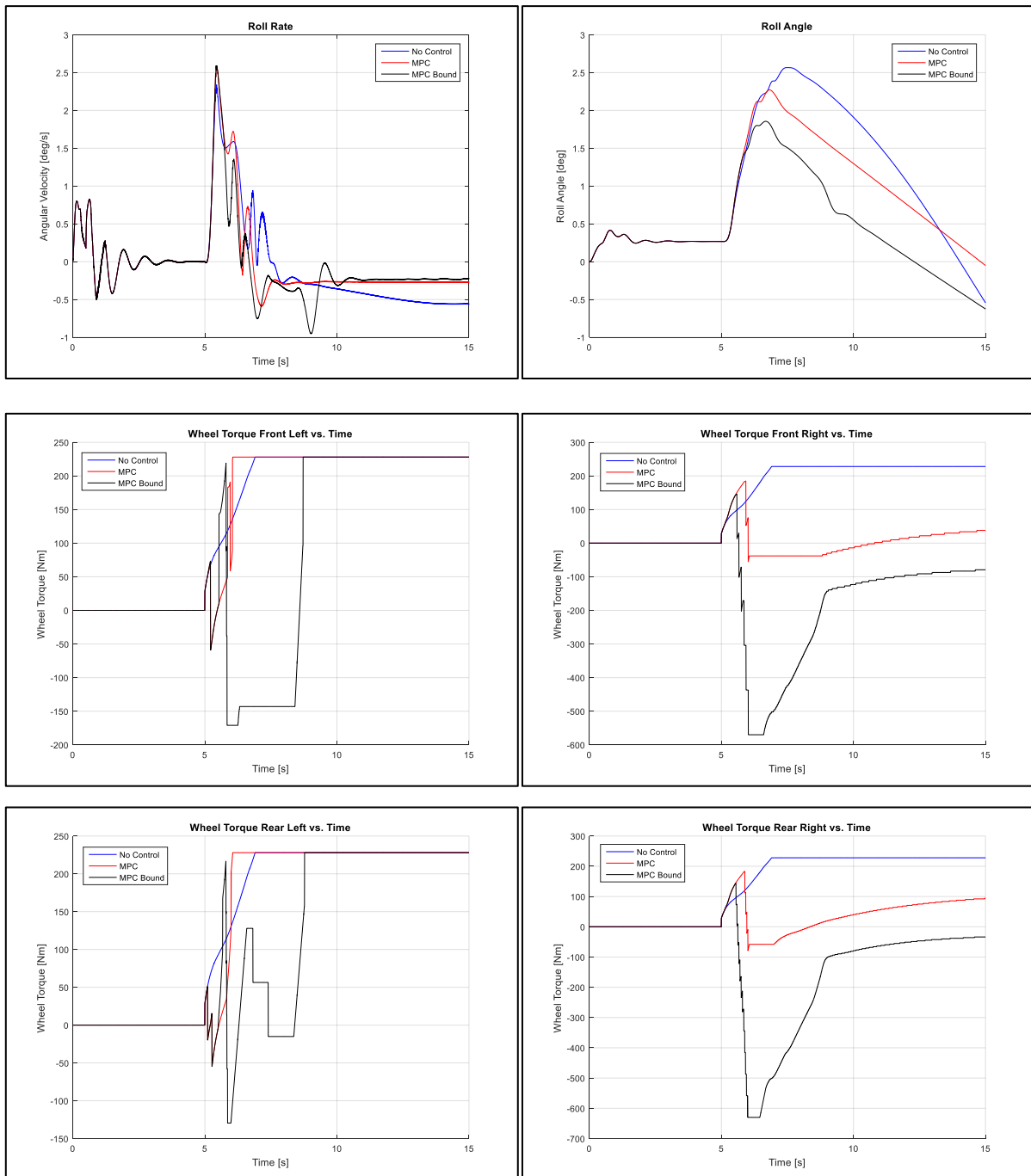
A.2 Sinusoidal Wave Steer Input with Roll Index Bounds



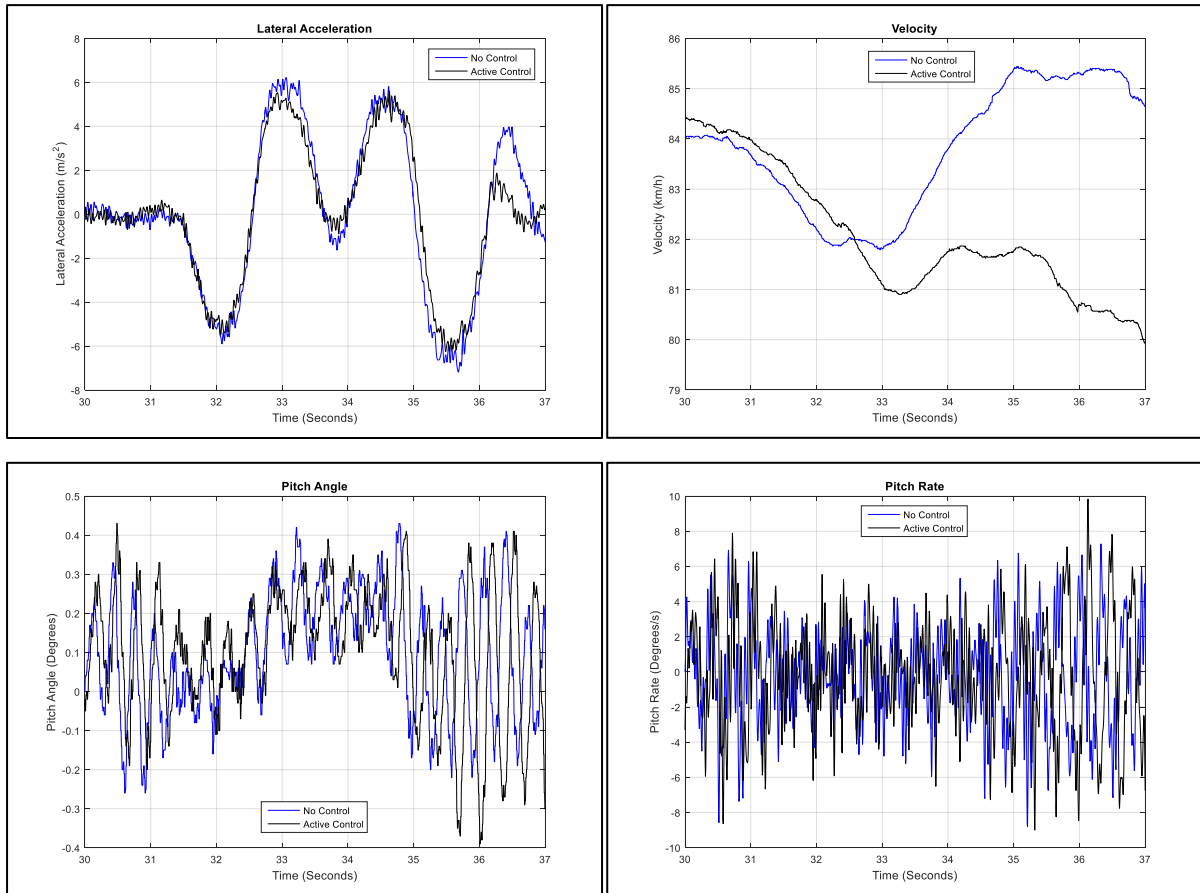
A.3 Step Steer without Roll Index Bounds



A.4 Step Steer with Roll Index Bounds



A.5 Severe Double Lane Change ISO3888-1



A.6 Severe Lane Change ISO3888-2 Obstacle Avoidance

